MacPoisson™ Supplement

Instructional Finite Element Analysis
Verification and Problem Sets

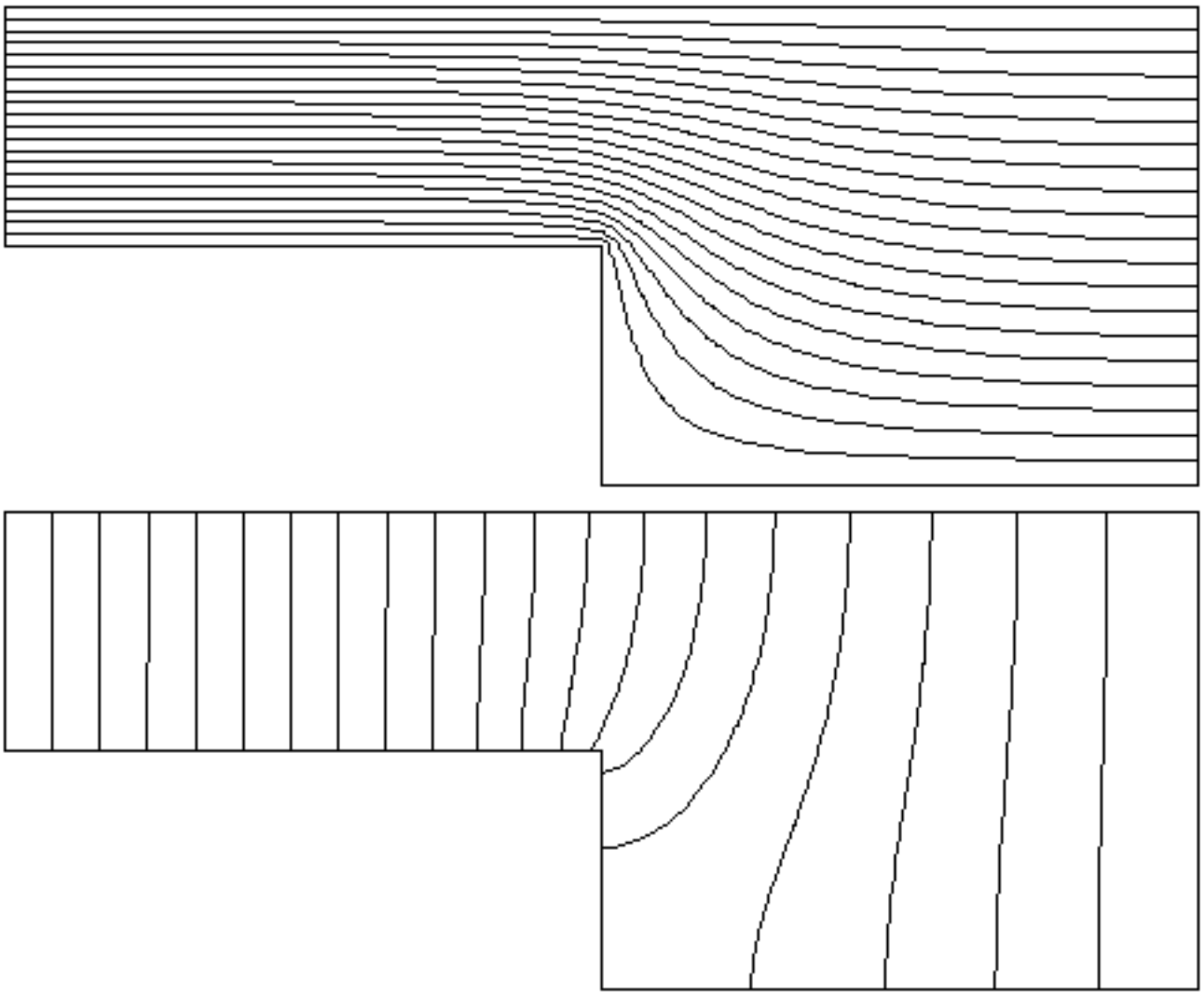

Contents

J. R. Cooke
D.C. Davis
E.T. Sobel
D.R. Raman

PDF version, December 1996

Contents

This chapter presents a collection of verification examples. We compare the MP results with the theoretical solution whenever feasible. These examples illustrate MP techniques and the strengths and weaknesses of the triangular element.

The first three examples appeared in the student guide, but are repeated here. At least one example for each type of problem is included. In addition to the necessary role of validation, these examples provide hints for using MP more effectively.

Format for problems

Title
Project name (as on diskette)
Description of the problem, including specific issues
Screen dumps of major parts of the solution
Output (graphical and tabular)
Theoretical solution (assumption, equations, etc.)
References
Addendum

List of problems (Click to select.)

Student version

Unrestricted professional version

Project 01: Heat conduction through a hollow cylinder.

Folder: Cylinder

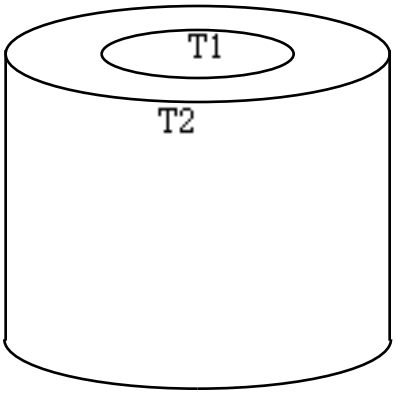

Fig 1.1.1 Cylinder

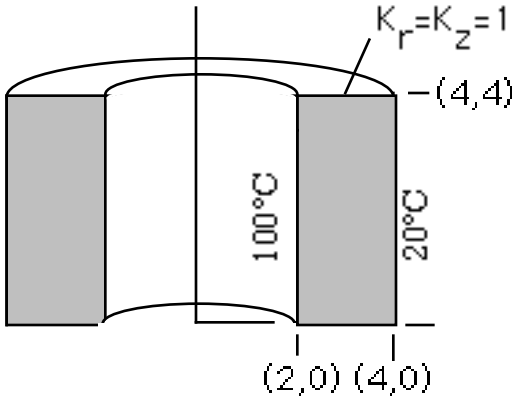

Fig 1.1.2 Cylinder schematic

This project models a hollow cylinder with an inside wall temperature of T1 and outside wall temperature of T2. Fig 1.1.1 is a sketch of the problem, while Fig 1.1.2 illustrates how you use the axial symmetry of the problem (i.e., the cylinder is represented by a rectangle rotated about the z-axis). The problem as posed could also be treated as a planar problem (a slice of two concentric circles).

The problem has dimensions as shown above, with a wall thickness of two meters, a height of 4 meters, and a thermal conductivity (k) of 1W / m°C. Take T1 as 100°C and T2 as 20°C.

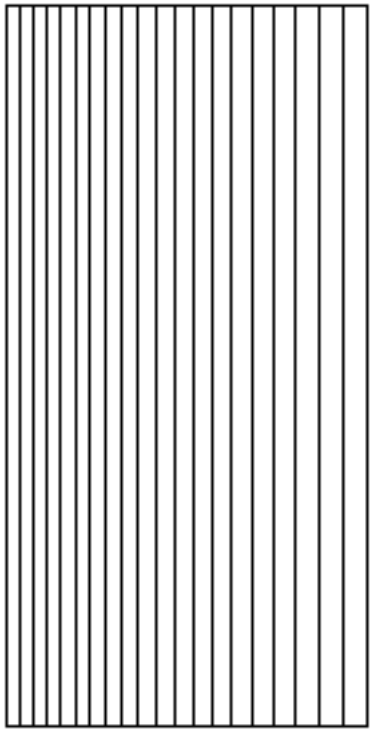

Fig 1.1.3 Constant temperatures

The equipotential lines resulting from this solution are shown in Fig 1.1.3. Notice that the lack of a z temperature gradient means that the problem is essentially one dimensional and could have been solved as a thin ring with only two nodes on the vertical side. A portion of the tabular output of the program (accessible via the library function, Fig 1.1.5) shows the temperature at different nodes along with the list (Fig 1.1.4) giving node position vs. node number and can thus be used to find the computed temperature at any node.

```
B55  2.00000000000000e+0 2.22044604925031e-16 b
B56  2.94736842105263e+0 3.55555555555556e+0 i
B57  2.84210526315789e+0 3.11111111111111e+0 i
B58  2.73684210526316e+0 2.66666666666667e+0 i
B59  2.63157894736842e+0 2.22222222222222e+0 i
B60  2.52631578947368e+0 1.77777777777778e+0 i
B61  2.42105263157895e+0 1.33333333333333e+0 i
B62  2.31578947368421e+0 8.88888888888889e-1 i
B63  2.21052631578947e+0 4.44444444444445e-1 i
B64  2.10526315789474e+0 2.22044604925031e-16 b
B65  3.05263157894737e+0 4.00000000000000e+0 b
```

Fig 1.1.4. Node position vs. node number for nodes 55 to 65

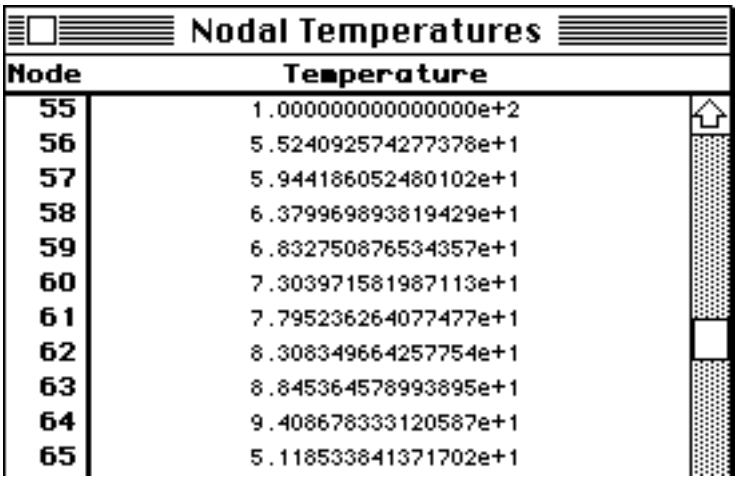

Fig 1.1.5 Nodal temperatures

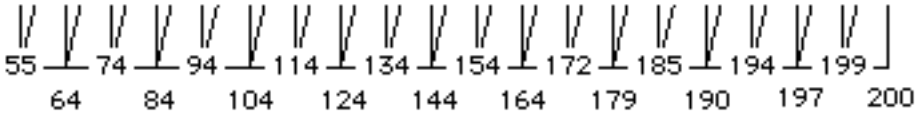

Fig 1.1.6 Node numbers in radial direction

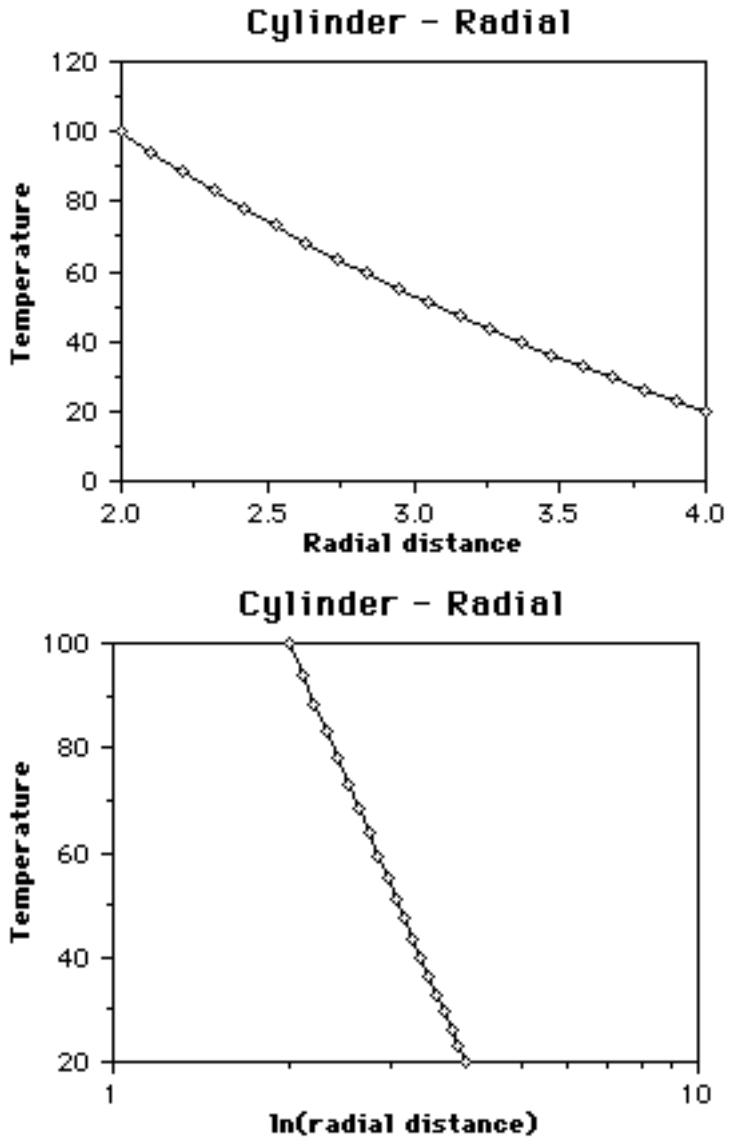

Fig 1.1.7 Temperature in radial direction (cf Fig 1.1.6)

Theoretical solution and comparison of results:

When you solve the differential equation governing steady state heat conduction in the tube, the result is: $T = c_1 \ln(r) + c_2$; with c_1 and c_2 easily calculated from boundary conditions. The solution assumes the tube to be of constant material properties, to have no heat sources or sinks within it, and to be very long axially, thus specifying no heat flow in the z direction. The radial variation in temperature is shown in Fig 1.1.7.

The following is the tabulated output comparing MP results (at nodes) to the results of the theoretical solution at those nodes.

Clearly, at this resolution (20 nodes in r-direction) you obtain very accurate results.

Pr-01 Cylinder

Radius	MP	Theory	Error
2.00	100.00	100.00	0.00%
2.11	94.09	94.09	0.01%
2.21	88.45	88.45	0.00%
2.32	83.08	83.08	0.00%
2.42	77.95	77.95	0.00%
2.53	73.04	73.04	0.00%
2.63	68.33	68.33	0.00%
2.74	63.80	63.80	0.00%
2.84	59.44	59.44	0.00%
2.95	55.24	55.25	0.01%
3.05	51.21	51.20	-0.03%
3.16	47.29	47.28	-0.02%
3.26	43.50	43.50	-0.01%
3.37	39.84	39.83	-0.01%
3.47	36.28	36.28	0.00%
3.58	32.84	32.84	0.00%
3.68	29.49	29.49	0.00%
3.79	26.24	26.24	0.00%
3.89	23.08	23.08	0.00%
4.00	20.00	20.00	0.00%

References: Eckert, E.R.G., and Drake, Robert M. Jr. 1972. *Analysis of Heat and Mass Transfer.* McGraw-Hill, p70.

An interesting variation on this problem is to assume the tube to have different material properties at different radii, thus making a composite tube. This problem also has an easily derivable, closed form solution. However, it is possible to change the problem in ways which render closed form solutions difficult, such as: by removing the "very long axially" restriction and assuming a convection loss along the top and bottom surfaces, or by assuming a small band of insulating or conducting material buried in the tube, or by assuming heat sources unevenly distributed within the tube.

Project 02: Electric potential between two eccentric metal cylinders.

Folder: Eccentric Cylinder

Two metal circular cylinders of different radii and different centers, one lying completely within the other are shown in Fig 1.2.1. The voltage on the inner cylinder is taken to be 200 volts, while the outer cylinder is taken as ground (0.0 volts). The potential distribution between the cylinders is desired.

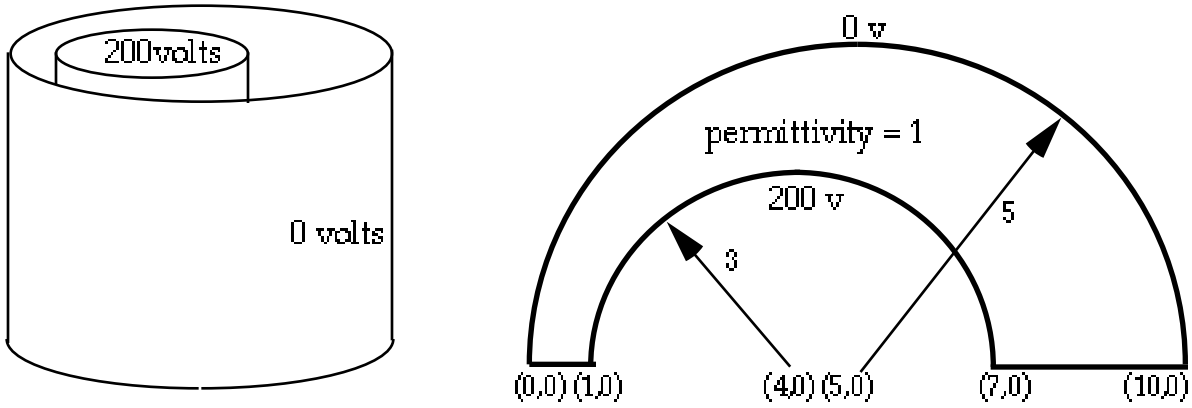

Fig 1.2.1 Eccentric cylinder capacitor

The geometry creation and subsequent mesh generation are tricky in this problem. The intermediate region generating points on the cylinders must be equally spaced to prevent incorrect mesh generation. Remember, MacPoisson uses a second degree curve fitting technique to connect two endpoints with an intermediate point on the curve. If, in this problem, you select regions which have unequally spaced intermediate points on the inner or outer cylinder, the result is a different paraboloid for each section, with non-continuous slope at the region borders.

Keep in mind the desirability of roughly equilateral triangles to promote accuracy in computations when specifying the node/size values for the problem. The left side of the problem tends to have longer, thinner elements if the node/side spacing is not adjusted carefully.

Once you create the mesh, the material property and boundary condition specification is straightforward. Figure 1.2.2 shows the solution of the problem as graphed by MacPoisson.

The theoretical solution to this problem is possible through the use of bicylindrical coordinates, wherein a family of orthogonal circles is defined by the relations:

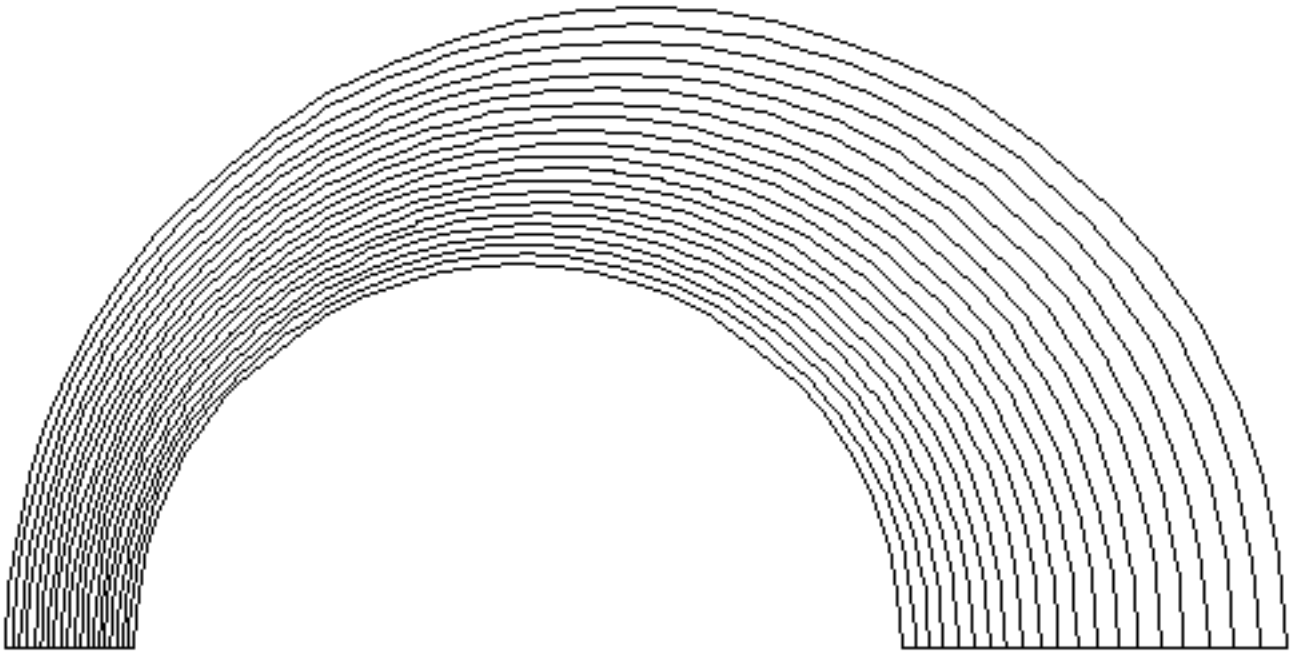

Fig 1.2.2 Equipotential lines for eccentric cylinder

$$x = \frac{a \sinh \eta}{\cosh \eta - \cos \theta}$$

$$y = \frac{a \sin \theta}{\cosh \eta - \cos \theta}$$

$$z = z$$

η = constant (circles about poles on x-axis at +a and -a).

θ = constant (orthogonal circles, centers on y axis).

The solution for the problem is easily shown to be:

$$V = 200 \frac{(\eta_1 - \eta_2)}{(\eta_1 + \eta_2)} \quad \text{where;}$$

η_1 corresponds to the inner 200v cylinder, and

η_2 corresponds to the outer grounded cyliner

To find V at any point given Cartesian coordinates, use the following relationship between x and y.

$$\eta = \sinh^{-1} \frac{x \sin \theta}{y}$$

$$\text{where } \theta = \tan^{-1} \frac{y}{x - a} - \tan^{-1} \frac{y}{x + a}$$

$$\text{with } a = \frac{1}{2s} \sqrt{s^4 - 2s^2 (r_2^2 + r_1^2) + (r_2^2 - r_1^2)^2}$$

where r_1 = radius of the smaller cylinder
r_2 = radius of the larger cylinder
s = distance between cylinder centers

Errors for Eccentric cylinder

Theoretical	MacPoisson	% Error	Node #
46.759037	44.792961	4.2	22
23.257677	22.017195	5.3	29
24.038365	22.554054	6.2	38
24.177020	22.466274	7.1	47
23.537626	22.196783	5.7	56
21.767392	20.854362	4.2	110
21.758951	20.637066	5.2	119
21.249613	20.252686	4.2	128
20.356016	19.539839	4.0	155

A computer program to solve the theoretically derived potential at each node was used to generate a table of the nodal values where the error exceeds 4.0% when compared to theory.

Clearly, even at a relatively low resolution (D.O.F. = 279), MacPoisson produces very good results, with a maximum error of 7.1%, and with only 3% of all nodes having an error of more than 4%.

Reference: Moon and Spencer. 1961. *Field Theory for Engineers*. D. Van Nostrand Company Inc. Ch 13.

Project 03: Bottom-heated pot revisited

Folder: HeatedPotIns

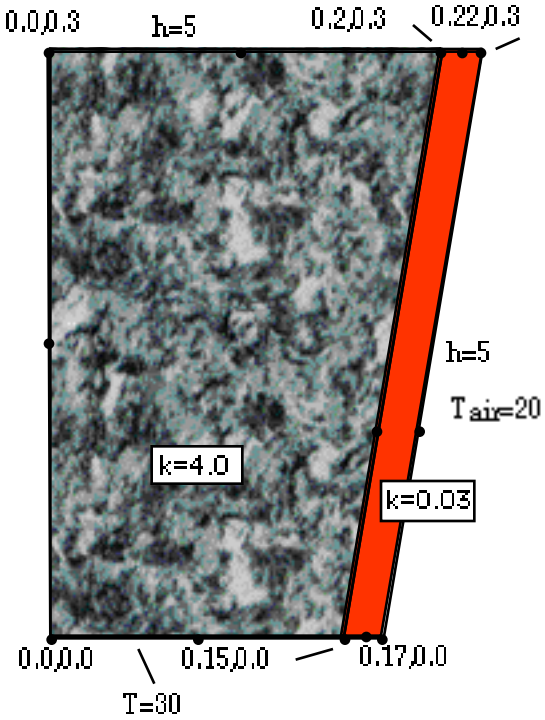

Fig 1.3.1 Pot with insulation

You wish to achieve a uniform temperature within the bottom-heated pot example discussed in Chapter 3. Suppose you want to consider the influence of the insulation of the pot on the temperature profile of the bottom-heated flower pot. One obvious possibility is the limiting case of a perfectly insulated wall, which we leave as an exercise. Consider the conditions depicted in Fig 1.3.1.

The formulation and solution are outlined in Figures 1.3.2 and 1.3.3.

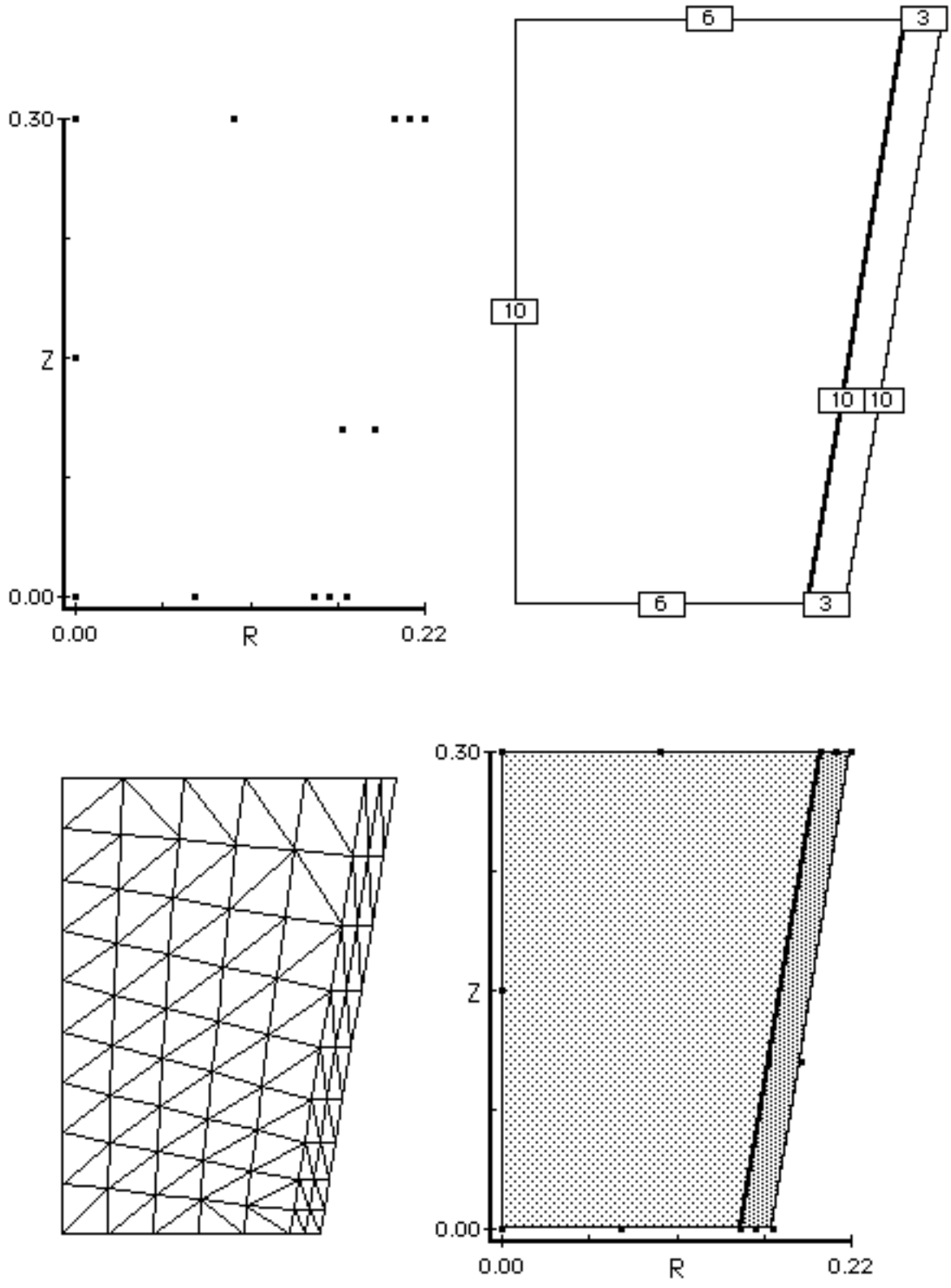

Fig 1.3.2 Mesh generation steps for insulated pot

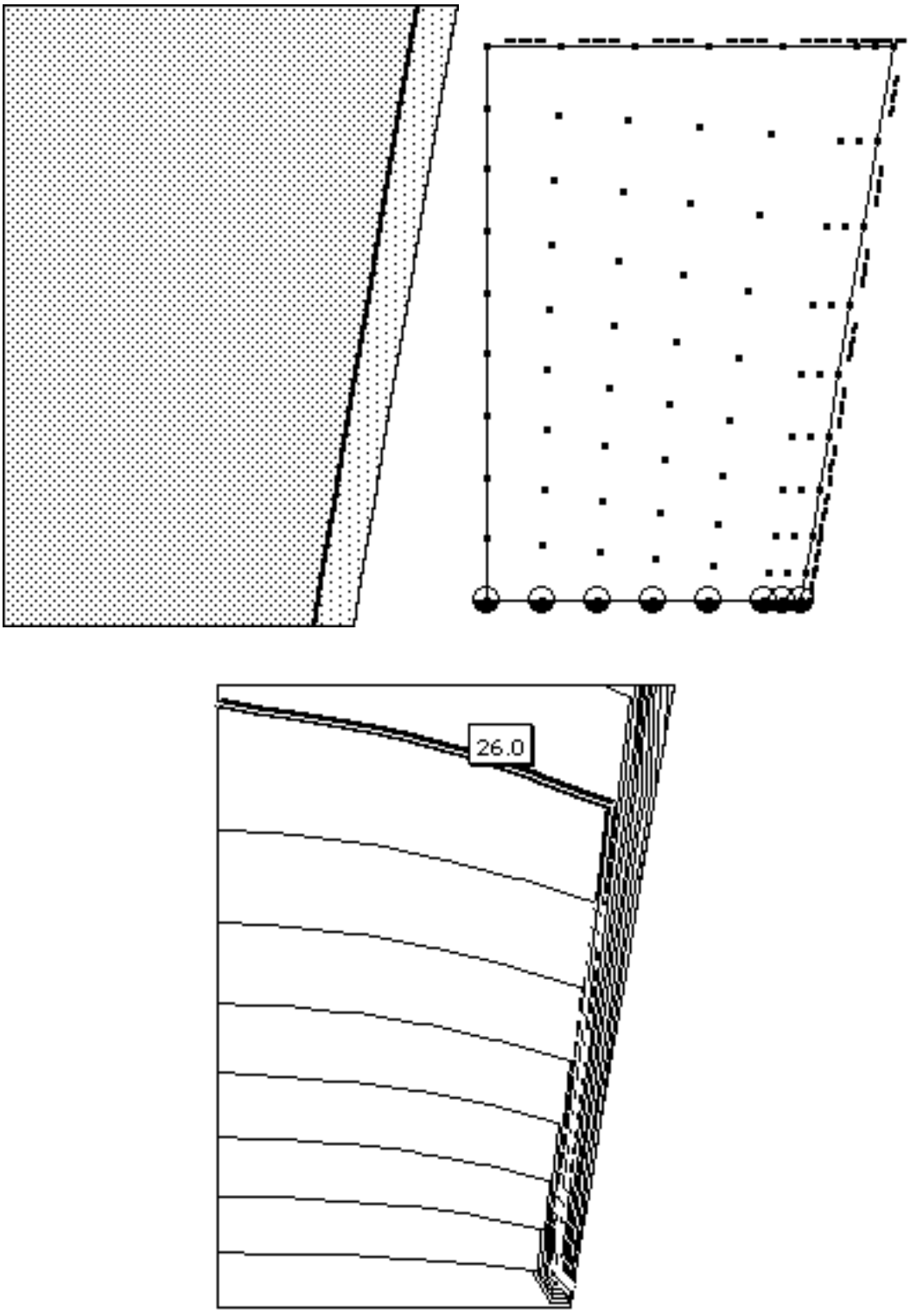

Fig 1.3.3 Properties, boundary conditions, and temperature profile

Compare the results with the example in Chapter 3 of the user guide.

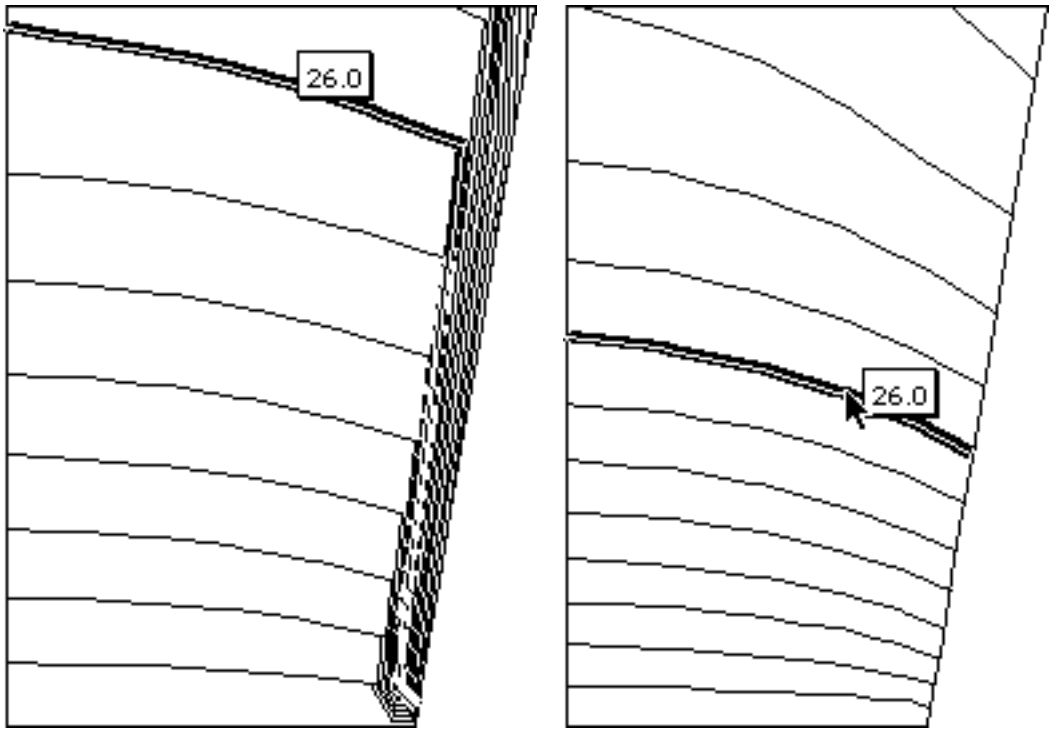

Fig 1.3.4 The insulated and uninsulated pot temperature profiles

Notice that the four degree drop occurs over a much greater distance than in the uninsulated case.

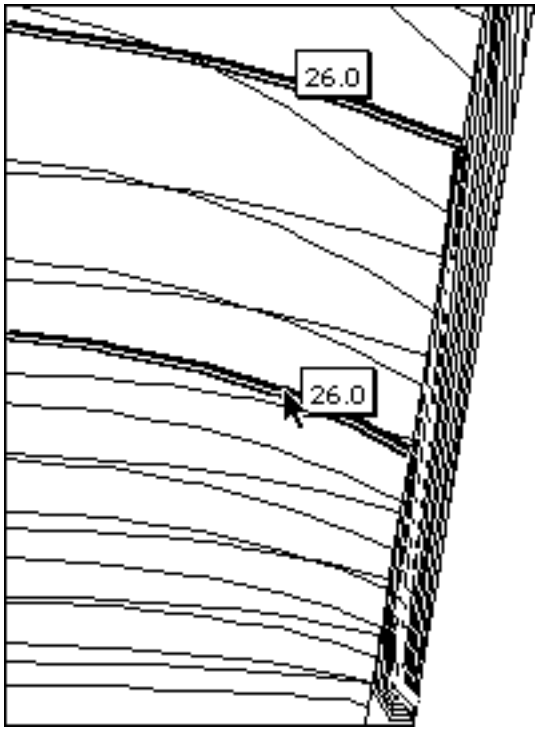

Fig 1.3.5 Insulated and uninsulated examples superimposed

The difference between the uninsulated and insulated cases can be displayed more clearly by superimposing the two results.

Reference: Yang, X. and L.D. Albright. 1985. Finite Element Analysis of Temperatures in a Bottom-heated Nursery Container. Acta Hort. No 175. pp155-165. (*Also:* ASAE Paper No. 85-4048 ASAE St. Joseph, MI)

Project 04: Insulated cylinder with convection.

Folder: InsPipe

A metal pipe of inner radius 0.15 ft, outer radius 0.25 ft, and conductivity 0.5Btu / (hr ft °F) is covered by insulation 0.10 ft thick of conductivity 0.5 Btu / (hr ft °F). The fluid inside the pipe is at 100°F and the fluid outside the insulation is at 50°F. The film coefficients are 20 and 2 Btu / (hr ft² °F) on the inner and outer surfaces, respectively. Find the temperature profile in the pipe and insulation.

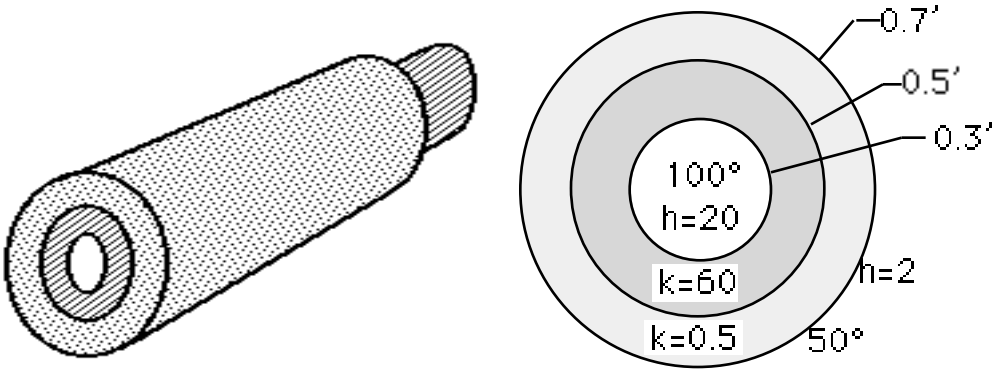

Fig 1.4.1 Insulated pipe and properties

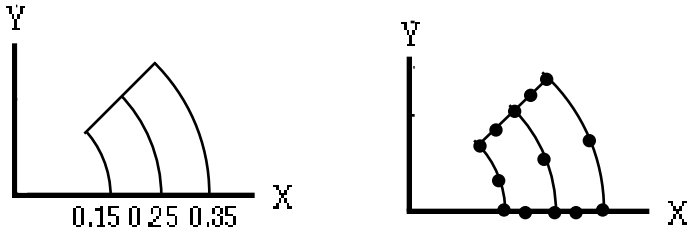

Fig 1.4.2 Geometry and region definition sketches

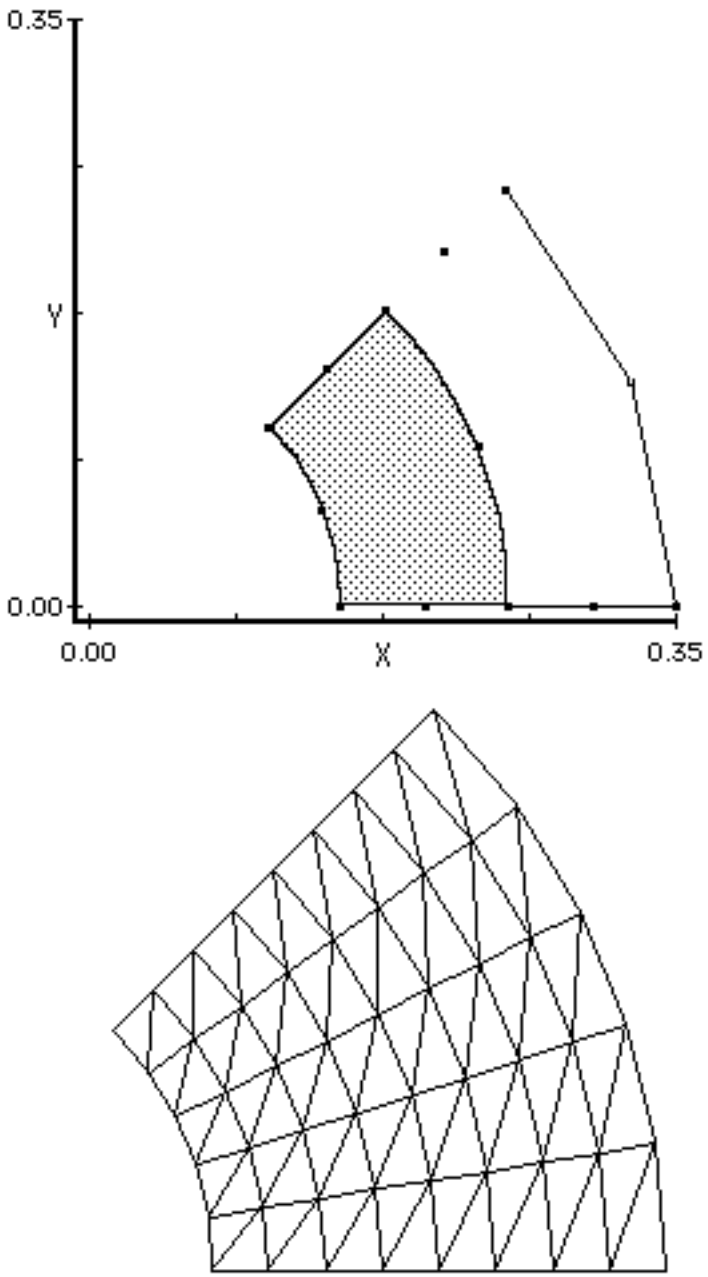

Fig 1.4.3 Mesh generation

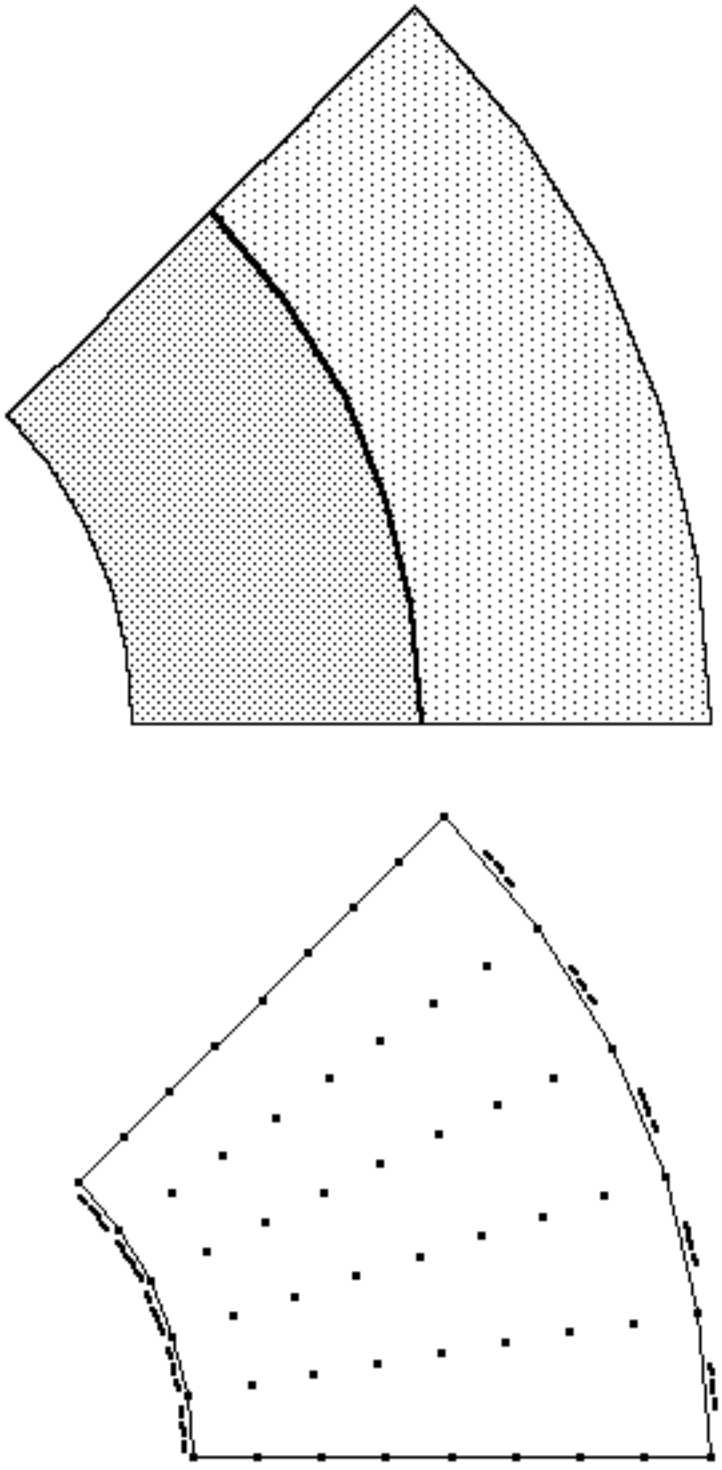

Fig 1.4.4 Properties and boundary conditions

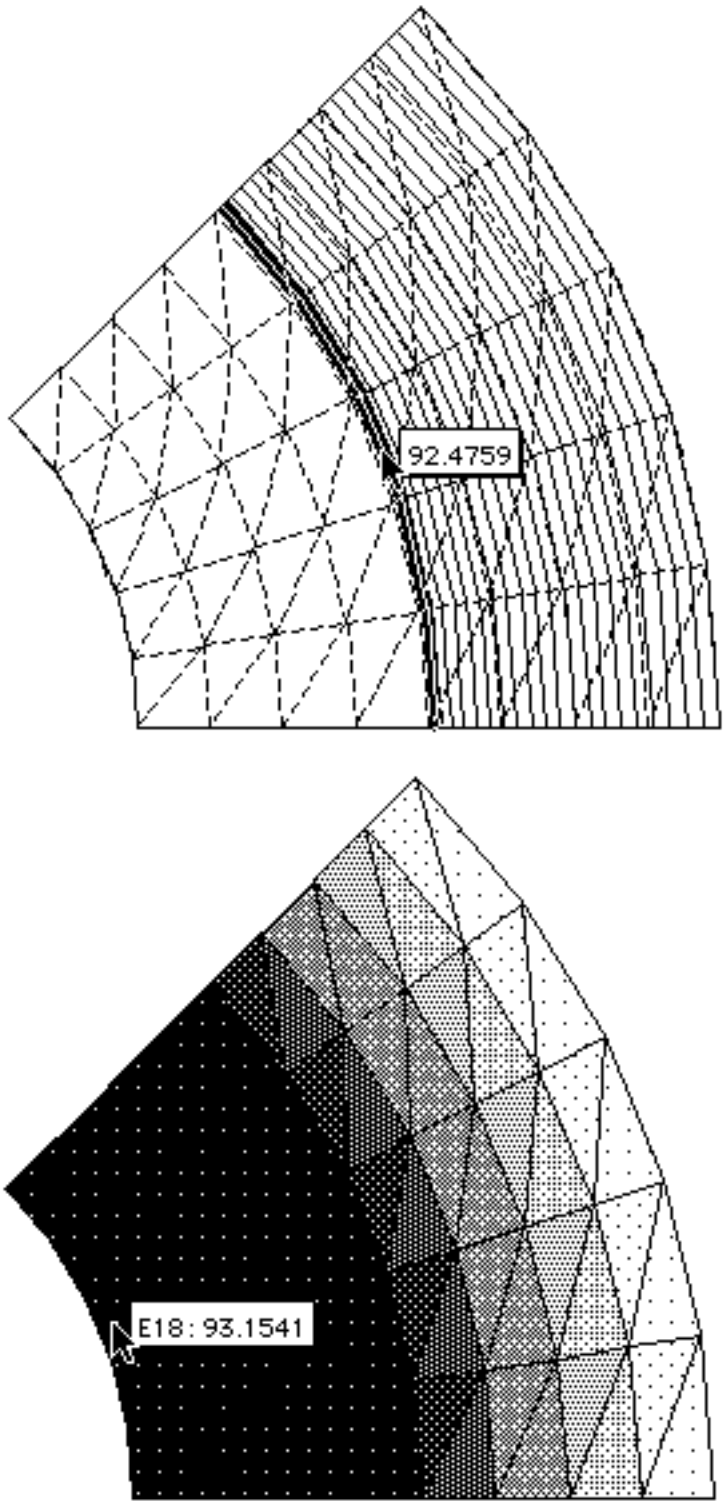

Fig 1.4.5 Computed temperatures

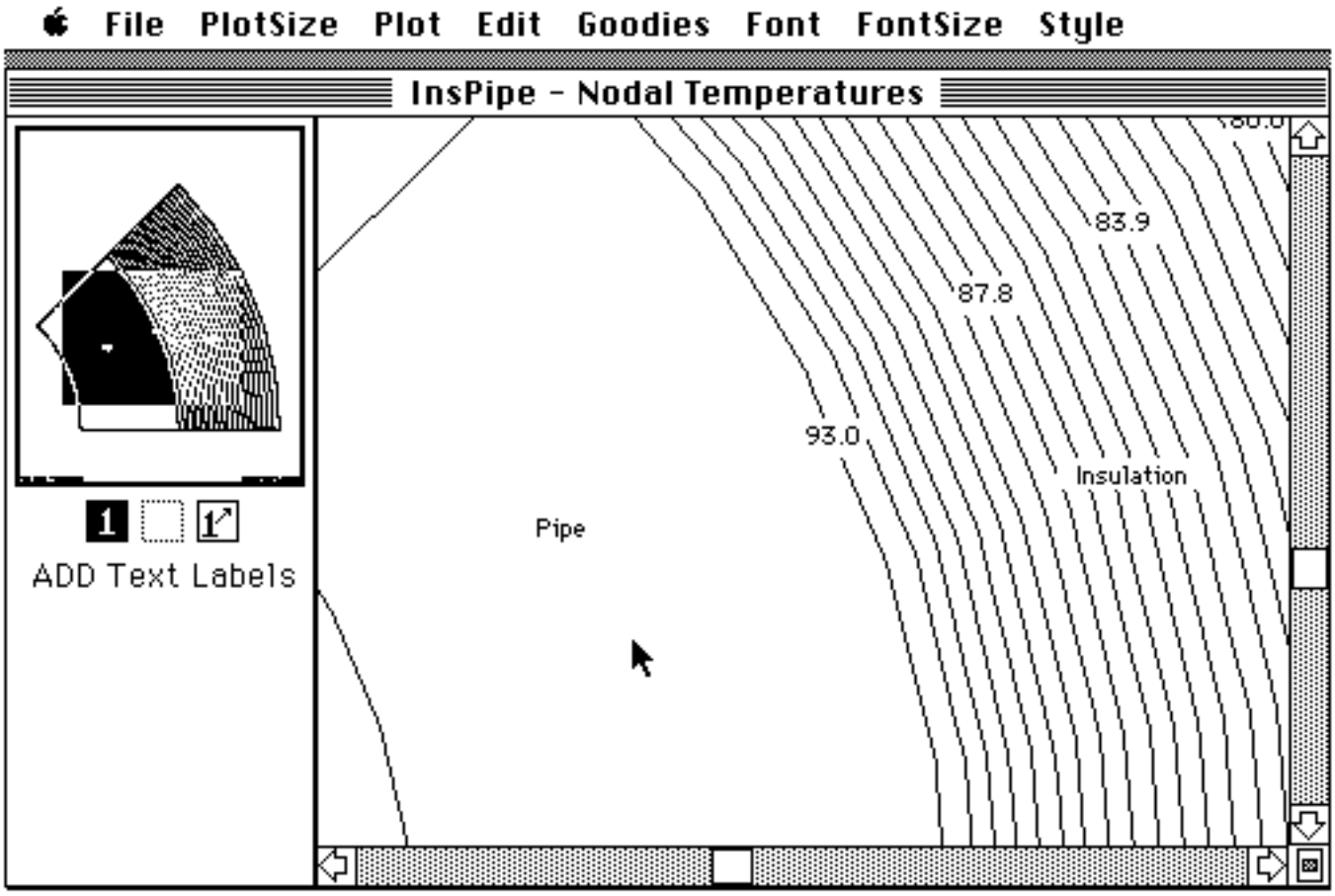

Fig 1.4.6 Plot with labels

The problem solving steps are outlined in Figures 1.4.2 through 1.4.6. Under certain circumstances in heat conduction from small-diameter tubes the application of insulation actually increases heat loss.

Reference: Eckert, E.R.G. and Robert M. Drake. Jr. 1972. *Analysis of Heat and Mass Transfer.* McGraw-Hill Book Co. NY. Ch 3.

Project 05: Chimney temperature.

Folder: Chimney

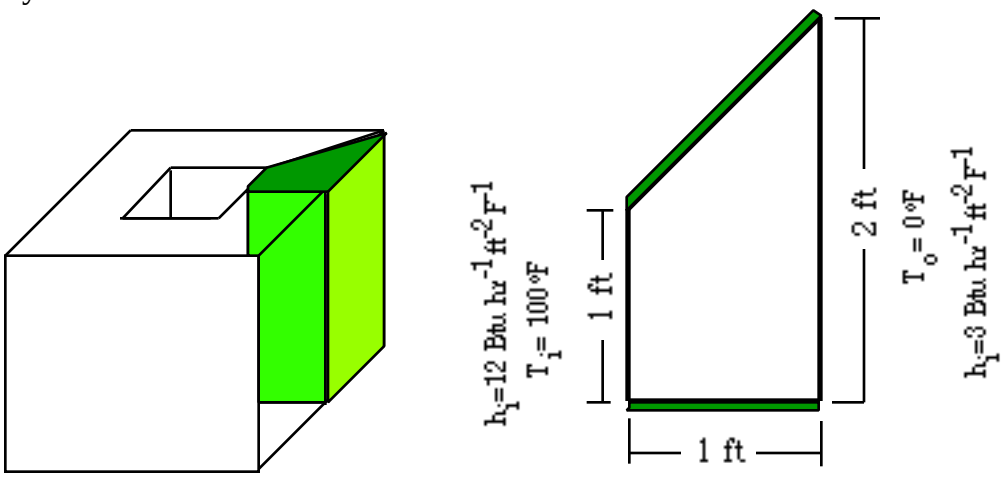

Fig 1.5.1 Chimney temperature

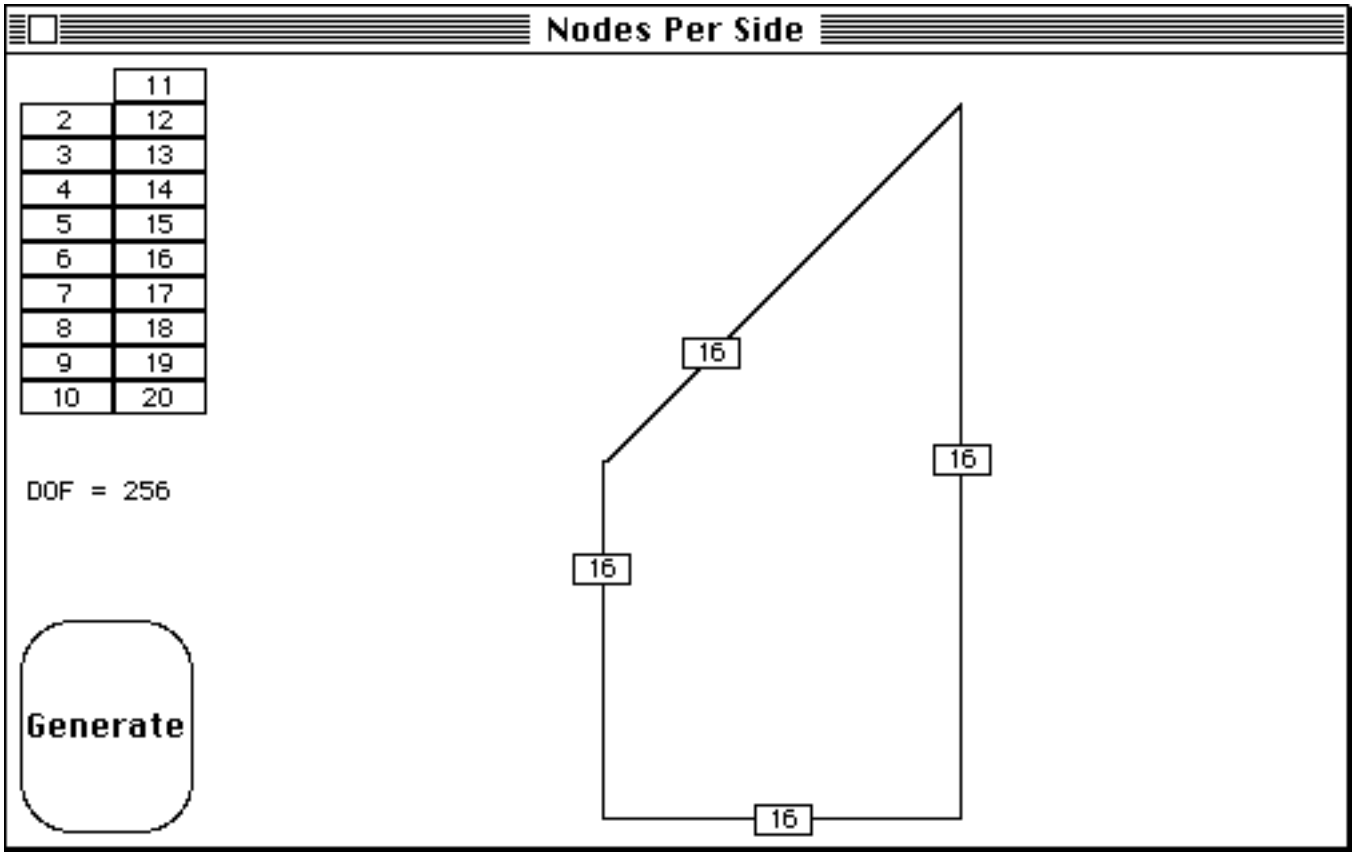

Fig 1.5.2a Mesh generation

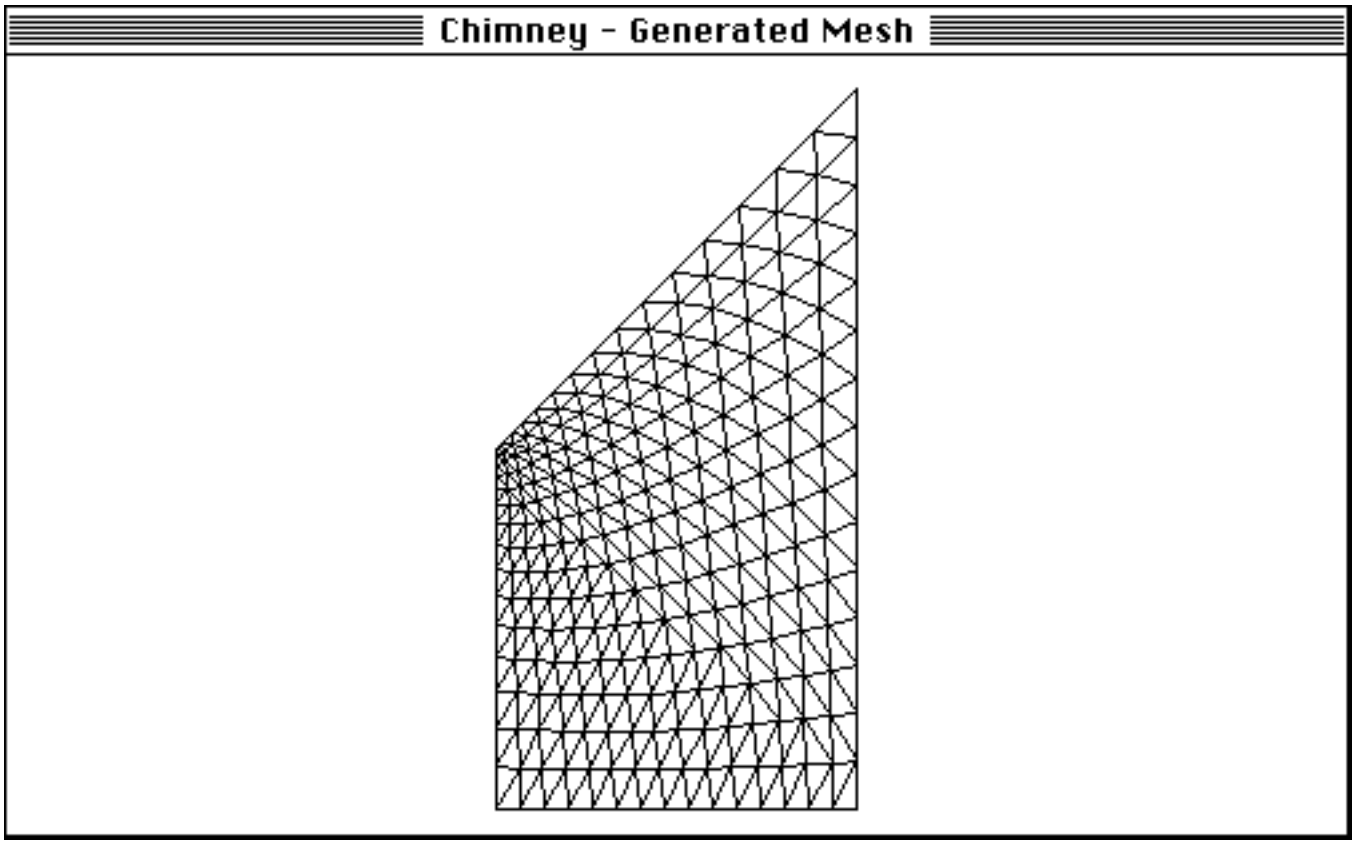

Fig 1.5.2b Mesh generation

You can easily find the steady- state temperature within the walls of a square chimney (Fig 1.5.1). By utilizing symmetry, you need only consider one eighth of the chimney (Fig 1.5.2). A uniform mesh is adequate.

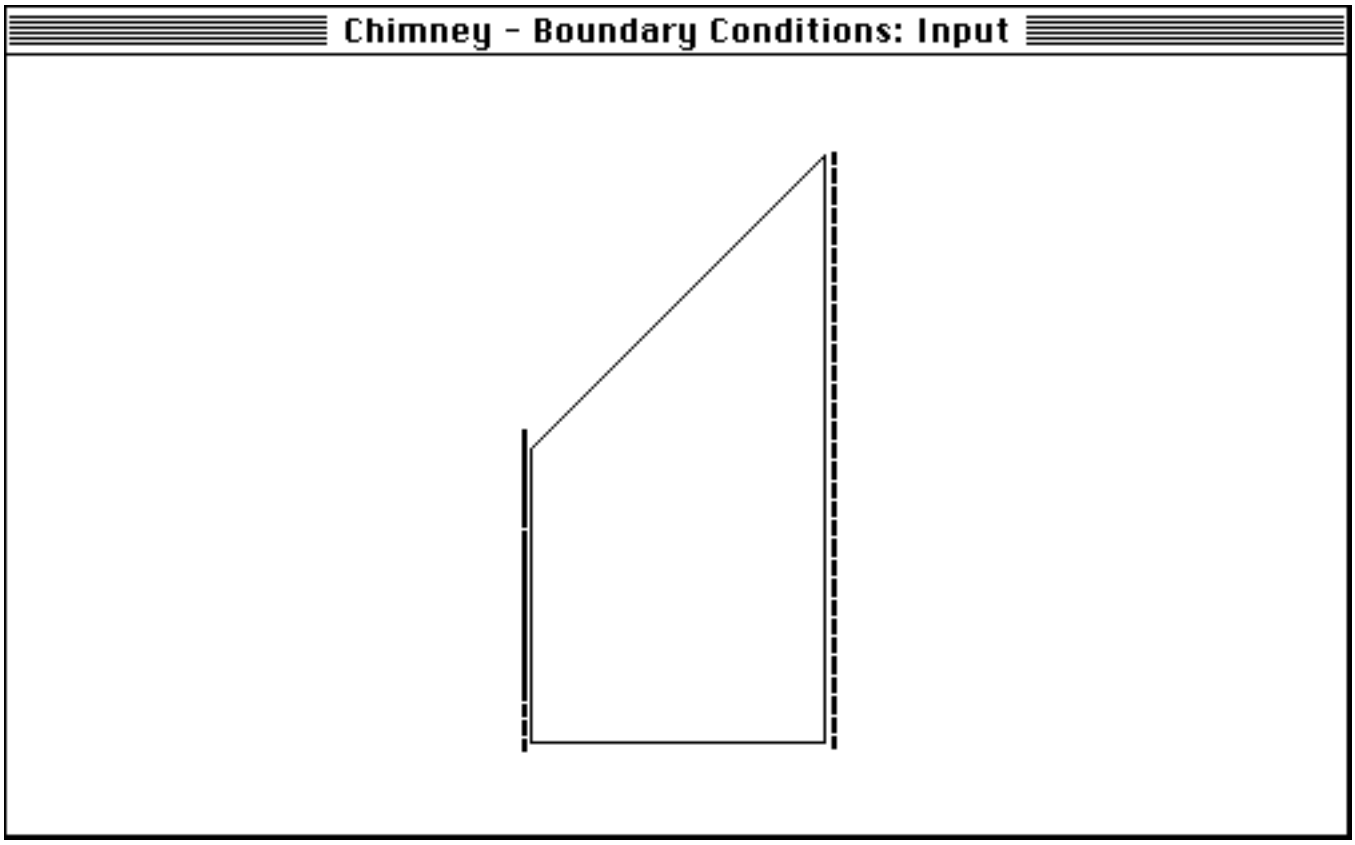

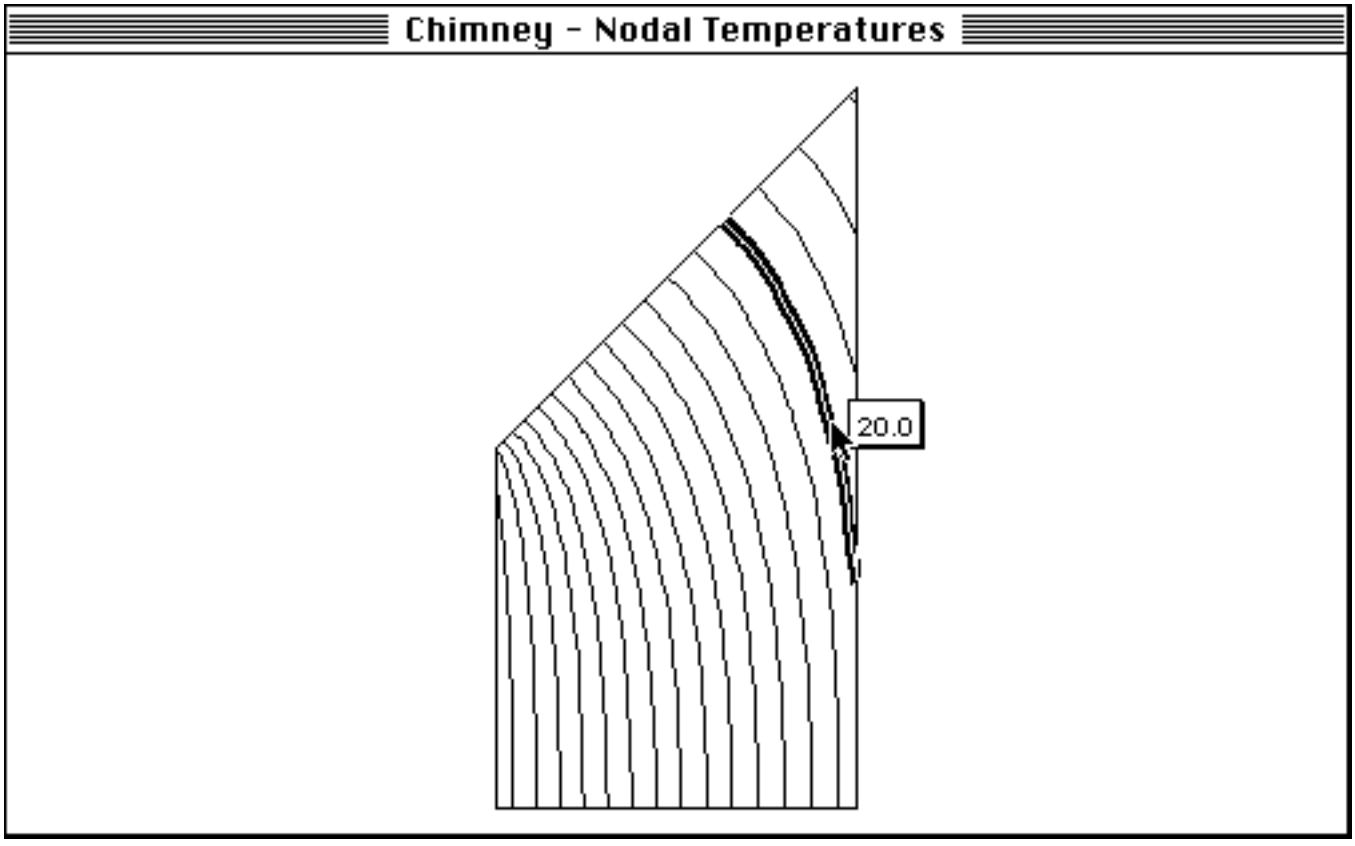

Fig 1.5.3 Boundary conditions and solution

The inner and outer walls are exposed to different constant temperatures. The surface coefficient is different for these two walls. Due to symmetry, you can apply a no-flux condition to the other two walls.

The constant temperature lines intersect the end walls at right angles, as expected for no-flux conditions. MP provides automatic lookup of the temperature contours.

Project 06: Illustrative heat conduction example.

Folder: Illustrative heat

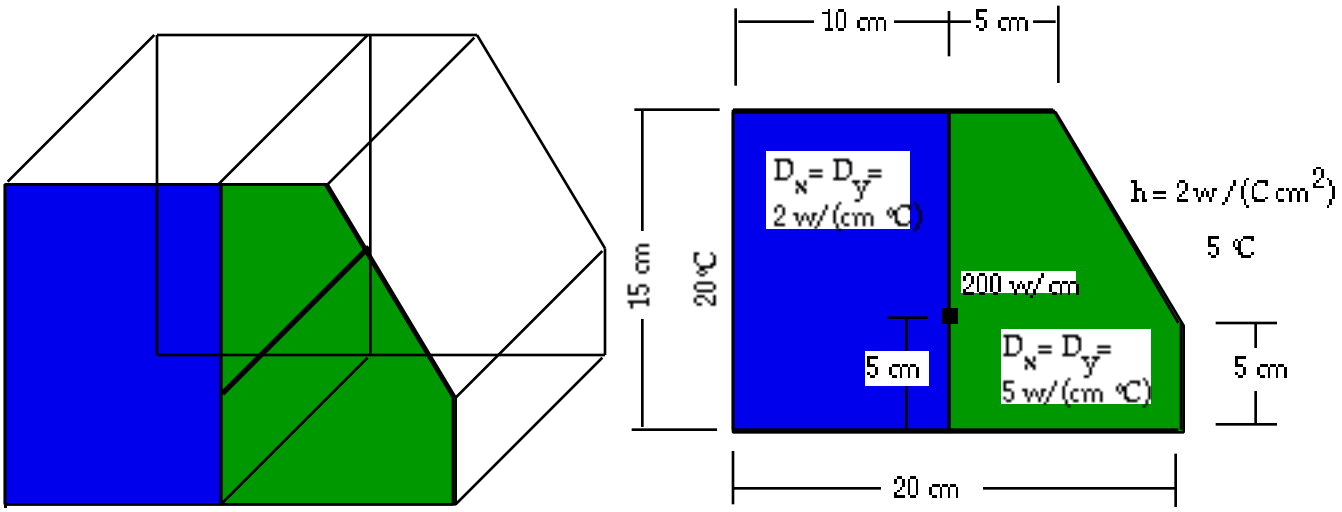

Fig 1.6.1 Illustrative example

The problem depicted in Fig 1.6.1 was created by Segerlind (2nd edition, pp. 219 - 223) to illustrate the application of the various boundary conditions (temperature, flux, and convection) and a line source. This example provides a comparison with a non-graphical formulation, including the input data.

You can construct the mesh using two mesh generating regions; the two regions correspond to two different material properties. The changes in material properties must match element boundaries. Note that the choice of mesh generating regions assures that this requirement will be met.

Since you must apply a line source at a node, the mesh you create must have a node at the desired location. In addition, you expect the temperature to change rapidly in the vicinity of a source so the elements should be smaller there.

Reference: Segerlind, L.J. 1984. *Applied Finite Element Analysis*. John Wiley & Sons. NY. (2nd edition, p219 - 223)

Figures 1.6.2 through 1.6.7 show solution steps. Four mesh generating regions were used (Fig 1.6.2). The placement of the intermediate points on the regions causes the elements (Fig 1.6.3) created near the line source to be smaller. Figs 1.6.4 and 1.6.5 show the property assignments and boundary conditions, respectively. Figs 1.6.6 and 1.6.7 show two representations of the computed results.

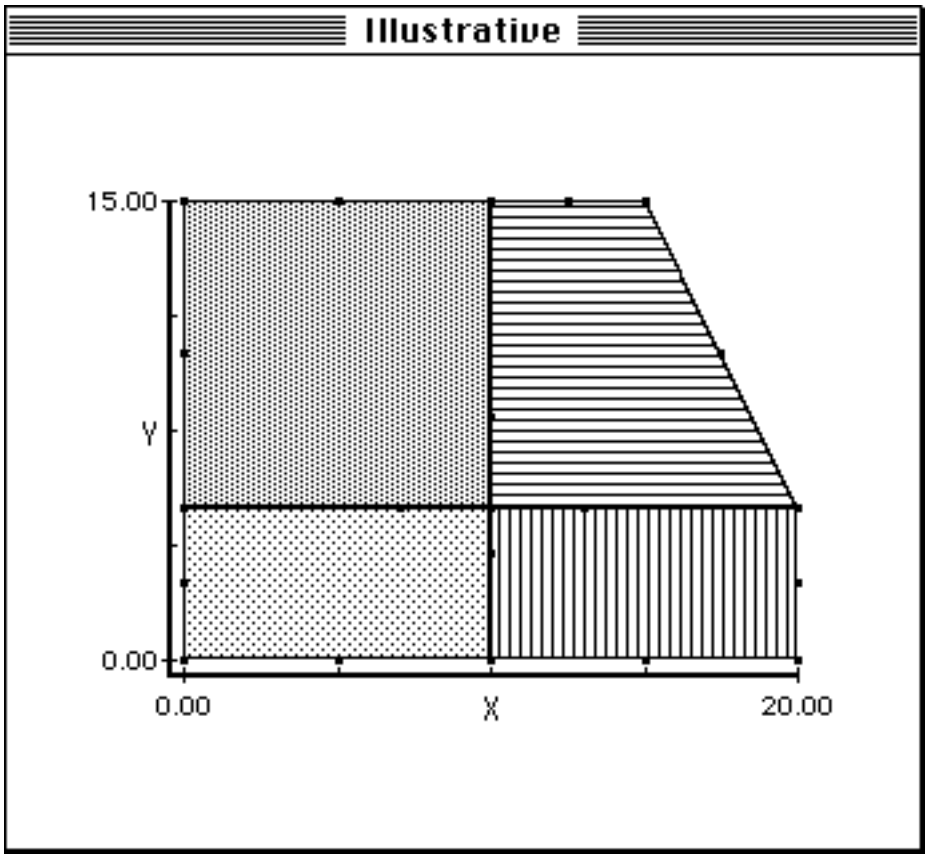

Fig 1.6.2 Mesh generating regions

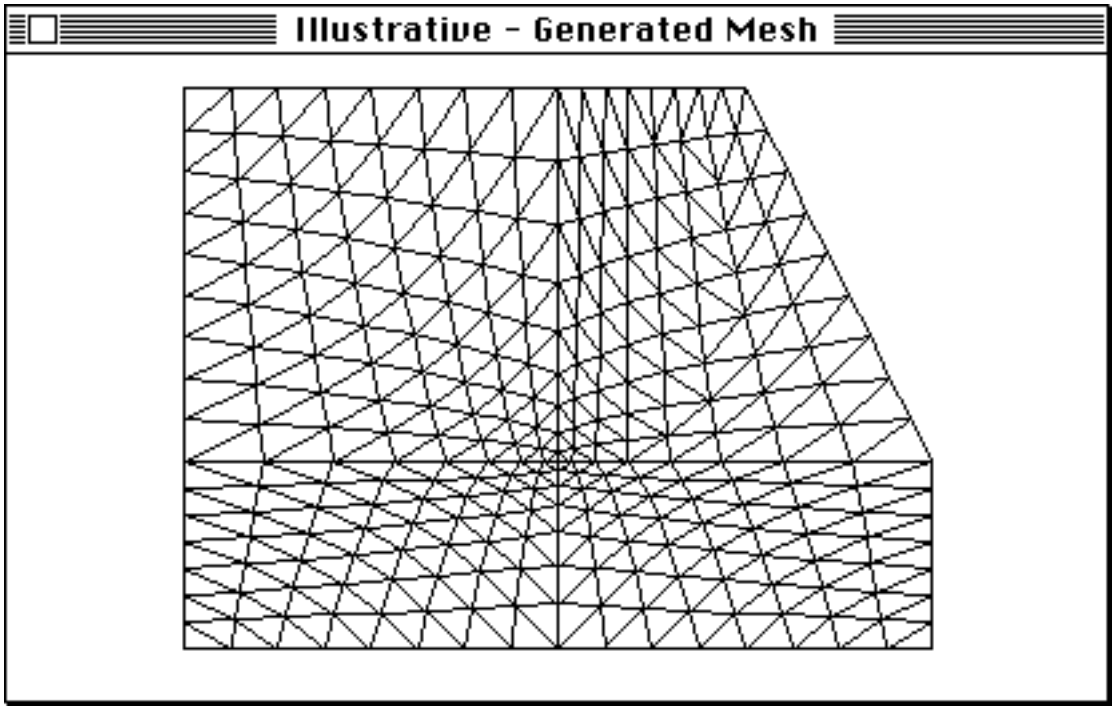

Fig 1.6.3 Mesh

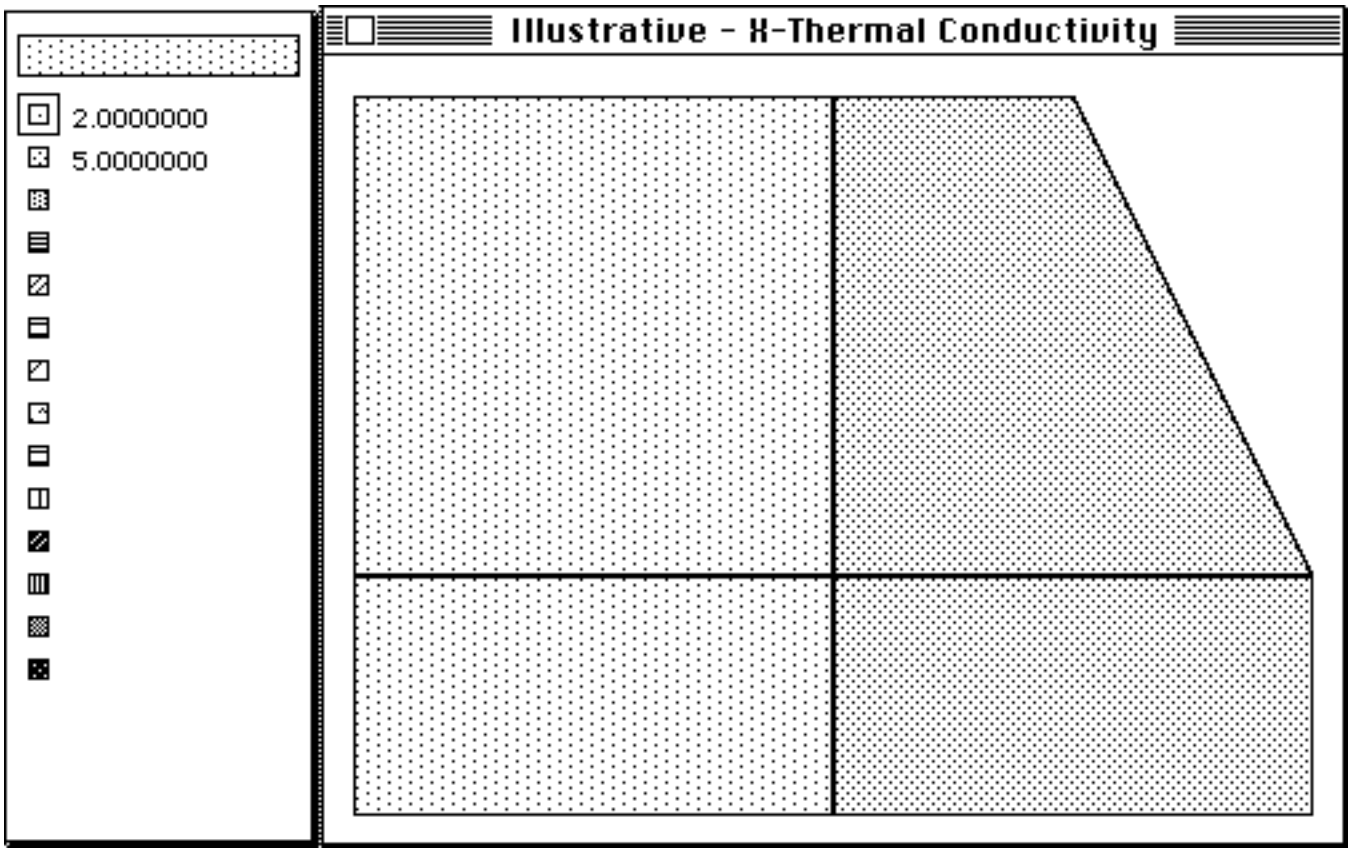

Fig 1.6.4 Properties

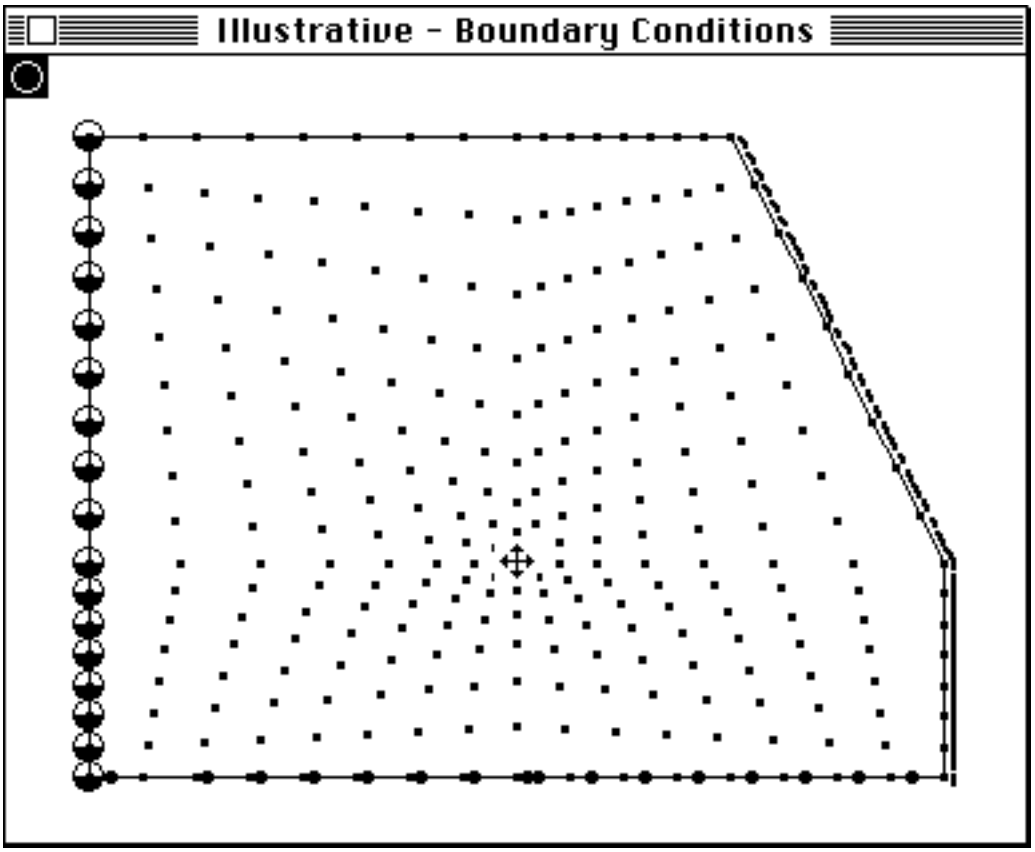

Fig 1.6.5 Boundary conditions

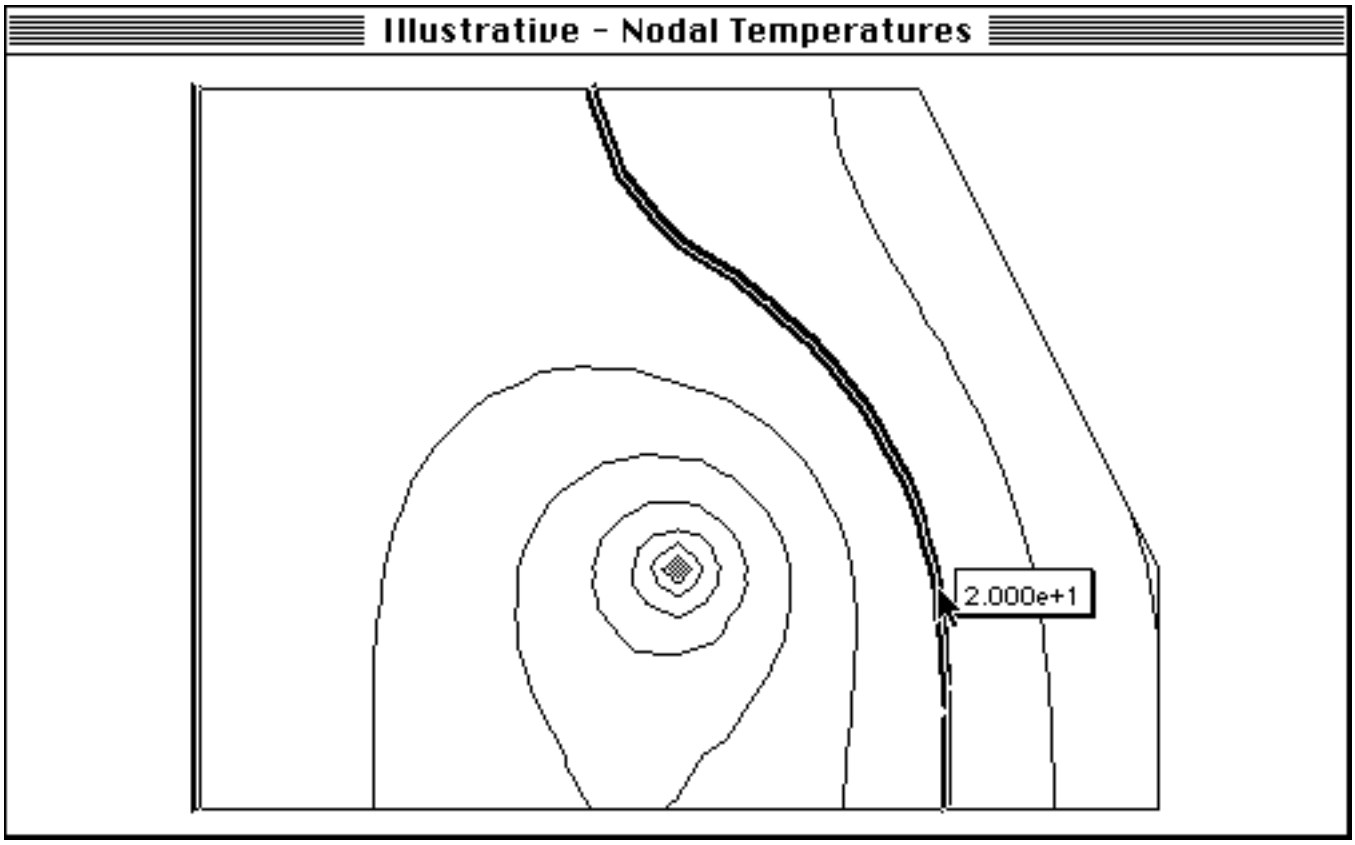

Fig 1.6.6 Constant temperature lines

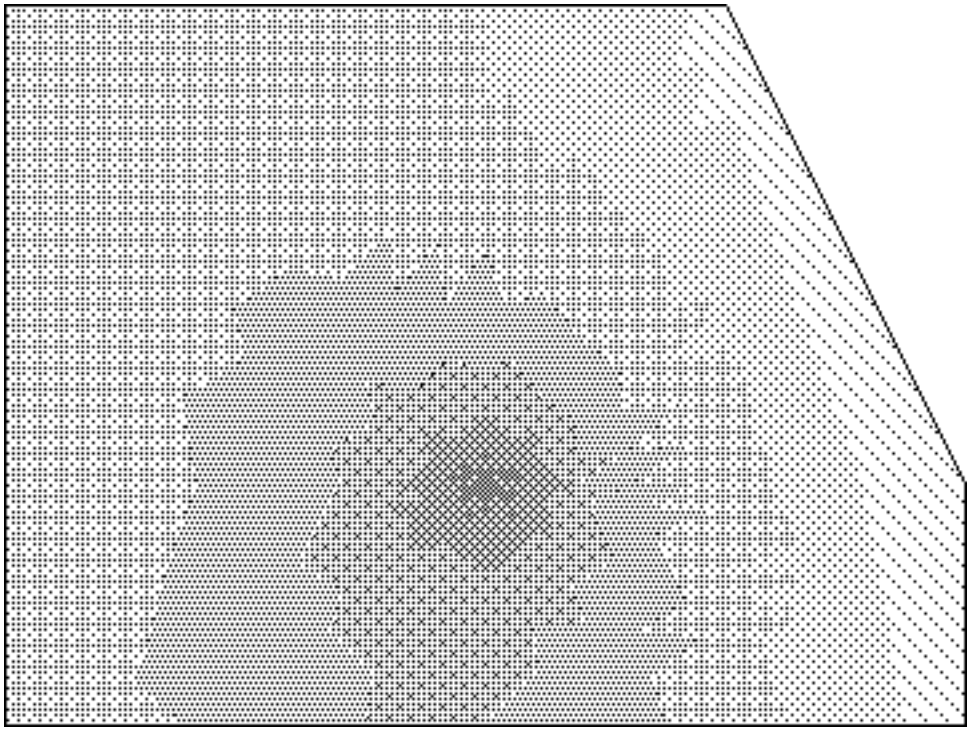

Fig 1.6.7 Average temperature

Project 07: Barge with grain.

Folder: Barge

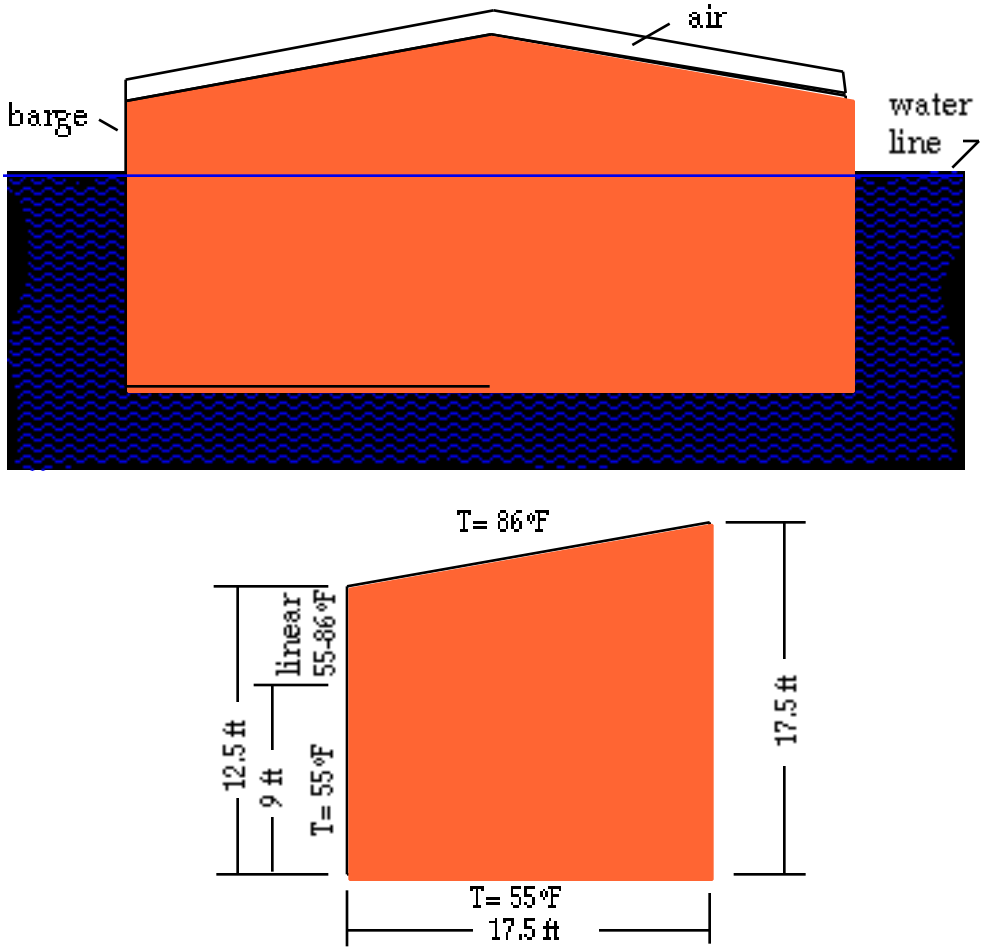

Fig 1.7.1 Barge with grain

Suppose a barge load of grain (Fig 1.7.1) is floated in water at 55°F while the air space above the grain is at 86°F. Find the temperature profile.

Note: This problem was suggested by Richard Stroshine.

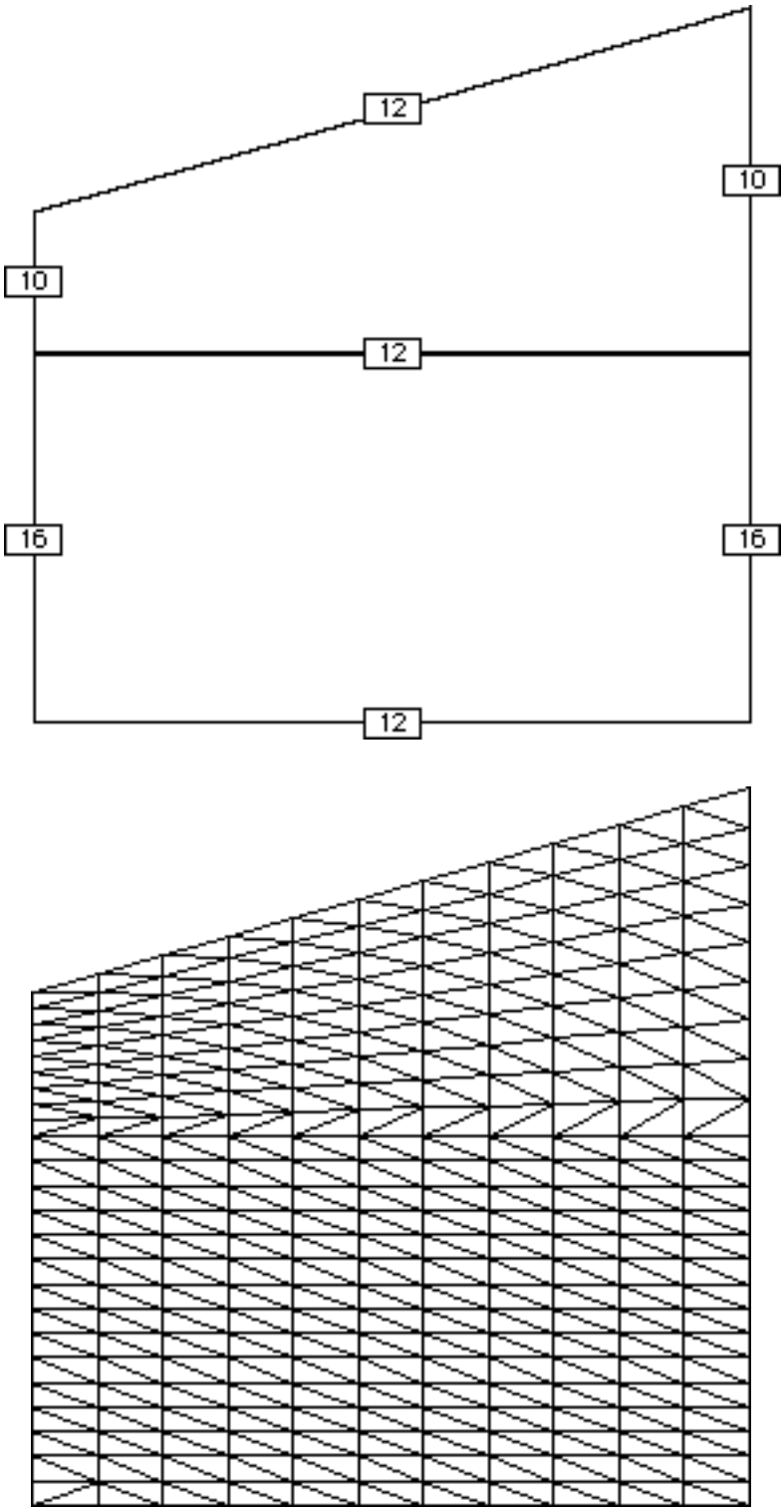

Fig 1.7.2 Mesh generation

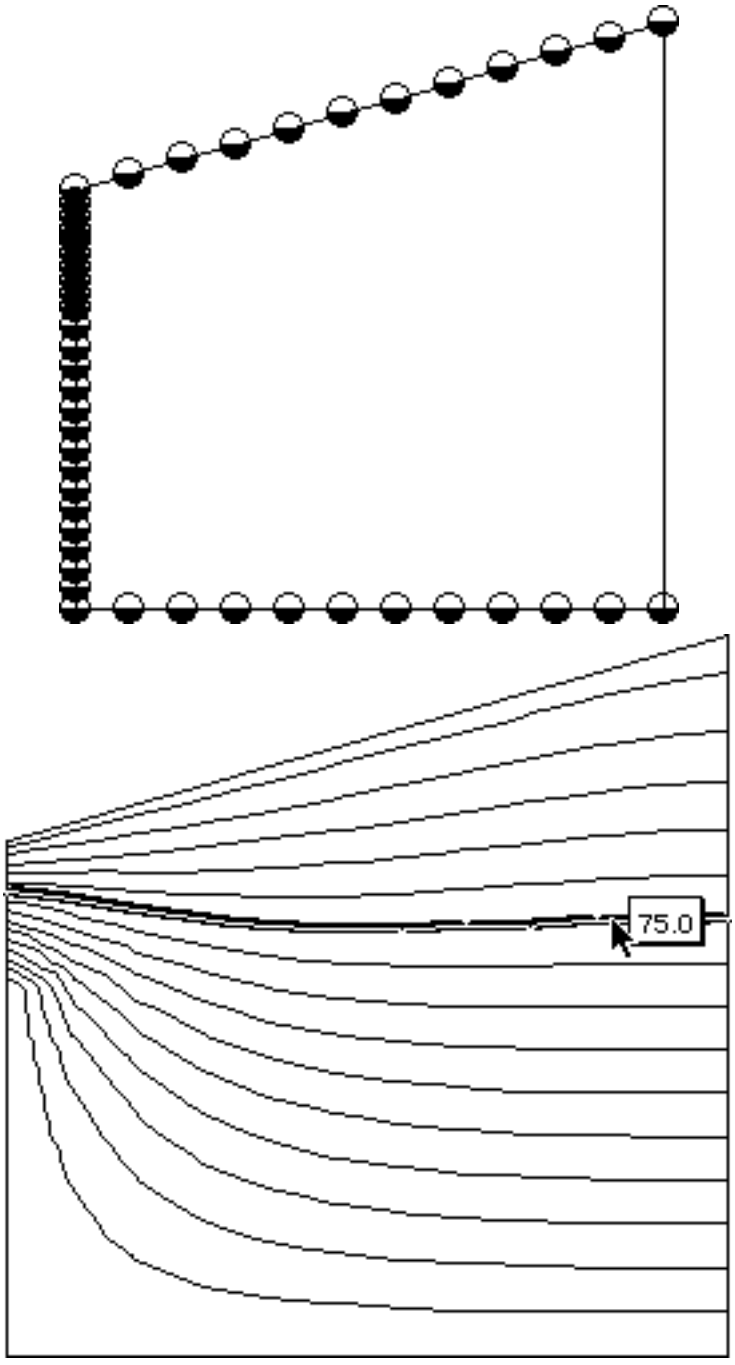

Fig 1.7.3 Boundary conditions and solution

Project 08: Temperature in a slab with internal heat generation.

Folder: HeatedSlab

In many problems, the source of heat energy is generated in the conducting body. MP can easily handle diffuse energy source problems, as shown in this simple example of a wall with internal heat generation and convection boundary conditions (Fig 1.8.1).

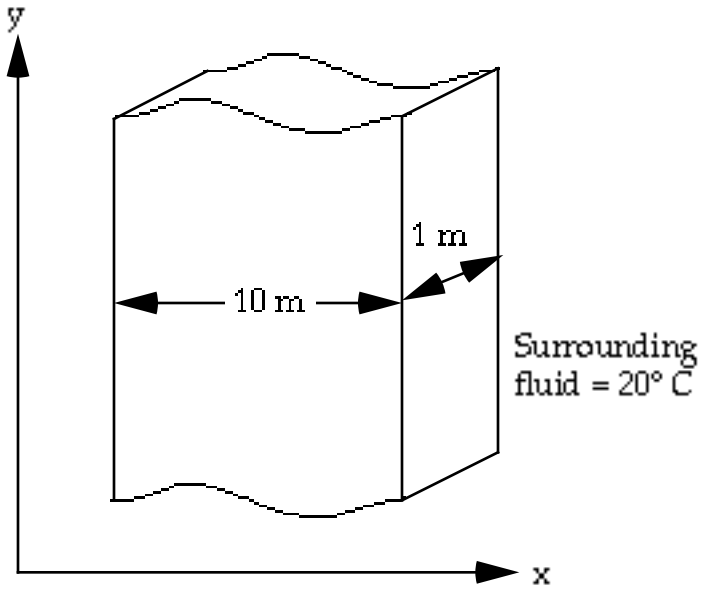

Fig 1.8.1 Slab with internal heat generation

Assume the wall's length to be much greater than its thickness, thus implying zero y-direction flux. The problem is, therefore, essentially one-dimensional, so use maximum resolution in the x-direction and minimum resolution in the y-direction.

The important constants are:

Thermal conductivity:
k = 1.0 W / m°K
Heat per unit volume:
Q' = 10 W / m^3
Convection coefficient:
h = 10 w / m^2°K
Fluid temperature:
tf = 20°C

Geometry (Fig 1.8.2), mesh (Fig 1.8.3), and boundary conditions (Fig 1.8.4) follow.
The distributed heat source (Fig 1.8.5) is assigned in the properties section.

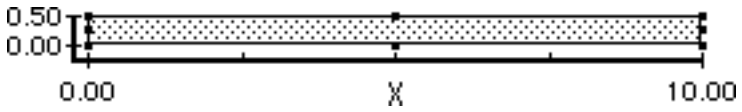

Fig 1.8.2 Geometry of slab

Fig 1.8.3 Generated mesh

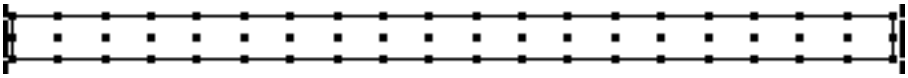

Fig 1.8.4 Convection-loss conditions set on both boundaries

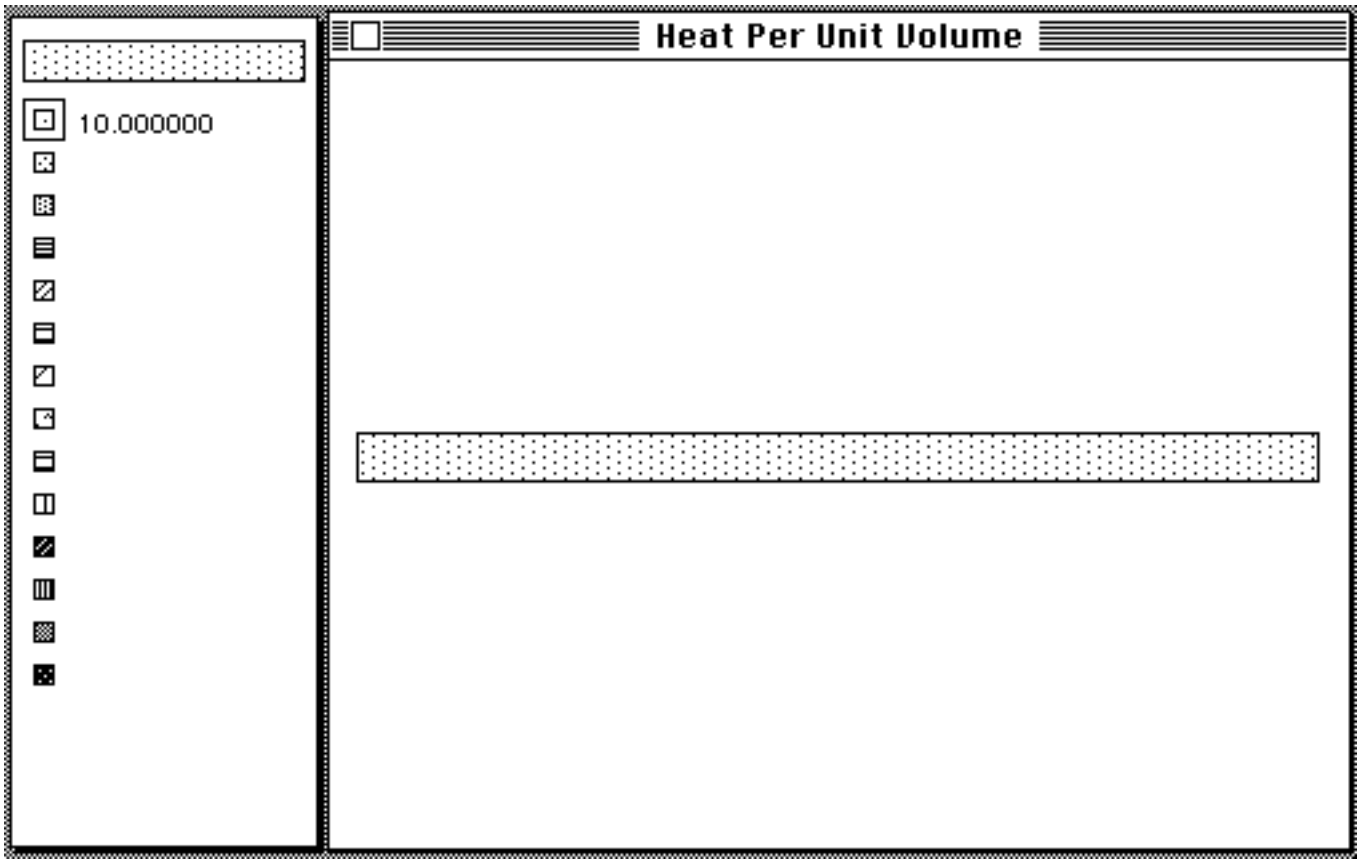

Fig 1.8.5 Assignment of heat per unit volume in properties definition section.

The theoretical solution to this problem is well known.

$$T = \frac{Q'}{2k}(l^2 - x^2) + \frac{Q'\,l}{h} + t_f$$

where:

T = temperature within the slab,
l = center to edge length of the slab, and
x = distance from center of slab.

Internal Heated Slab Results

Theoretical Value:	MacPoisson Output:	Percent Error:	Node Number:
25.000000	24.947821	0.208717	1
25.000000	25.052179	-0.208717	6
25.000000	25.052179	-0.208717	57
25.000000	24.947821	0.208717	60

Comparison of the MacPoisson solution on a node by node basis against the theoretical solution to the problem is shown at the left. All nodes with an error greater than 0.1% are shown.

The greatest error is one part in 479 for this problem, clearly demonstrating the potential for accuracy from the finite element formulation if you use high resolution.

Exercise: You could have used symmetry in this problem since no heat flows across the centerline; i.e., you could use half of the mesh with a no-flux condition at the center.

References: E.R.G. Eckert and Robert M. Drake. 1972. *Analysis of Heat and Mass Transfer.* McGraw-Hill. pages 95-98.
P. Moon and D.E.Spencer. 1961. *Field Theory for Engineers.* D.Van Nostrand Co. section 14.06.

Project 09: Floor heating.

Folder: Floor

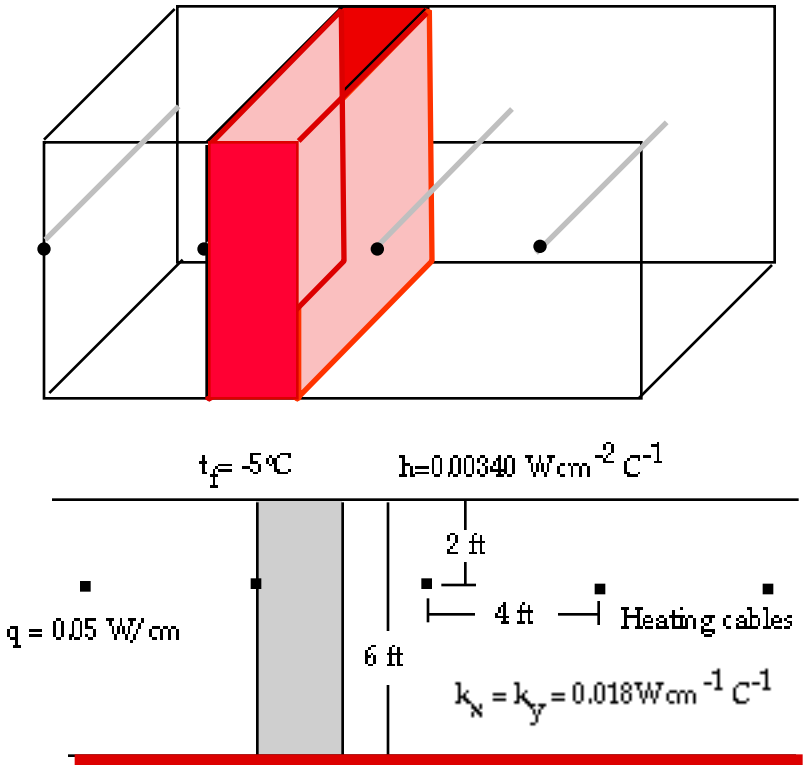

Fig 1.9.1 Electrical floor heating

Segerlind (1984, 148-151) describes this problem of a grid of heating cables embedded in a thin concrete slab for snow melting. A similar problem (Cooke, 1969 and 1970) has been examined as a basis for off-peak energy storage and for keeping the floor of a brooder for baby chicks warm and dry and, therefore, healthier. Will the floor become too hot? How deep should you place the heating cables?

References: Cooke, J.R. and D.R. Price. 1969. Analysis of subsurface electric heating. ASAE Paper No. 69-848.
Cooke, J.R. 1970. Summary of progress in electric floor heating studies. 27th Annual Progress Report to NY Farm Electrification Council. pp. 53-54.
Segerlind, Larry J. 1984. *Applied Finite Element Analysis*. Second edition. John Wiley & Sons, Inc. NY. pp. 149-151

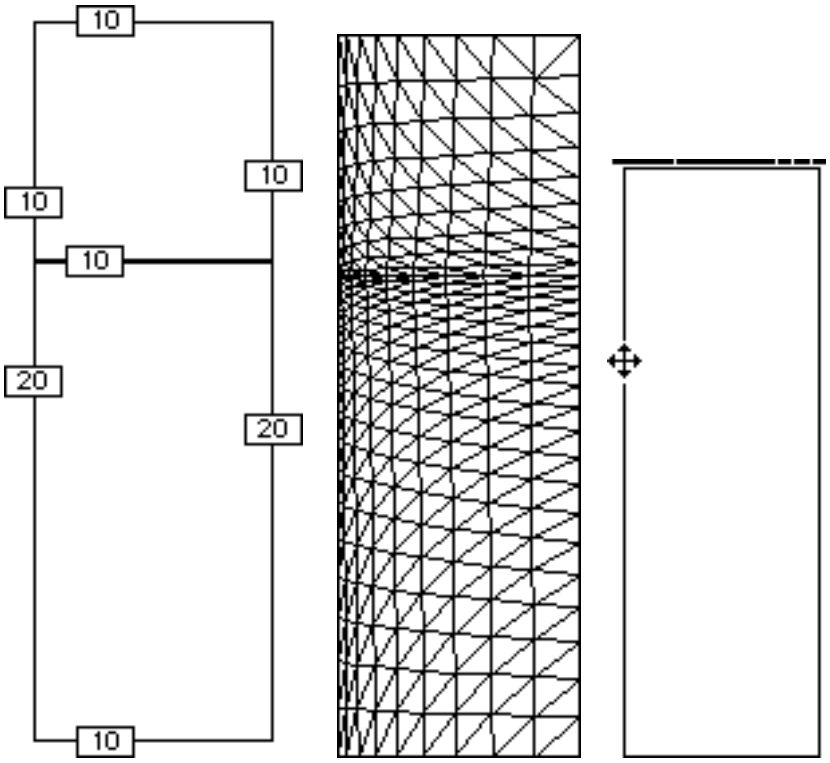

Fig 1.9.2 Floor heating problem formulation

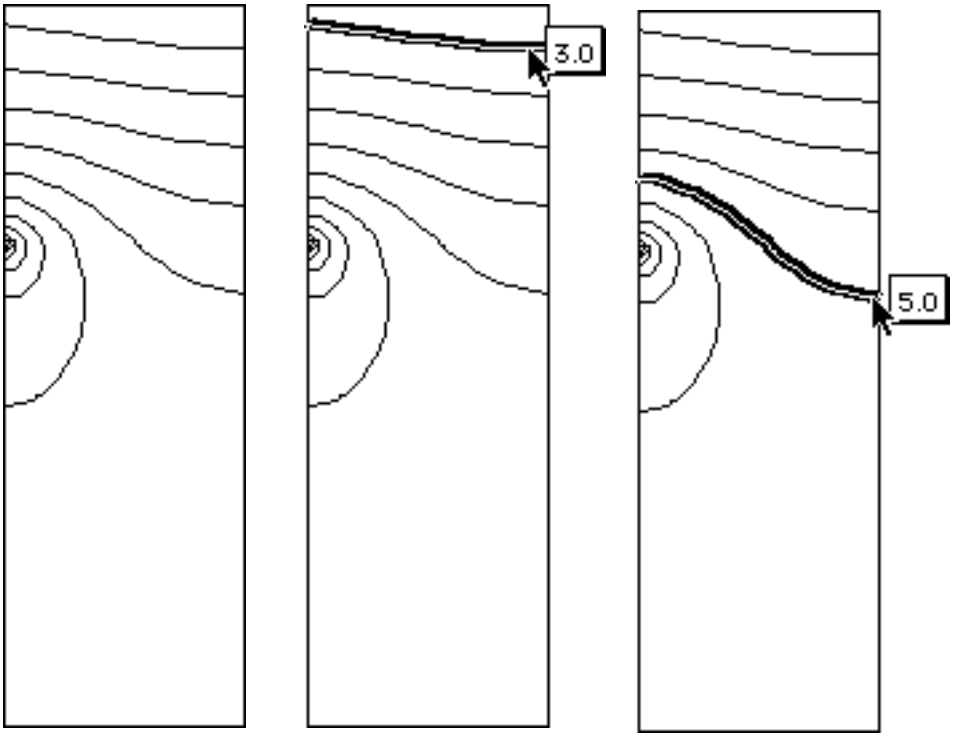

Fig 1.9.3 Temperature profile

Project 10: Sphere heated by sun.

Folder: SphereInSun

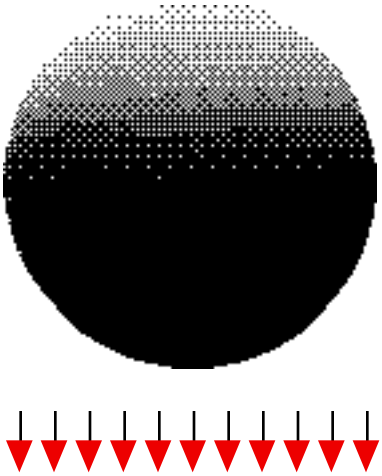

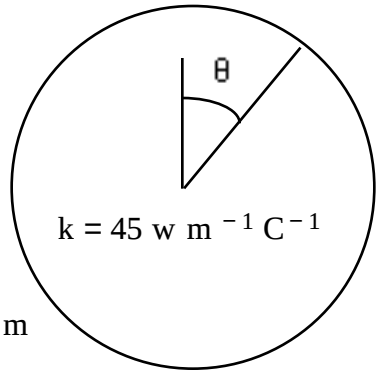

radius= 0.1 m

Equivalent fluid temperature

'convection coeficcient
ε = 20 w m $^{-2}$ C^{-1}

$$T(\theta) = \frac{D(\theta)}{\varepsilon} = \begin{cases} (4800 \text{ w m}^{-2}/\varepsilon)\cos\theta, & 0 \le \theta \le \pi/2 \\ 0, & \pi/2 < \theta \le \pi \end{cases}$$

Fig 1.10.1 Externally heated sphere

Find the temperature within a blackened cast iron sphere placed in sunlight. The problem is axisymmetric. Newton's law of cooling applies at the surface and the effective temperature of the surrounding fluid varies from a maximum at the point nearest the source and diminishes to zero at the "equator" according to a cosine function. The remainder of the surface blocked from the radiant pharosage is taken to be zero. This approach is equivalent to the sol-air approach used in building design.

We created the mesh depicted in Fig 1.10.2 using two degenerate mesh generating regions. Two sides of each generating region fall along the circular arc. We placed the intermediate node common to the two regions near the surface in order to produce smaller elements nearer the surface. The boundary fluid temperature varies along the upper half of the sphere. We used the

value at the midpoint of the element; therefore, the maximum value at the “north pole” is slightly underestimated.

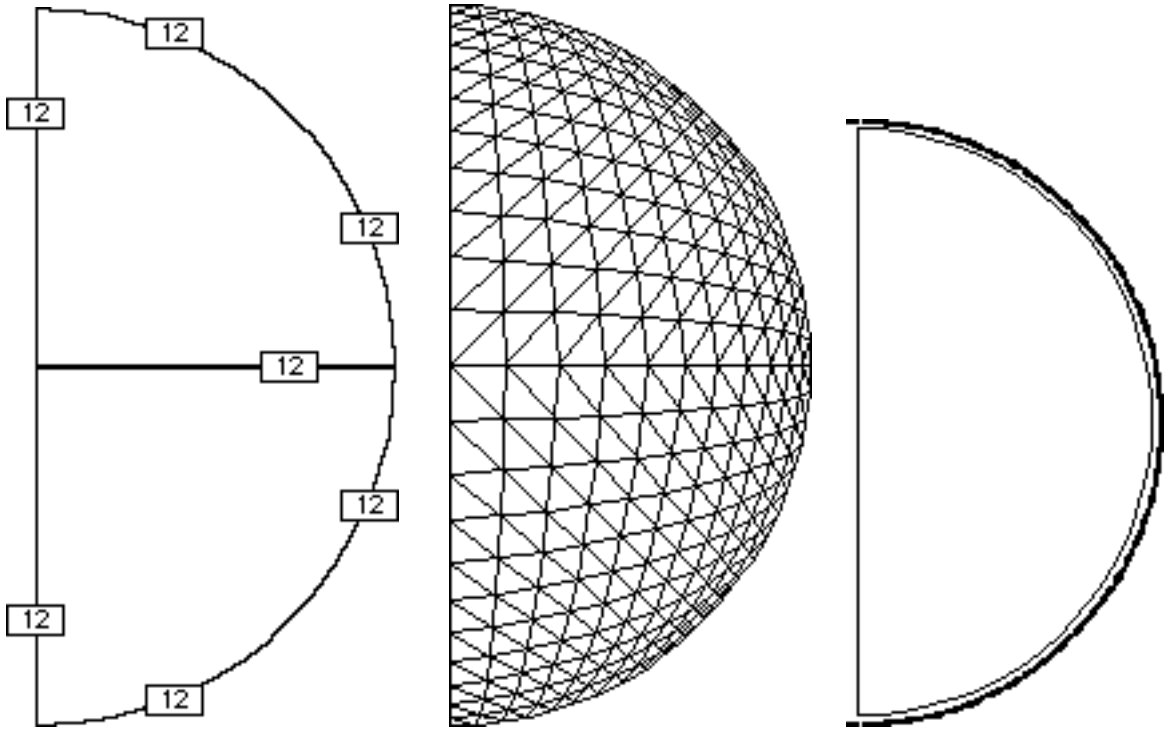

Fig 1.10.2 Problem formulation

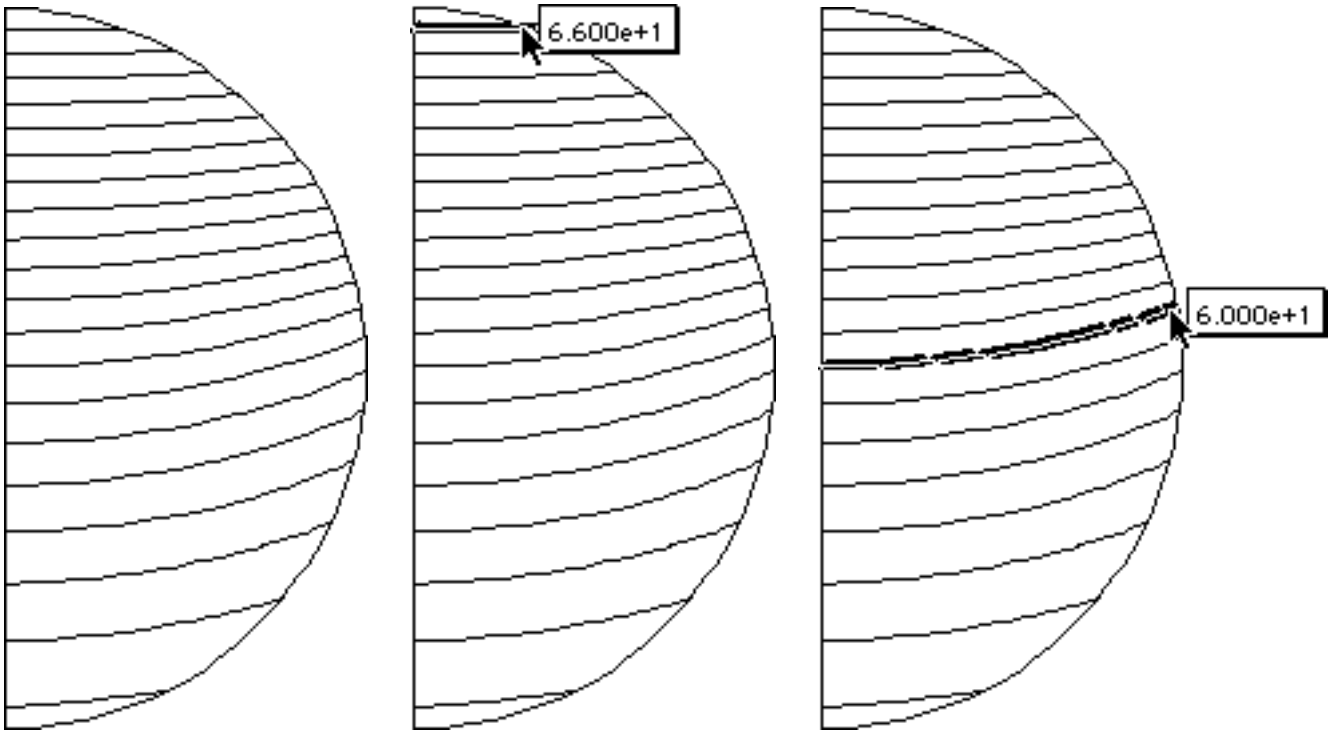

Fig 1.10.3 Temperature within sphere

Theoretical solution and references

Moon and Spencer (1961, 221-224) present the separation of variables solution for this problem developed originally by Lord Rayleigh and summarized by Byerly in *Fourier Series* (1893, p177, ch 5&6).

$$\varphi = \frac{(1-\rho)\, D(0)}{4\,\varepsilon}\left[1 + \frac{2\,\varepsilon\, a}{k + \varepsilon\, a}\left(\frac{r}{a}\right)\cos\theta + \frac{5\,\varepsilon\, a}{4\,(2\,k + \varepsilon\, a)}\left(\frac{r}{a}\right)^2 P_2(\cos\theta)\right.$$

$$\left. - \frac{3\,\varepsilon\, a}{8\,(4\,k + \varepsilon\, a)}\left(\frac{r}{a}\right)^4 P_4(\cos\theta) + \right]$$

The solution is expressed as a series of Legendre polynomials where surface reflectance $r = 0$; $D(0)$ incident radiant power per unit area; and "a" is sphere radius. Note: The Moon and Spencer equation 8.16 contains a typographical error in the multiplier and has been corrected here.

Using the general expression for the series coefficients from Byerly (1959,177) and the recurrence relation for Legendre polynomials from Abramowitz and Stegun (1965, 340,344) we obtained 66.6, 60.0, 59.0 and 56.3 degrees at the "north pole", "center", "equator", and "south pole" respectively. The corresponding MP values are 66.37, 59.97, 59.01, and 56.37 with a relative error of less than three tenths of a percent.

Project 11: Ideal fluid flow past elliptic cylinder and prolate spheroid.

Folder: Elliptic cylinder; Prolate Spheroid

In this example consider ideal fluid flow past an elliptical cylinder and past a prolate spheroid. Suppose an ellipse with semi-minor axis is 2.0 and the semi-major axis is 4.0 is placed in a uniform velocity field. Find the streamlines for both the planar and the axisymmetric cases.

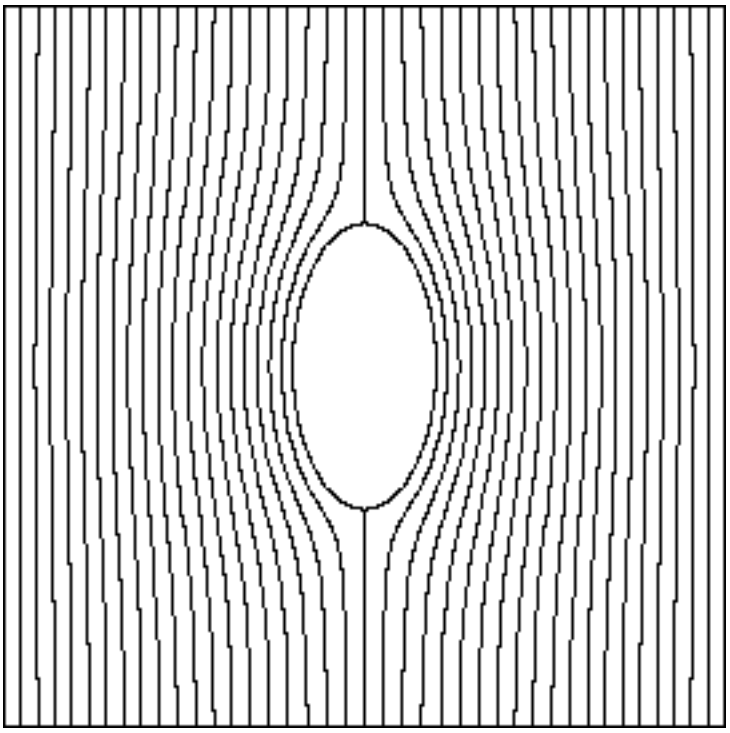

Fig 1.11.1 Elliptical cylinder in a uniform flow

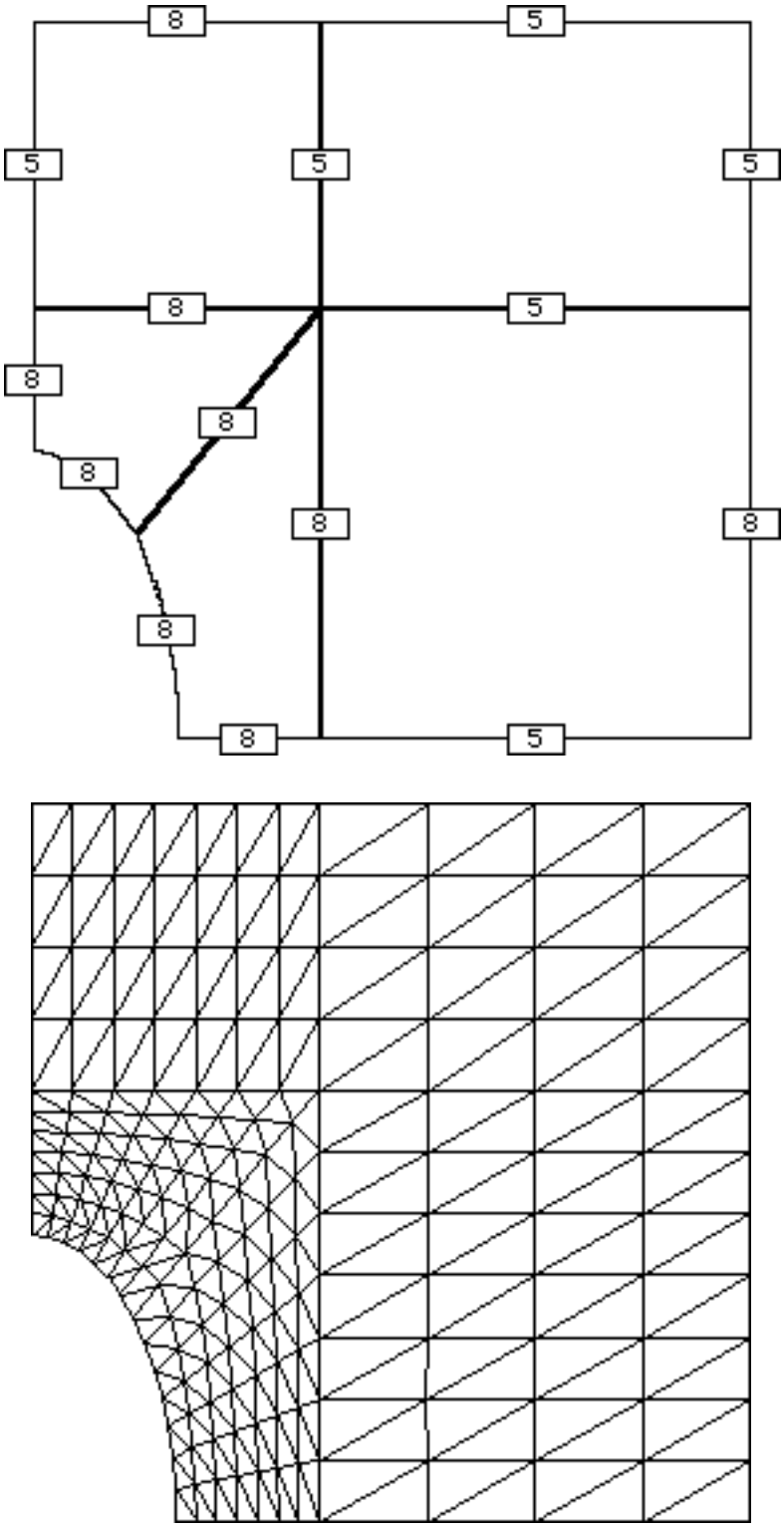

Fig 1.11.2. Mesh and boundary conditions

The mesh and boundary conditions are shown in Fig 1.11.2. Note we refined the mesh in the vicinity of the ellipse. We used the ellipse generating tool to construct the generating regions.

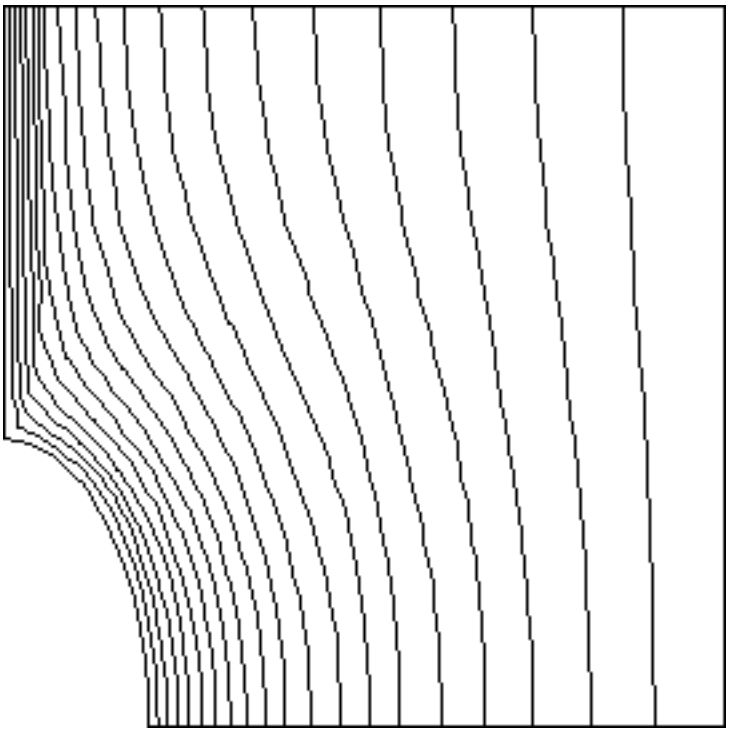

Fig 1.11.3 Planar solution

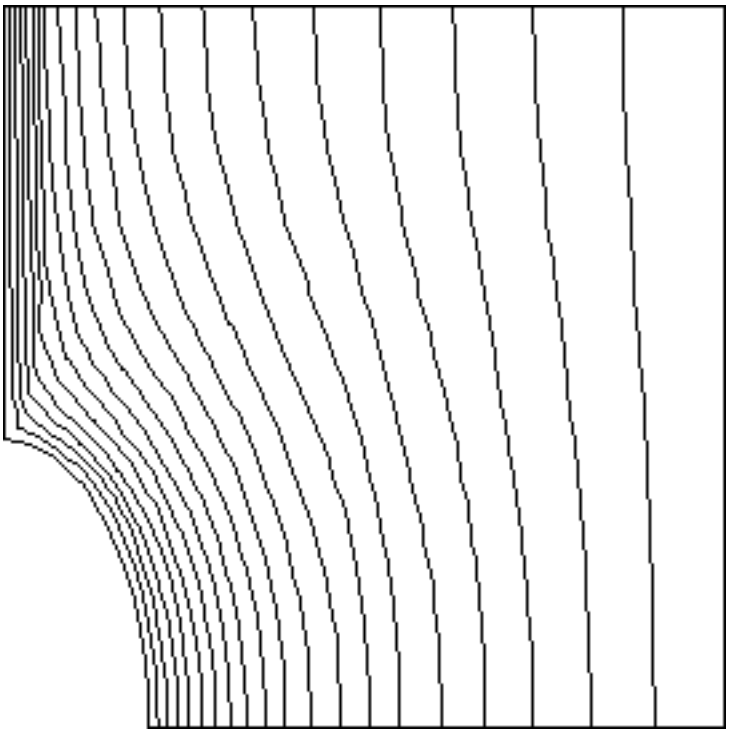

Fig 1.11.4 Axisymmetric solution

Fig 1.11.5 is an overlay of the planar and axisymmetric solutions for a direct comparison.

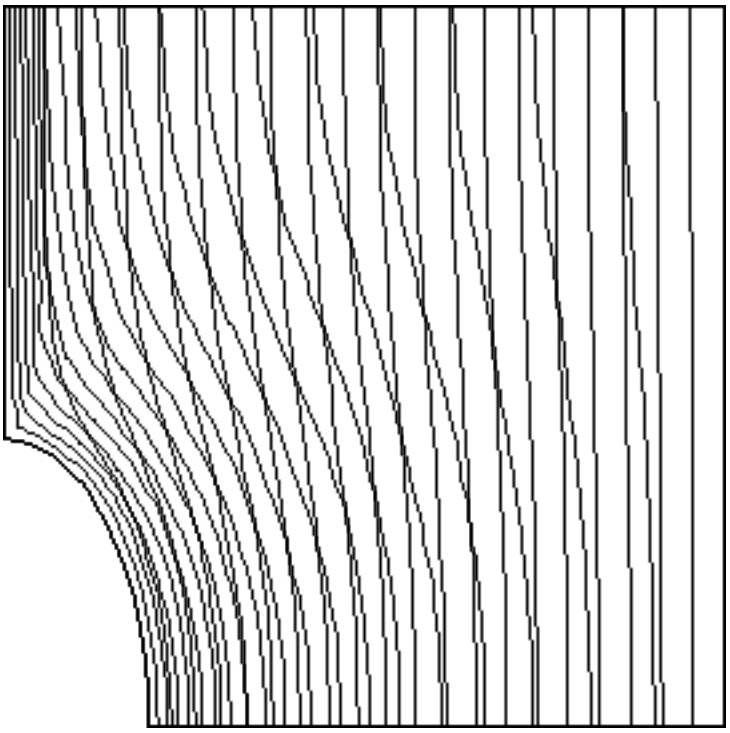

Fig 1.11.5 Planar and axisymmetric solutions superimposed

Reference: L.M. Milne-Thomson. 1967. Theoretical Hydrodynamics. MacMillan Co. §6.33.

Project 12: Ideal fluid flow in channel with abrupt enlargement.

Folder: Enlargement

Ideal fluid flow (inviscid, irrotational) is governed by Poisson's equation. A classic problem from hydrodynamics is the two-dimensional flow in a channel (Fig 1.12.1) which has an abrupt change in width (Milne-Thomson, 1967; Lamb, Hydrodynamics, 1945). A Schwarz-Christoffel transformation is often used to solve this problem. Walker (1964, p62) presents a detailed discussion of this problem and a figure.

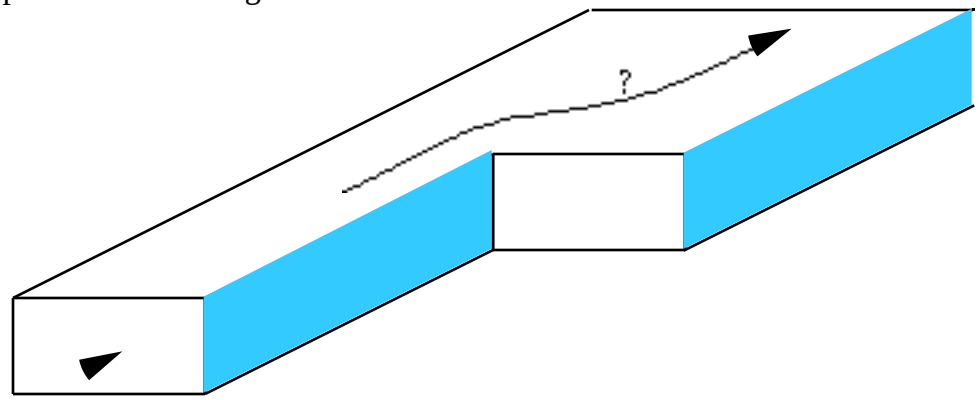

Fig 1.12.1 Ideal fluid flow in a channel with abrupt width change

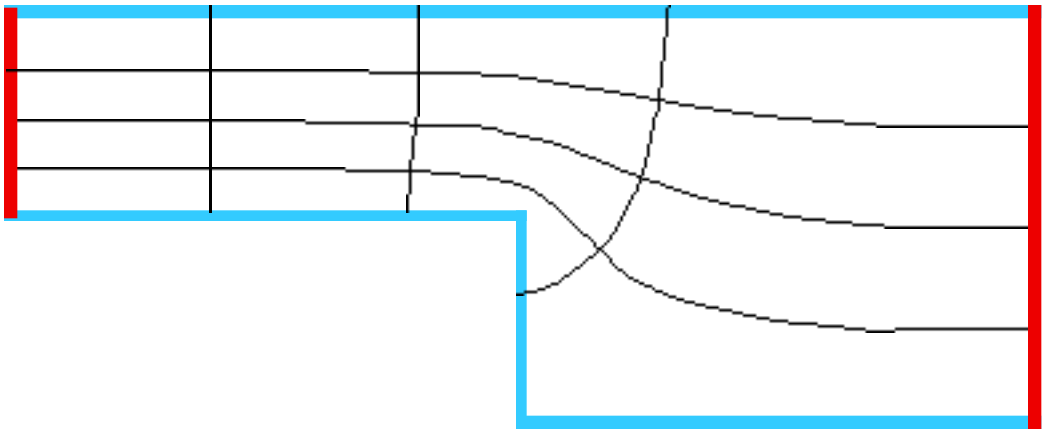

Fig 1.12.2 Expected ideal fluid flow pattern

You can find the streamlines (Fig 1.12.2) if you assign 1.0 to the top boundary and 0.0 to the lower boundary which has two abrupt turns. The left and right ends have a zero normal gradient; in MP a boundary left undesignated automatically corresponds to one having a zero normal gradient.

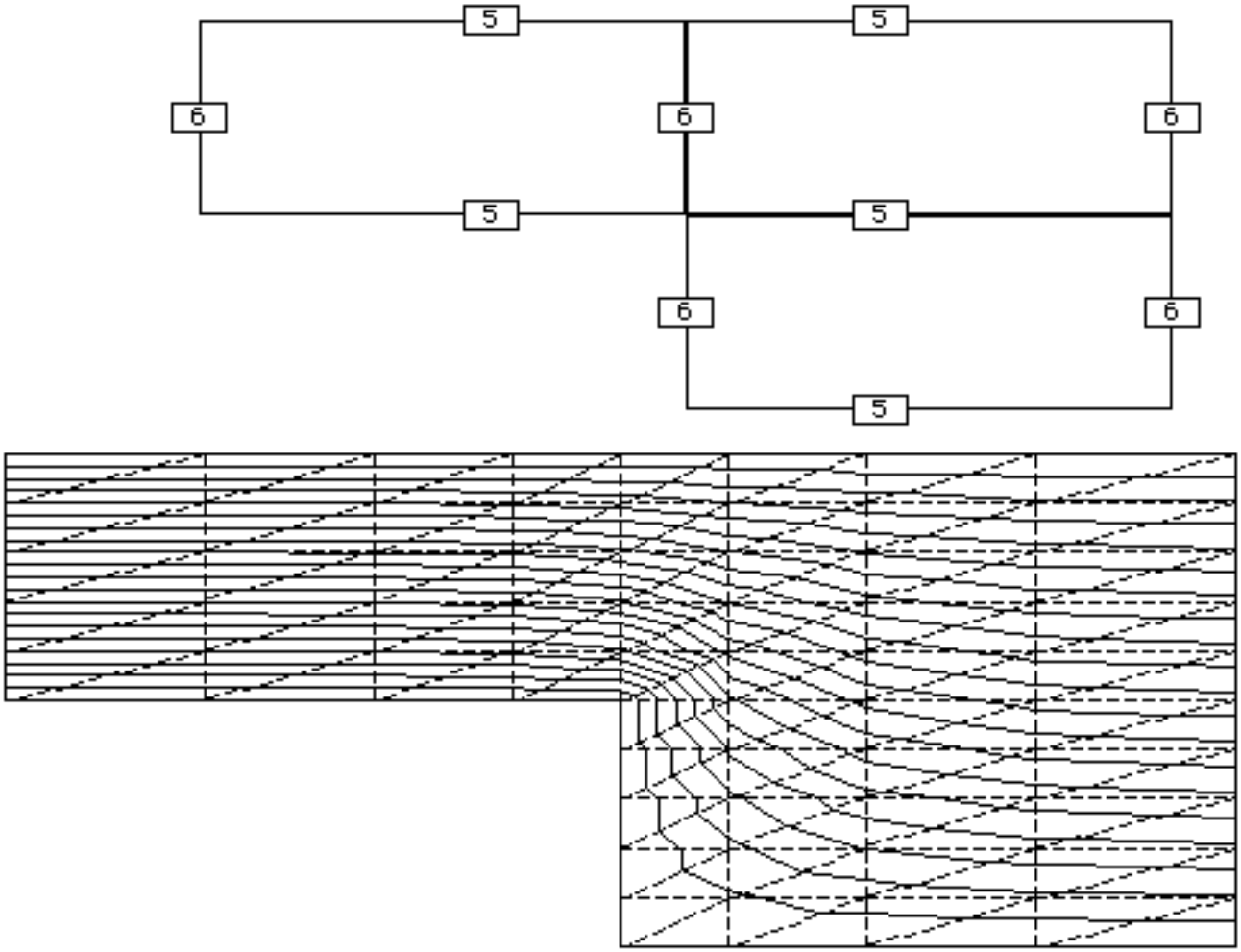

Fig 1.12.3 Coarse mesh (79 dof)

An examination of the mesh generation process is instructive. Recall that the automatic mesh generator requires quadrilateral regions. Let's subdivide the region into three rectangular mesh generating regions as follows.

This rather coarse mesh (dof=79) produces surprisingly good results (Fig 1.12.3). As expected, the contours in the vicinity of the corners are the most uneven. By refining the mesh you can obtain a smoother result, i.e., a better approximate solution. The following figures illustrate ways to improve the results.

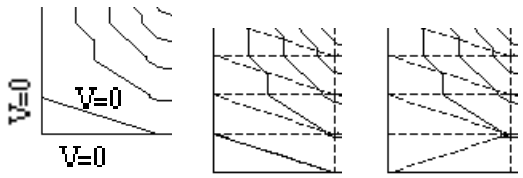

Fig 1.12.4 Diagonals

The simple triangular element allows only multilinear interpolation within an element. Therefore, if two sides of an element (Fig 1.12.4) have the same value, the entire element must

also have that same value because MP uses a linear element. If you need greater resolution in the corner, switch the diagonal using the redefine tool in Modify mesh of the Goodies menu in the mesh module.

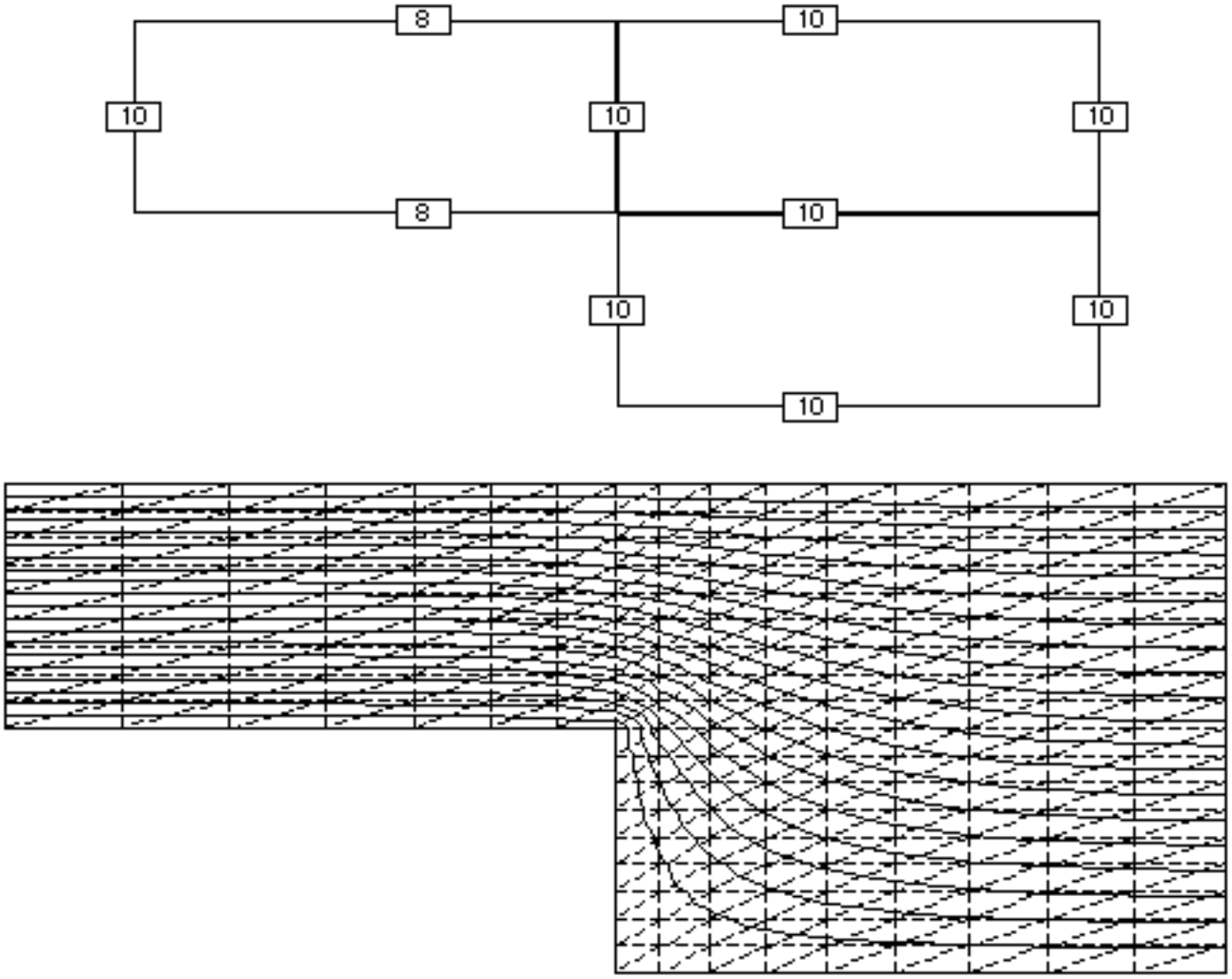

Fig 1.12.5 Second mesh (260 dof)

The easiest and most obvious technique to improve the result is to increase the number of elements. Of course, there is always a practical limitation of available RAM and computation time. In this instance, increasing the degrees of freedom from 79 (Fig 1.12.3) to 260 (Fig 1.12.5) produces a smooth plot.

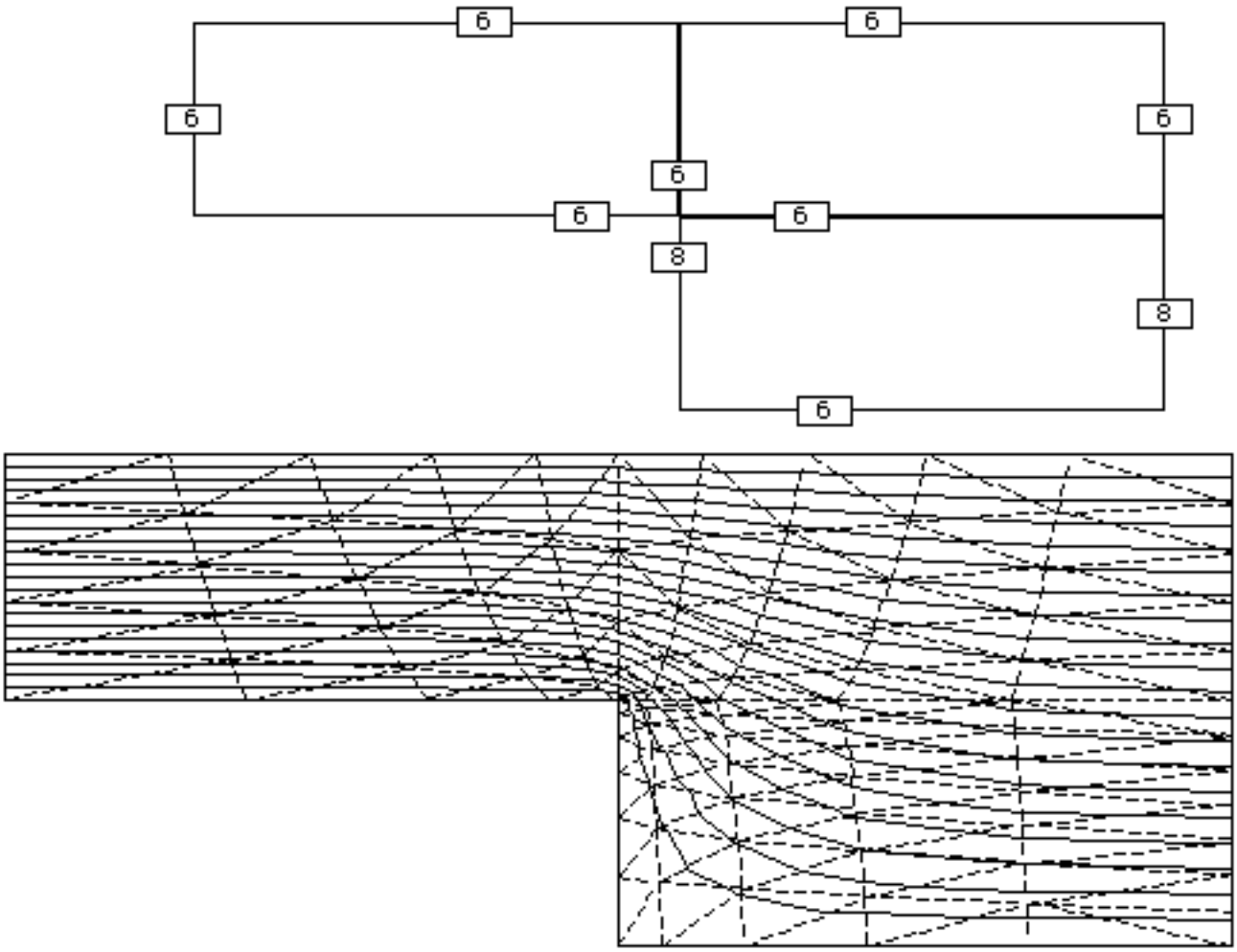

Fig 1.12.6 Third mesh (108 dof)

MP provides other mesh modification techniques which improve performance. You can obtain results roughly comparable to the 260 dof solution (Fig 1.12.5) with 108 dof (Fig 1.12.6).

You can make the elements smaller in the vicinity of the abrupt enlargement by moving the points on the side of the mesh generating region (in the geometry module) nearer the abrupt change. The nodes per side assignments (Fig 1.12.6) also reflect this adjustment.

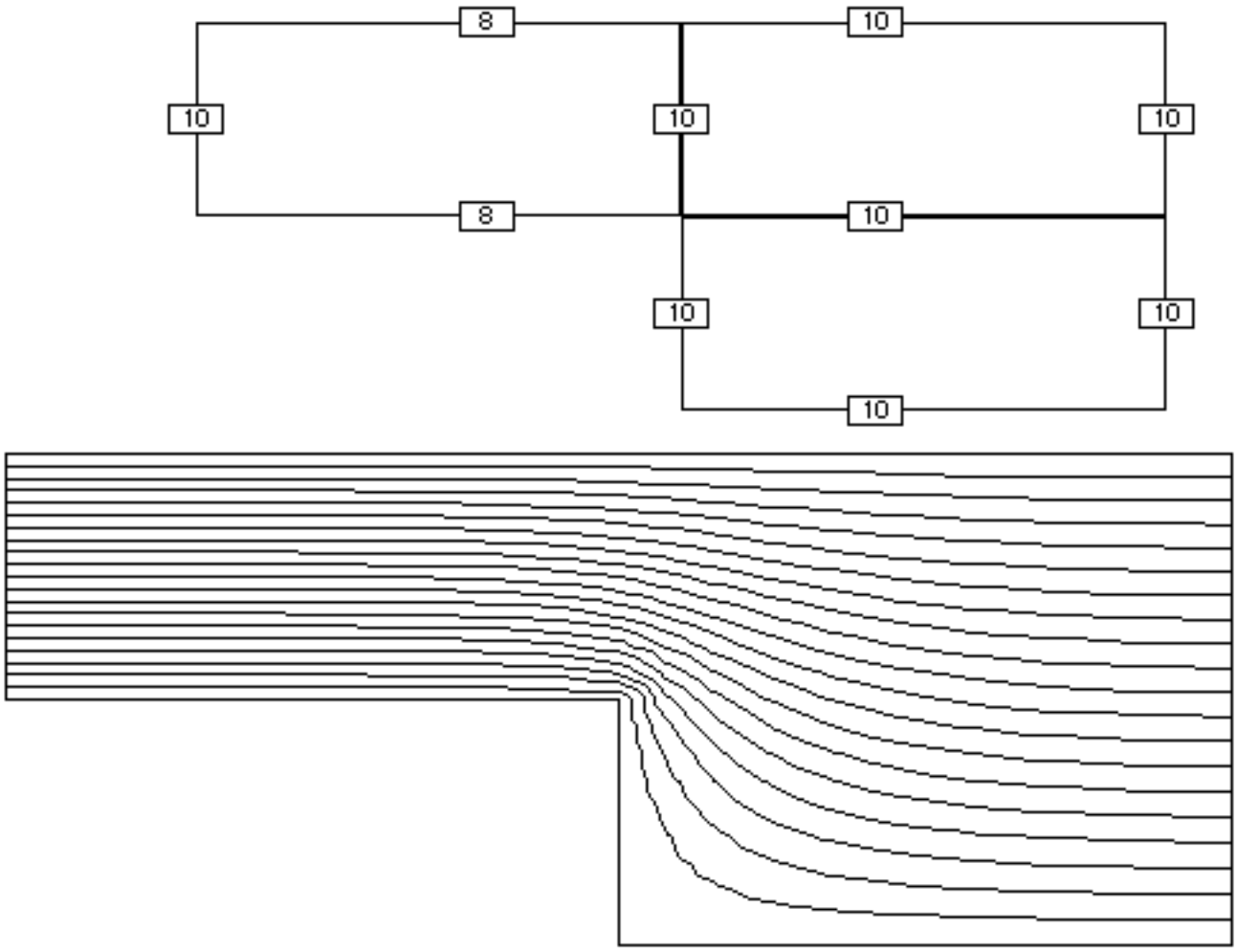

Fig 1.12.7 Fourth mesh (260 dof)

The student version (max. 300 dof) is capable of obtaining a smooth result even with regular element shapes and 260 dof.

For purposes of illustration Fig 1.12.8 shows the result you can obtain with a Macintosh SE with one Meg of memory (1020 dof).

You can find the conjugate problem (a family of curves everywhere orthogonal to the streamlines) by swapping the constant potential and no-flux boundary conditions (Fig 1.12.8).

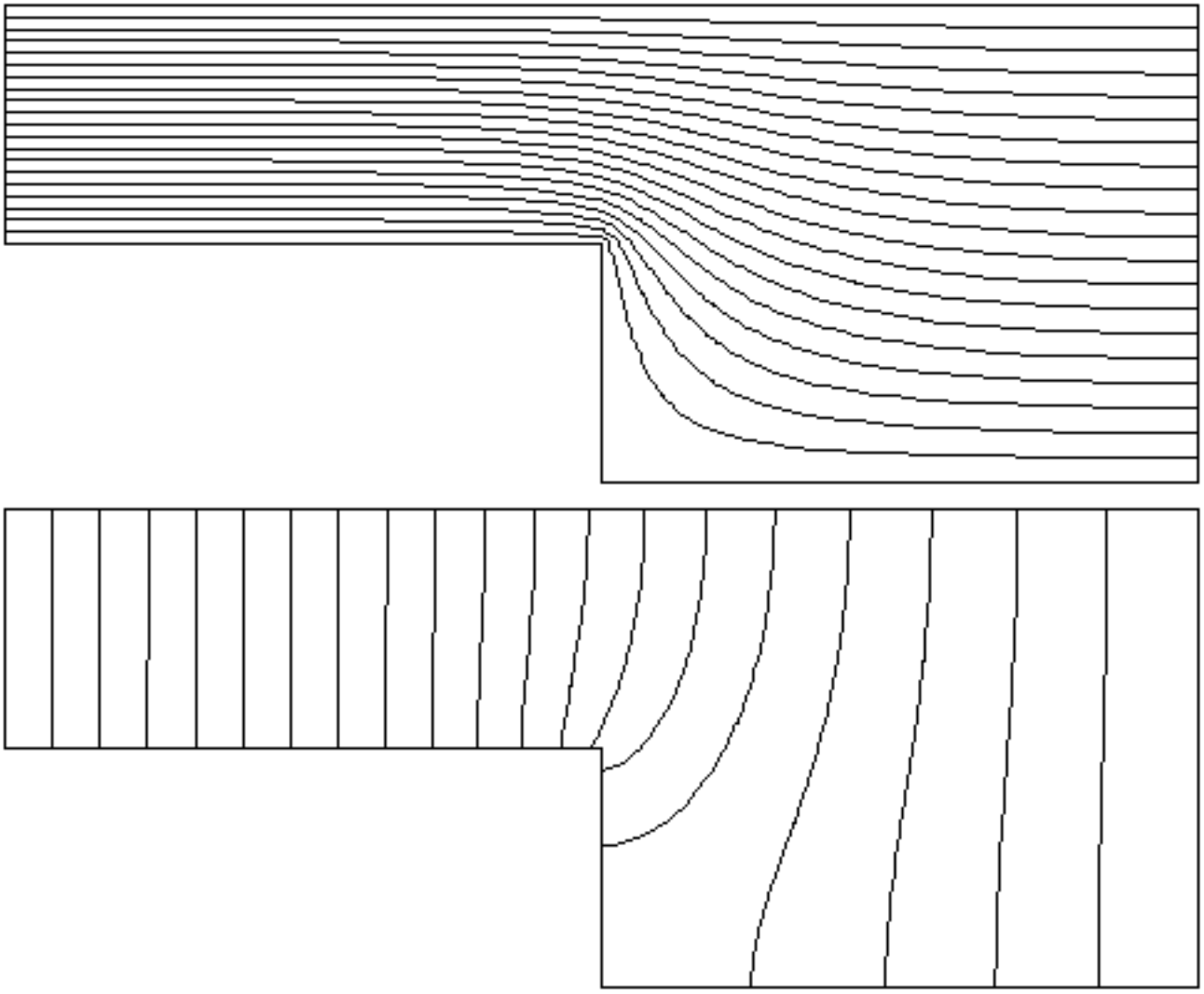

Fig 1.12.8 Fifth mesh (1020 dof)

The convenience and speed of the finite element method are striking in dealing with complex geometries. With the conformal mapping technique the computational details for all but the simplest geometries quickly become very complex.

References: Lamb, Horace. 1945. *Hydrodynamics*. Dover Publications. NY.
Milne-Thomson, L.M. 1967. *Theoretical Hydrodynamics*. MacMillan. NY.
Walker, Miles. 1964. *The Schwarz-Christoffel Transformation and Its Applications*. Dover Publications. NY. pp. 53-65.

Project 13: Diffusion through cylinders of different radii.

Folder: Stomatal Diffusion

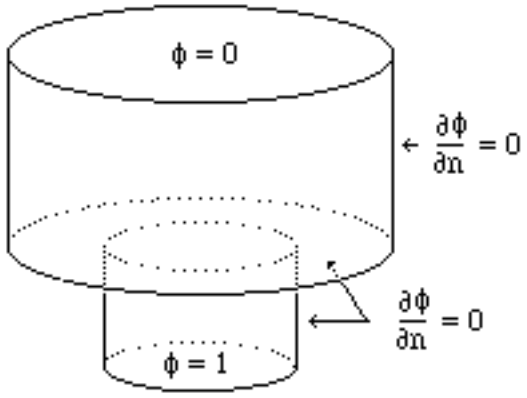

Fig 1.13.1 Diffusion through connected cylinders

Now suppose you wish to generalize the channel problem (Project 12) into an axisymmetric problem (Fig 1.13.1). This problem arises in connection with gas exchange through stomatal pores on the leaves of plants. Higher plants depend upon the entry of carbon dioxide through pores for the source of carbon for photosynthesis. Refer to Chapman and Parker (1981) for the analytical solution to this problem. The complex variables method is no longer applicable, and the direct use of separation of variables and integral transform methods is troublesome due to this slight complication in geometry. Even if the length of the smaller cylinder were reduced to zero, you would have to solve a mixed boundary value problem of significant difficulty.

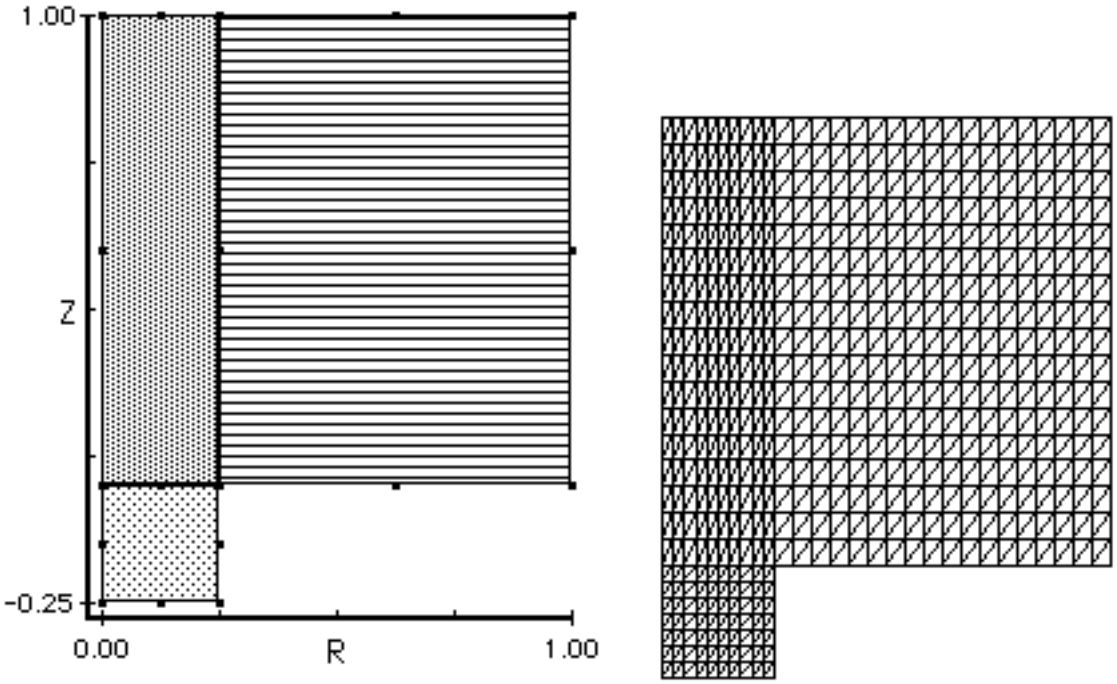

Fig 1.13.2 Mesh generation

First, formulate the problem geometry using a mesh of elements to describe the geometry. Fig 1.13.2 shows the first step in this process—regions defined for use with the automatic mesh

generator. These regions typically match geometric boundaries and changes in material properties. Next the mesh generator uses these regions to produce the elements shown in Fig 1.13.2. The program automatically creates the data structures, displays the node and element numbers, and provides tools for refining the mesh, i.e., improving element shapes and sub-dividing elements in the vicinity of greatest change of the dependent variable. Automatic node renumbering reduces the memory requirements and increases computational speed.

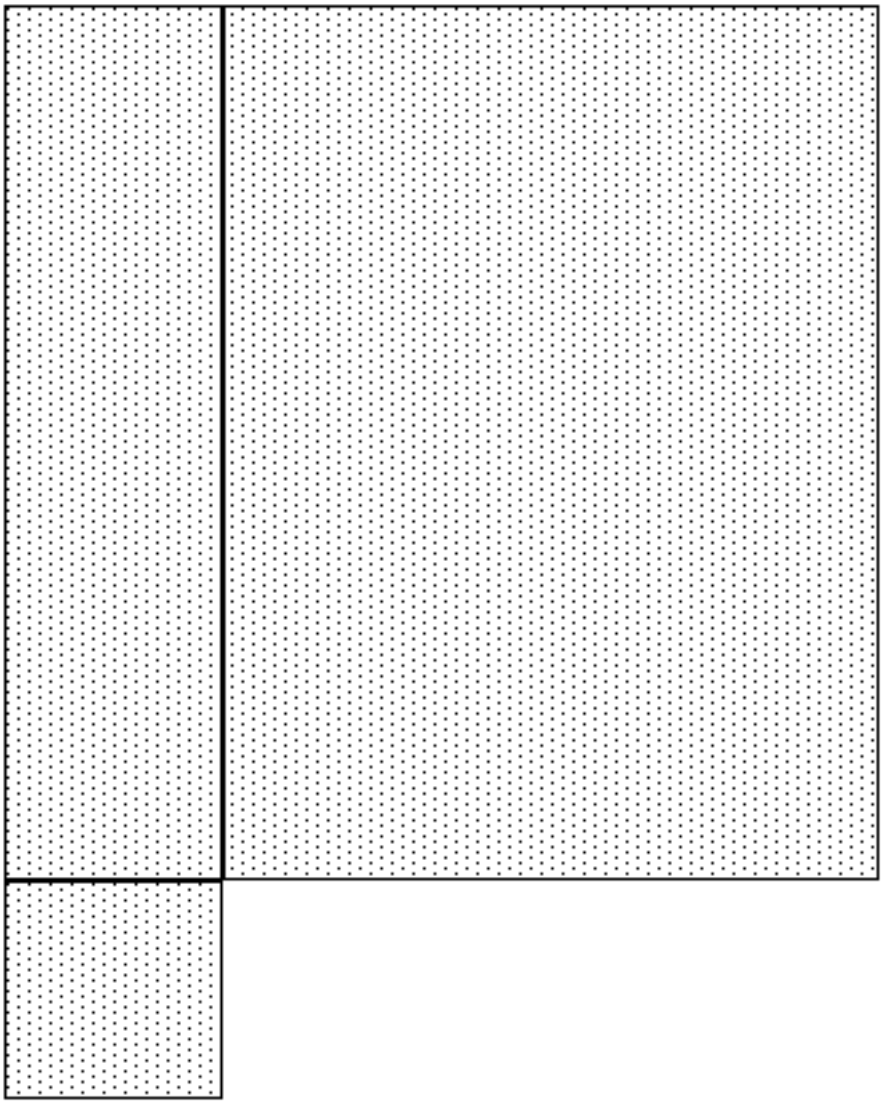

Fig 1.13.3a Properties

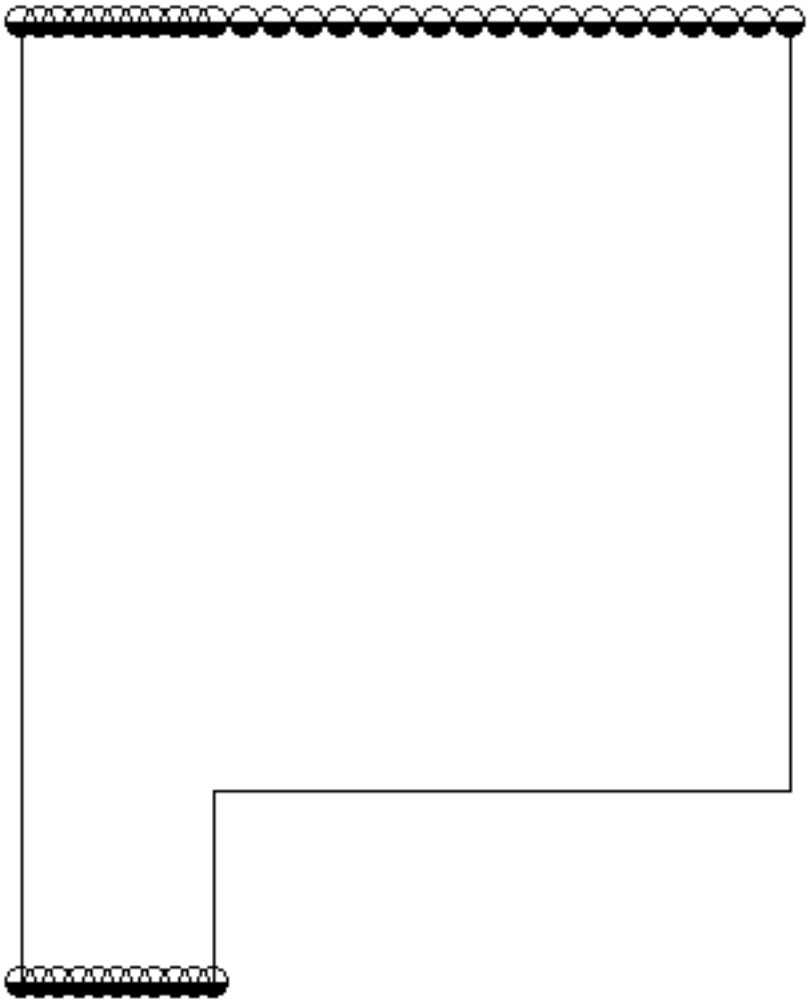

Fig 1.13.3 Boundary conditions

Second, supply the properties. Assign each different property value to a shading pattern; then "paint" the elements with these shades. Although not required here, the r and z components can vary arbitrarily from element to element in Fig 1.13.3. Third, supply the boundary conditions to complete the formulation of a well posed problem (Fig 1.13.3).

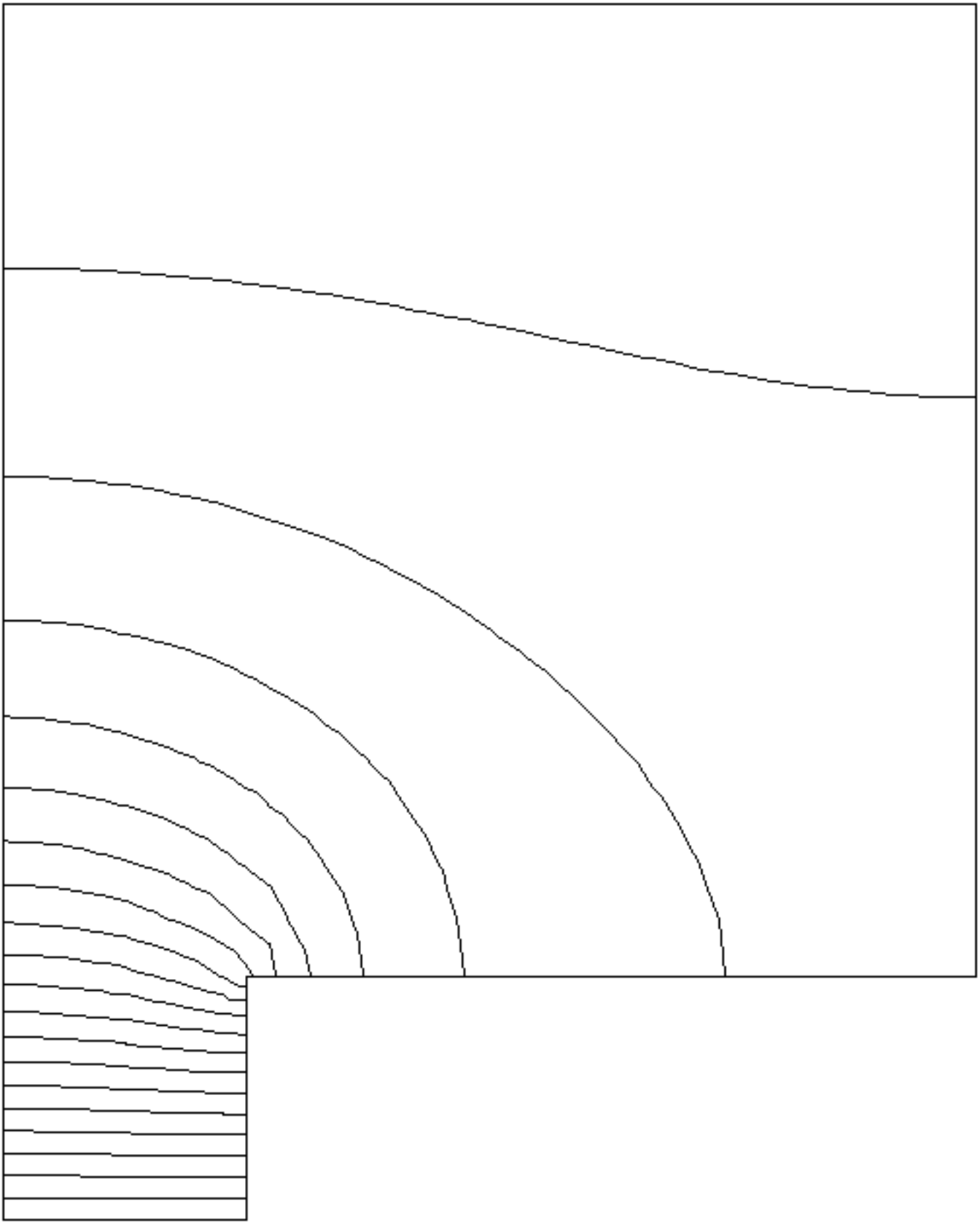

Fig 1.13.4a Constant potential lines

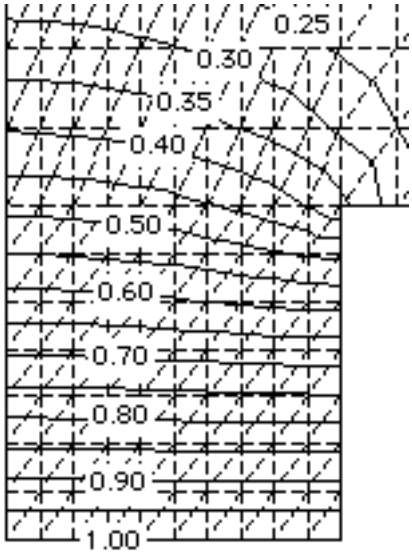

Fig 1.13.4b Enlargement of corner

Figs 1.13.4 and 1.13.5 display the calculated potential. The tabular results are also available, should you need additional calculations. The calculated diffusion resistance differs from the Chapman and Parker result by less than 2 percent.

The above problem also describes the analogous direct current resistance problem and ideal fluid flow through a cylinder having an abrupt enlargement, as well as the problem of immediate interest—the diffusion of carbon dioxide through connected cylinders of different radii.

The finite element formulation provides even more generality than suggested by this example. Suppose there were obstructions within the cylinders. Or suppose the cylinders were made of composite materials. These more general solutions are immediately available; simply assign different properties and boundary conditions to the elements. Even if the permeability or conductivity components were not the same in the r and z directions, the calculation still would proceed smoothly.

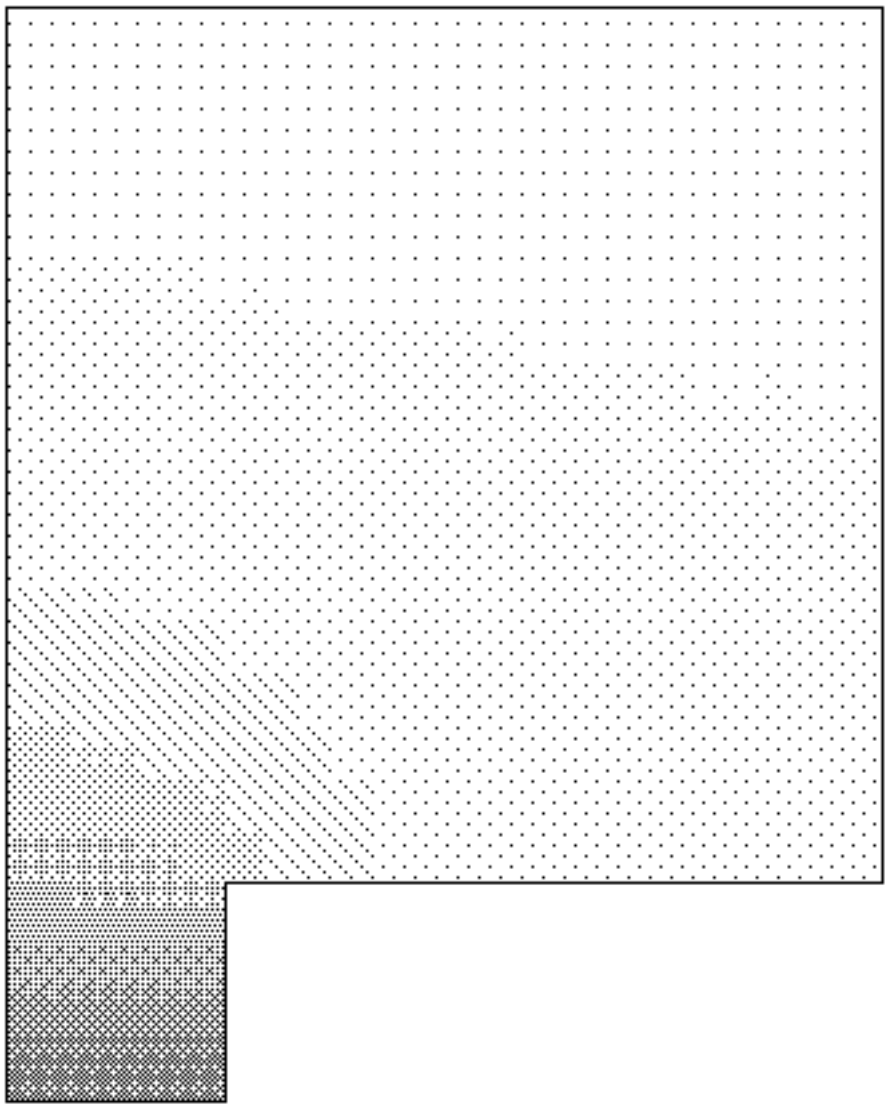

Fig 1.13.5 Element average concentration

References: Chapman, David C. and Robert L. Parker. 1981. A Theoretical Analysis of the Diffusion Porometer: Steady Diffusion Through Two Finite Cylinders of Different Radii. Agricultural Meteorology v23 pp. 9-20.

Cooke, J. Robert. 1988. Instructional Sofware Makes The Finite Element Method Accessible. *Academic Computing*. Sept 1988. pp. 34-35, 54.

Cooke, J. R., S.K. Upadhyaya, M.J. Delwiche, R. H. Rand, N. S. Scott and E.T. Sobel. 1988. StomateTutor™: An Introduction to Stomatal Control of Gas Exchange in Plants. Cooke Publications, Ithaca, NY. (A HyperCard application).

Holcomb, D.P. and J.R. Cooke. 1977. Diffusion resistance of porometer calibration plates determined with an electrolytic tank analog. ASAE Paper No. 77-5509. 60 pages. St. Joseph. MI.

Holcomb, D.P. and J.R. Cooke. 1977. An electrolytic tank analog determination of stomatal diffusion resistance. ASAE Paper No. 77-5510. 56 pages. St. Joseph. MI.

Project 14: A point charge eccentrically placed in a conducting sphere.

Folder: Point Charge in Sphere

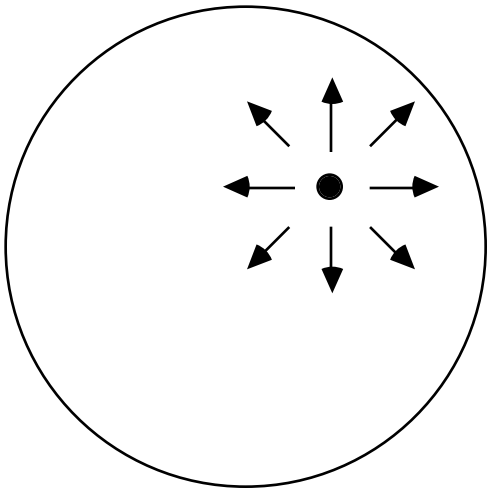

Fig 1.14.1 Eccentric point charge in a sphere

A point charge (Fig 1.14.1) lies eccentrically in a hollow conducting sphere. What is the potential distribution?

Use the radial symmetry in the formulation of this problem—an axisymmetric semicircle of equipotential with a point source located on one axis of symmetry. The problem is relatively simple to set up as you need only one region, a semicircular one with the axis of the semicircle lying on the z-axis. This shape generates a sphere when it is rotated about the z-axis. MP produces results within 15% of theoretical results (except at node source) with an 11x11 mesh for 121 D.O.F. Solution time is low (on the order of 1 minute on a 512KE Mac).

Find the potential field associated with a point charge q eccentrically located a distance d from the center of a conducting sphere of radius a (Fig. 1.14.2).

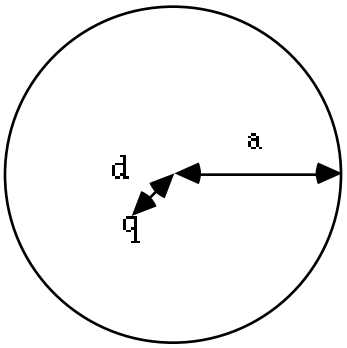

Fig 1.14.2 Schematic of point charge in sphere

Find the solution (Fig 1.14.2) using the method of images to solve for V (Pugh & Pugh, p 90). Compare the results with the finite element method using MacPoisson.

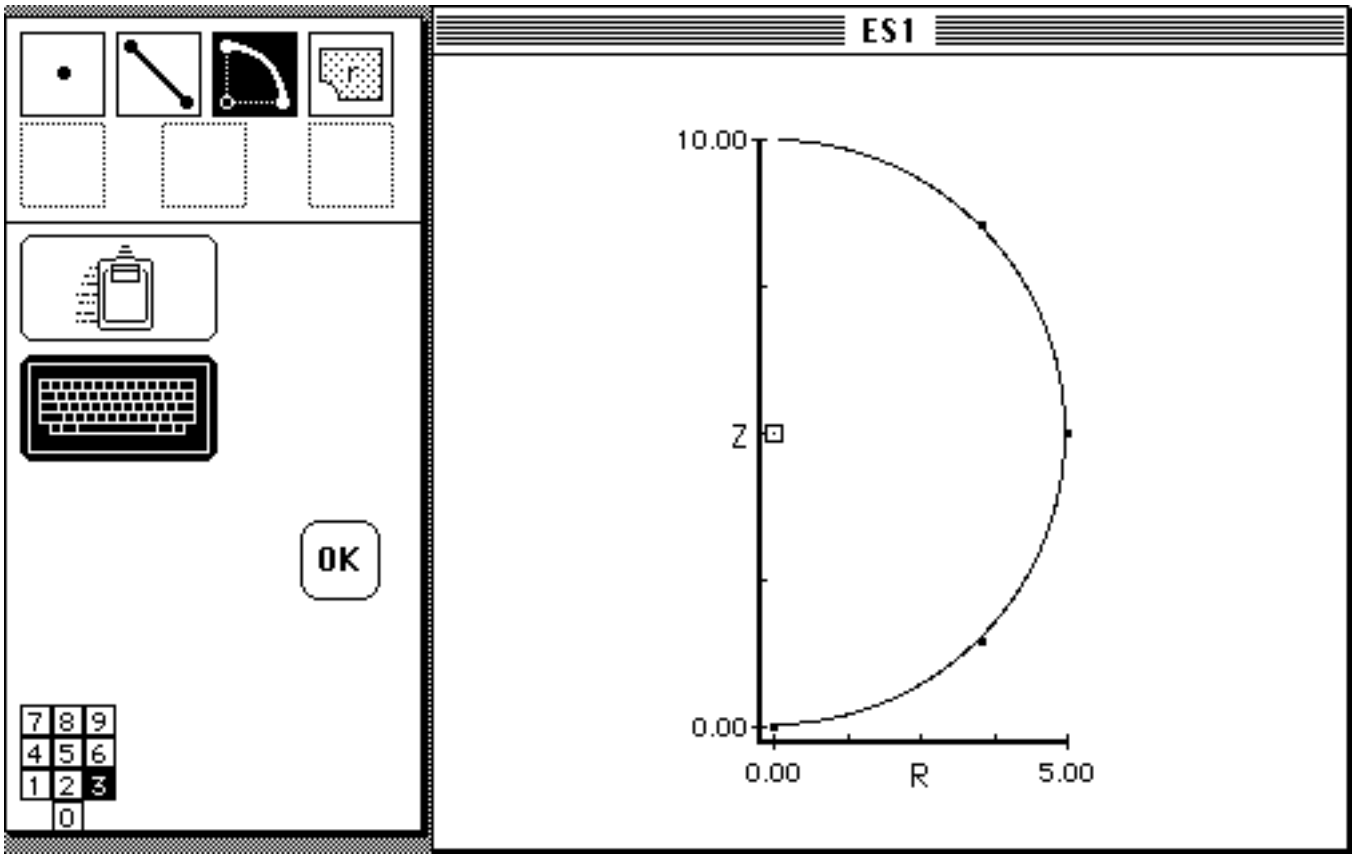

Fig 1.14.3 Geometry

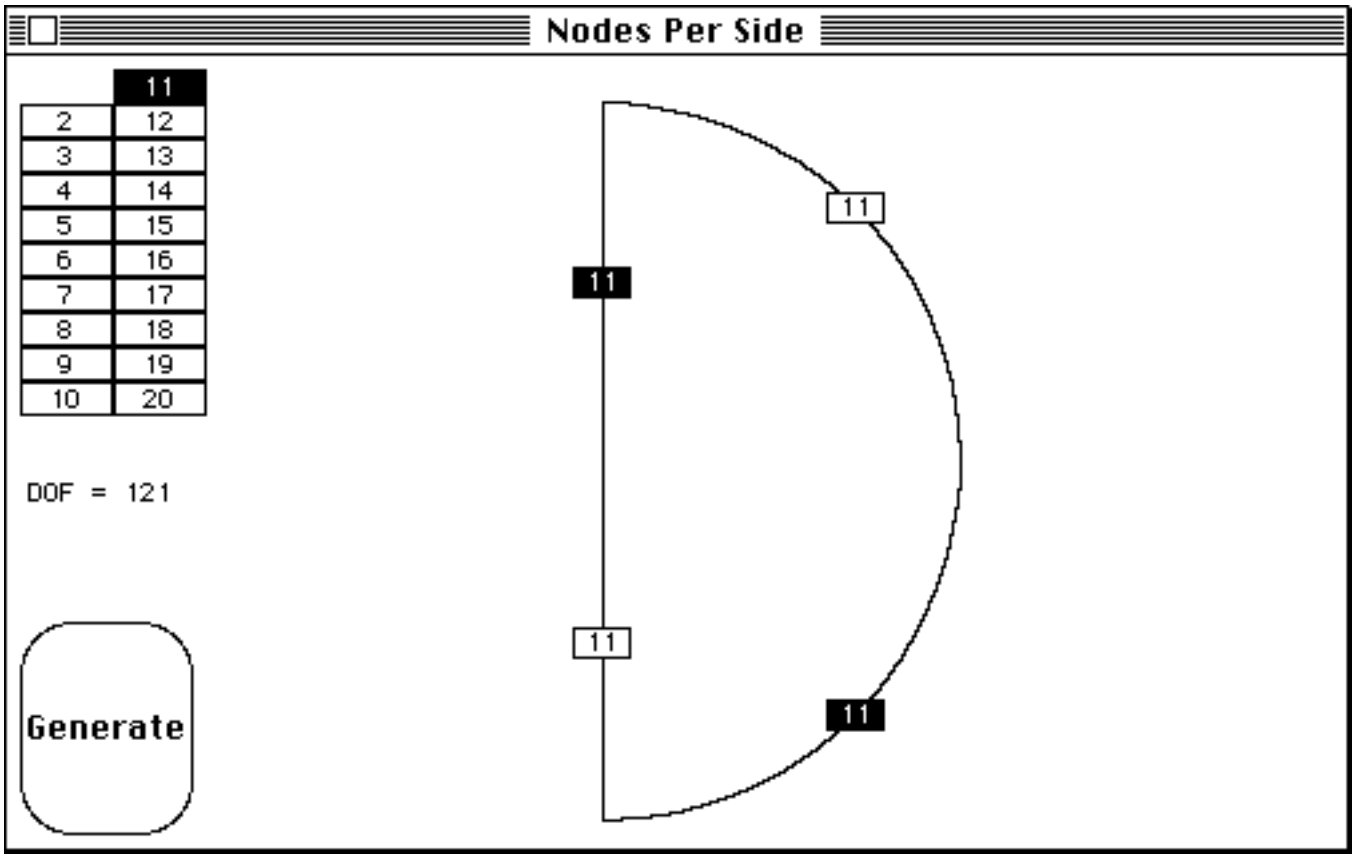

Fig 1.14.4 Nodes per side

Geometry:

For the sample problem, assume a sphere of radius 5.0 meters with a point charge of 1.0 microCoulomb located 2.0 meters from the center of the sphere.

Use the axial symmetry of the problem to your advantage by specifying axisymmetric coordinate axes when prompted at the beginning of the geometry definition section. The semi-circle lies vertically on the z-axis (Fig 1.14.3), you should, therefore, set the r-range to 0.0 to 5.0 and use the default z-range of 0.0 to 10.0.

Begin to define the region. Choose the arc command and use keyboard input. MP prompts for the arc's center point. Enter 0.0, 5.0; then click OK. (Use the return key to go from the upper to lower box.) MP asks for the arc's starting point. Enter 0.0, 0.0; then click OK. Since you want a semicircular region, type 180 into the box asking how many degrees counterclockwise the arc should run. MacPoisson now draws the arc for you and asks how many intermediate points you want. Because it is convenient to have eight points along the entire boundary of the region, select three intermediate points; then press OK (Fig 1.14.3). (You have three points on the circle, two at vertices, and three on the z-axis, thus making eight total.) Now, to quickly add the last three points, select line mode, keyboard entry. Put 0.0, 10.0 for the starting point; 0.0, 0.0 for the ending point; and again select three intermediate points. Click OK.

Select the area by going to the region selection mode, moving the circle to the vertex at 0.0, 0.0, and choose the subsequent counterclockwise dots. After you select the eighth dot, the timer appears; and MacPoisson fills the region.

You are now ready to go on to the mesh generation section. Pull down the File menu and select Mesh. Save the geometry data. A menu appears and you should click on >>Generate Mesh.

Mesh: Because MacPoisson views the semicircle as a degenerate curvilinear quadrilateral, you are prompted to select the nodes/side value for both pairs of sides; namely the upper-arc/lower-radius pair and the lower-arc/upper-radius pair (Fig 1.14.4). Use 11 as a first try, this gives a reasonable amount of resolution while not taking too much computing time. (11 is preferable to 10 in this problem because it results in 11 nodes and, therefore, 10 spaces over the 5 meter radius, making source placement easy to calculate.) If you want greater resolution, use a higher number of nodes; if you want faster processing, use a lower number.

Click on the Generate button and MacPoisson draws the mesh. When the drawing is complete, pick different node numbers (by clicking the box in the generated picture window to show the original screen) or use the generated mesh by selecting End Generation under the Generate menu.

You are again at a menu, this time showing Generate Mesh with a checkmark next to it and offering Other Calculations below it. Choose Other Calculations to finish the mesh generation computations and ensure minimal processing time later in the program. Regardless of whether or not you achieved bandwidth reduction, you must save the renumbered data and the line information.

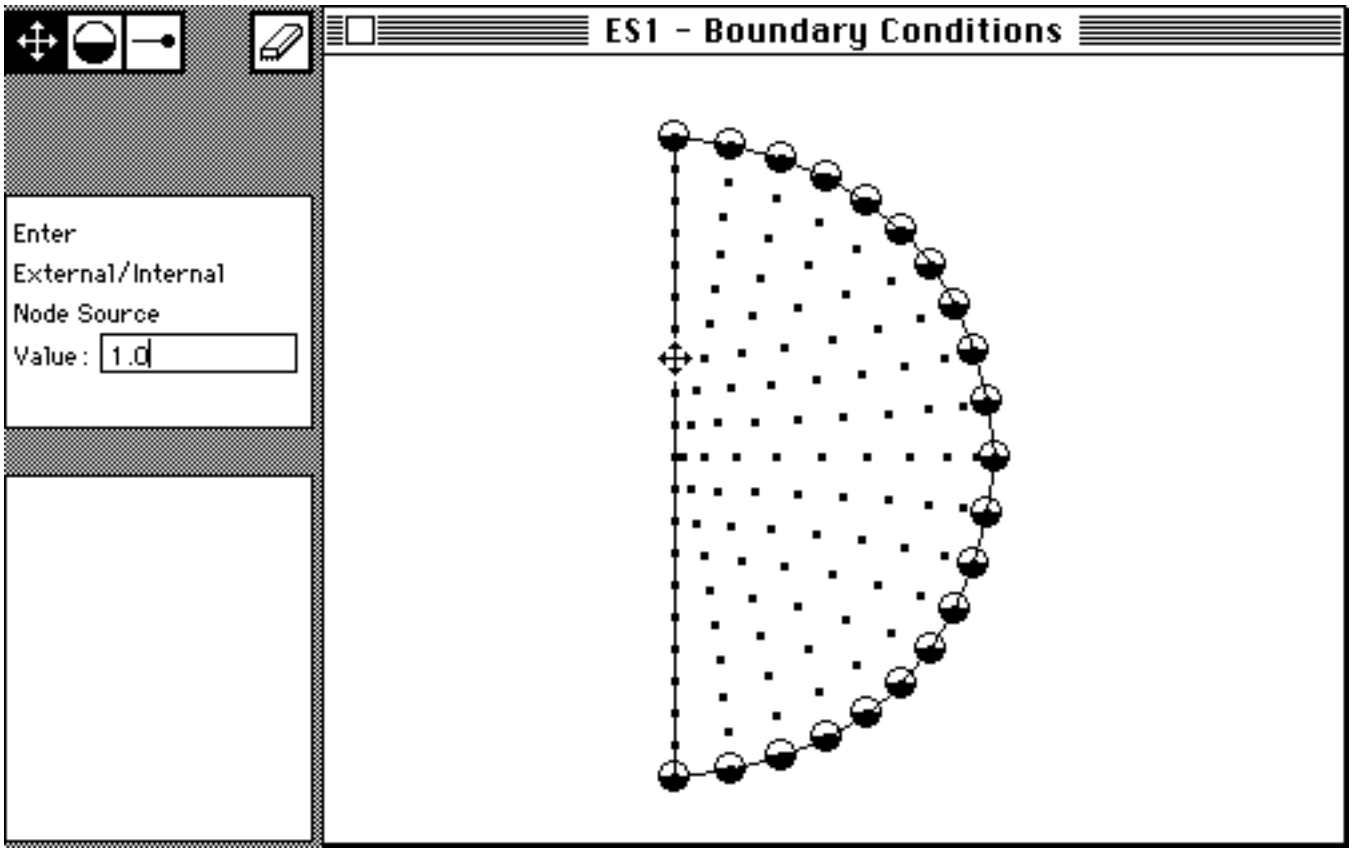

Fig 1.14.5 Boundary conditions

Boundary Conditions: Select >>Enter Boundary Conditions. MP draws the geometry you created along with mesh node points. Set the node source value to 1.0 for a 1 microCoulomb charge. Since the source in this problem is 2.0 meters from the center of the sphere, and since you have the relationship of 1 node space equal to 0.5 meter, you place the cursor on the 4th node from the center and click the mouse (Fig 1.14.5).

To model the grounded conducting sphere, select node potential by pointing at the black and white circle icon and clicking. The default potential is zero, which is correct for a grounded sphere. You can individually set the outer nodes to zero now, by moving the pointer onto each of them and clicking; however, it is much more convenient to use the perimeter feature of MP. Place the pointer on the lower vertex of the semicircle, press the keyboard shift key, and click once. Now go to the upper vertex and do the same; MP fills in the nodes in a counterclockwise manner.

Now select End Boundary Conditions Definition under the B.C. menu, save the boundary conditions, and proceed with the solution.

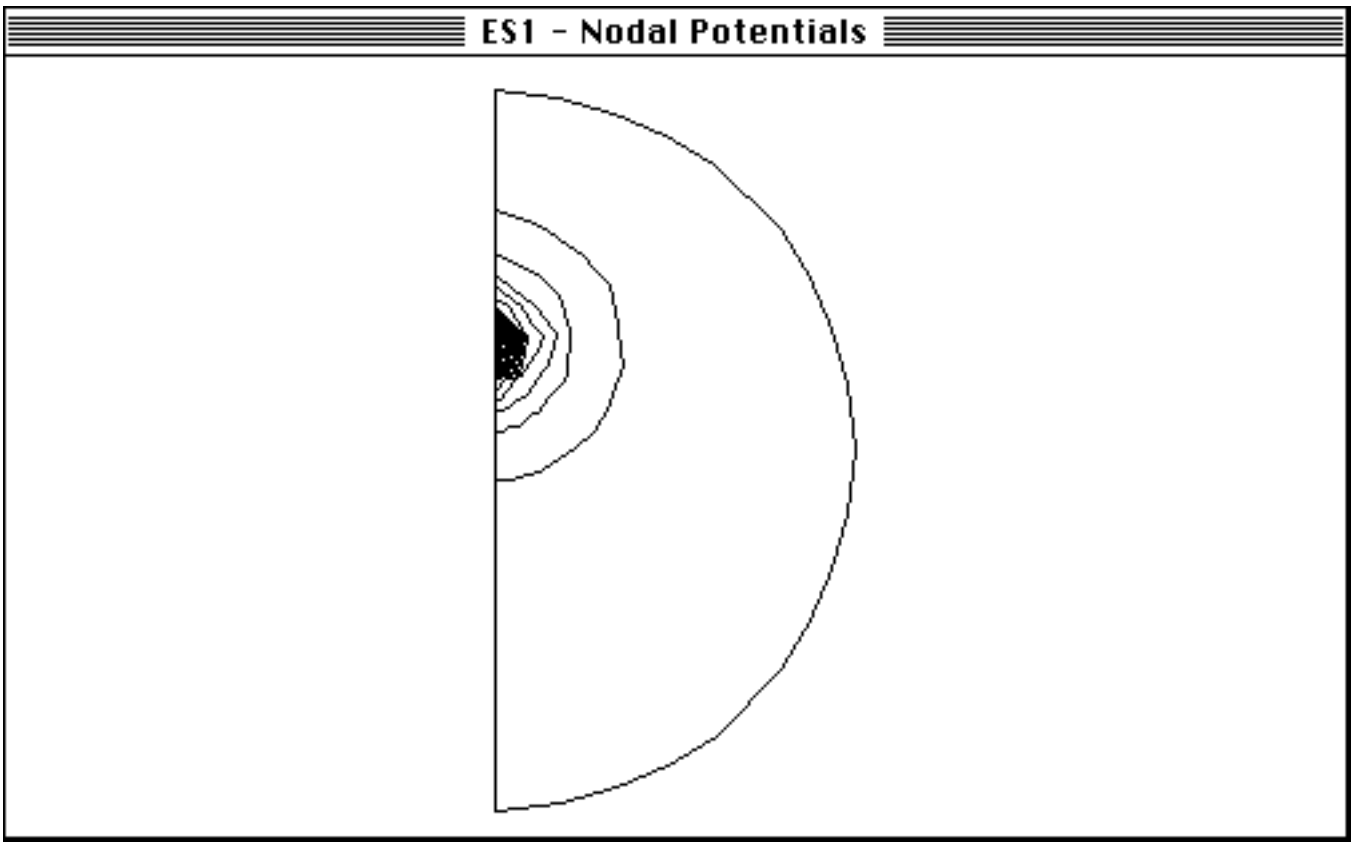

Fig 1.14.6 Nodal potentials

Solving and Plotting: Finish the problem by clicking on >>Solve to reach the Solve menu. As you did in the heated pot demo, first solve for the nodal potentials, then for potential gradients and other calculations. MP insures that you proceed in the correct order by dimming the non-allowed menu choices.

Having solved the problem, click on >>Plot to get to the plot screen. Use the screen plotsize first to observe the potential plot at default plot values. Notice that the equal spacing causes MacPoisson to draw a graph with too much unusable resolution near the center (Fig 1.14.6); this is due to the inverse-square relationship between potential and distance. To produce a plot with greater resolution at the edges of the plot, specify different limits on the plot values, such as 0.0 to 0.4 (Fig 1.14.7). If the information you want is shown on the graph, select 8x10 plot size and produce a high quality final draft of the problem's solution (Fig 1.14.8). If you'd like greater resolution elsewhere, get it by choosing the appropriate limits on the plot choice menu.

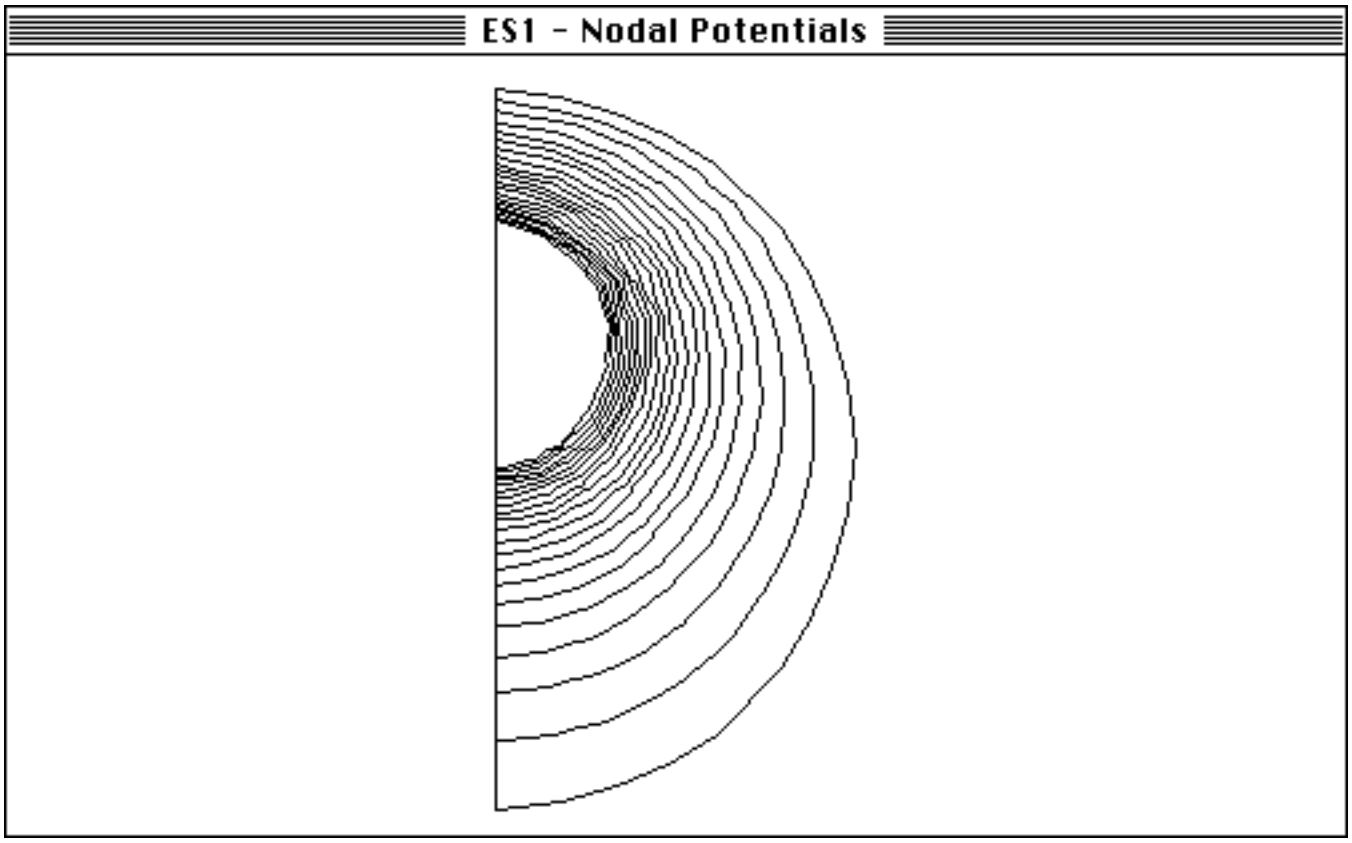

Fig 1.14.7 Rescaled plot. (0.0 to 0.4 range)

The potential becomes infinite at the line source, so the error is expected to be large there. As an exercise, solve the problem with a refined mesh, i.e., one with more elements and smaller elements near the source.

Project 15: Parallel plate capacitor.

Folder: Parallel Plate

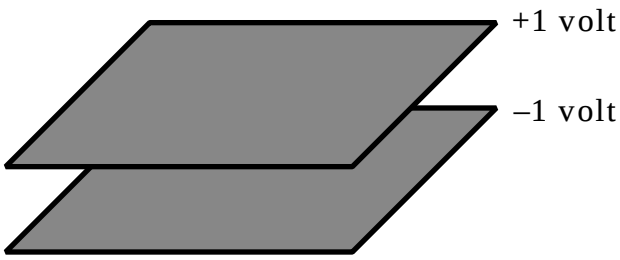

Fig 1.15.1 Parallel plate capacitor

One of the classical problems of electrostatics is the fringing of a parallel plate capacitor. The simplest approximation used in introductory electrostatics books ignores the fringing effect at the edges of the capacitor. You can analyze this problem using conformal mapping in complex variable theory. The results using the Maxwell curves is presented in the *Field Theory Handbook* (Moon and Spencer, 1971, p65 and Moon and Spencer, 1961, p341). [Note: The mathematically equivalent problem for ideal fluid flow, i.e., a liquid flowing from a large reservoir into a canal bounded by two thin parallel walls, is presented by Lamb (1945, p74).]

$$z = \frac{a}{\pi}(w + 1 + e^{w})$$

This describes a capacitor of spacing '2a' with potential of +p and - p .

$$x = \frac{a}{\pi}(u + 1 + e^{u}\cos v) \qquad y = \frac{a}{\pi}(v + e^{u}\sin v)$$

The x = 0, y = 0 origin is at the right edge of the plates and midway between the two. The no-fringing approximation appears to be a surprisingly useful approximation.

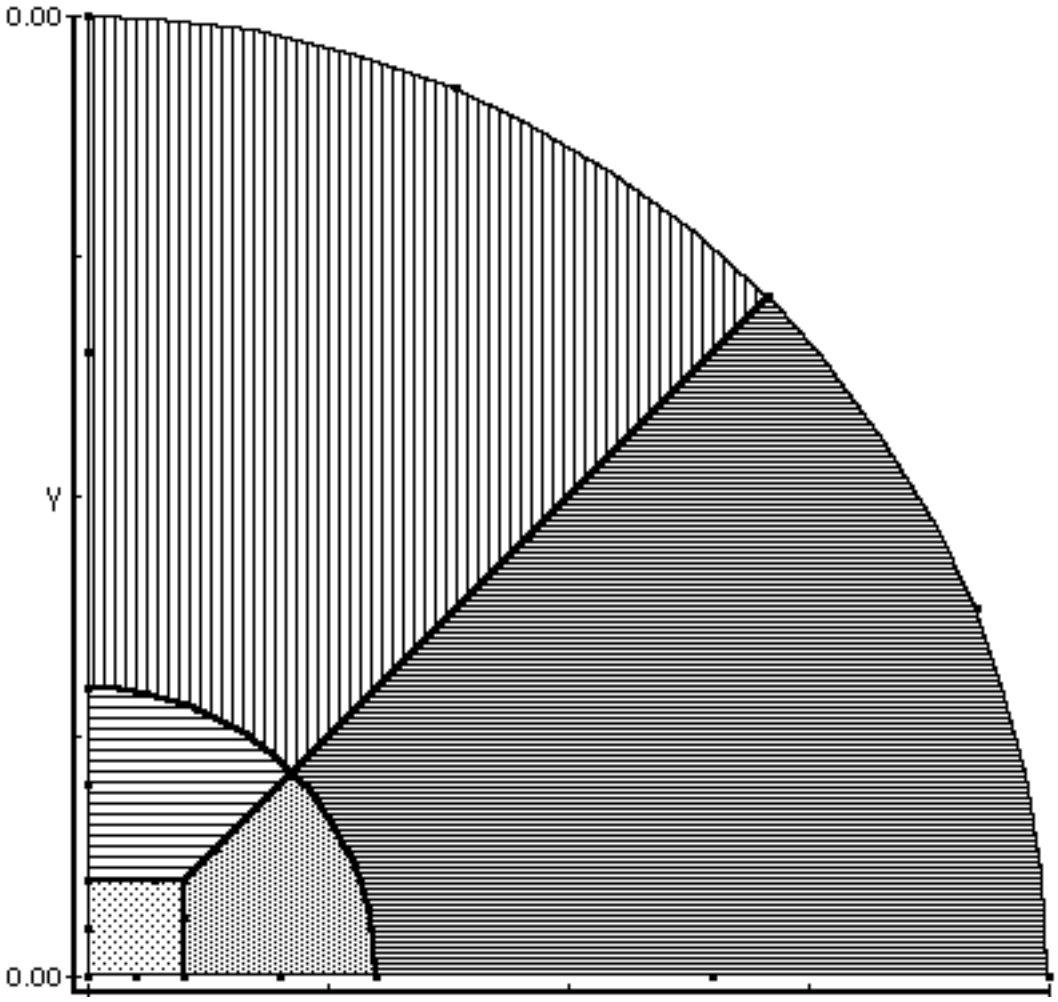

Fig 1.15.2 Mesh generation

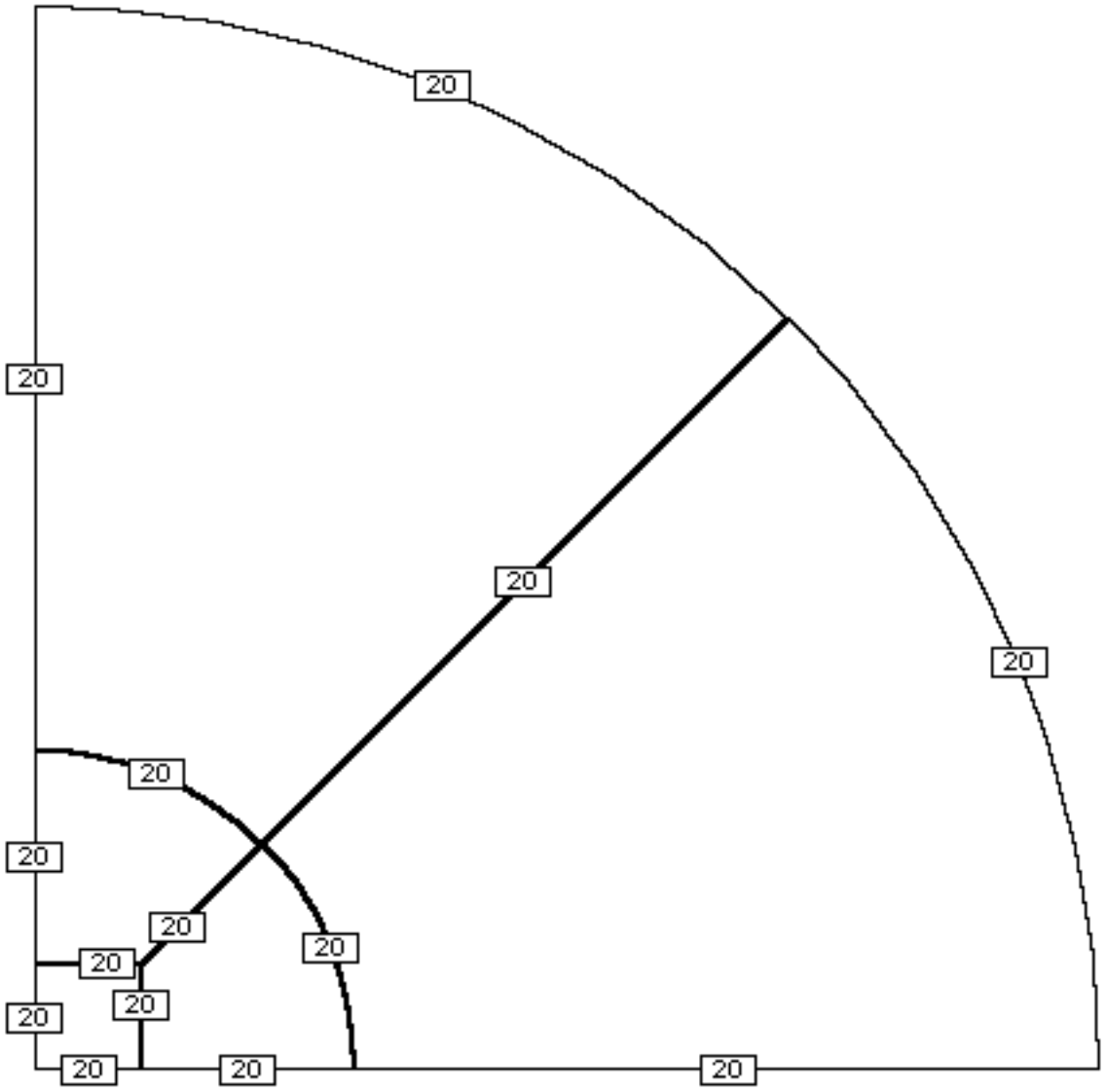

Fig 1.15.2b Mesh generation

Although you can solve this problem using the student version, the mesh shown (Fig 1.15.2) shows the refinement which is possible with 2 megabytes of memory (and 1882 degrees of freedom). Since you must locate the boundary in MP a finite distance from the origin, use a quarter circle a “large distance” from the origin. Set the gradient of the potential to zero at this large, but finite distance from the capacitor (Fig 1.15.3).

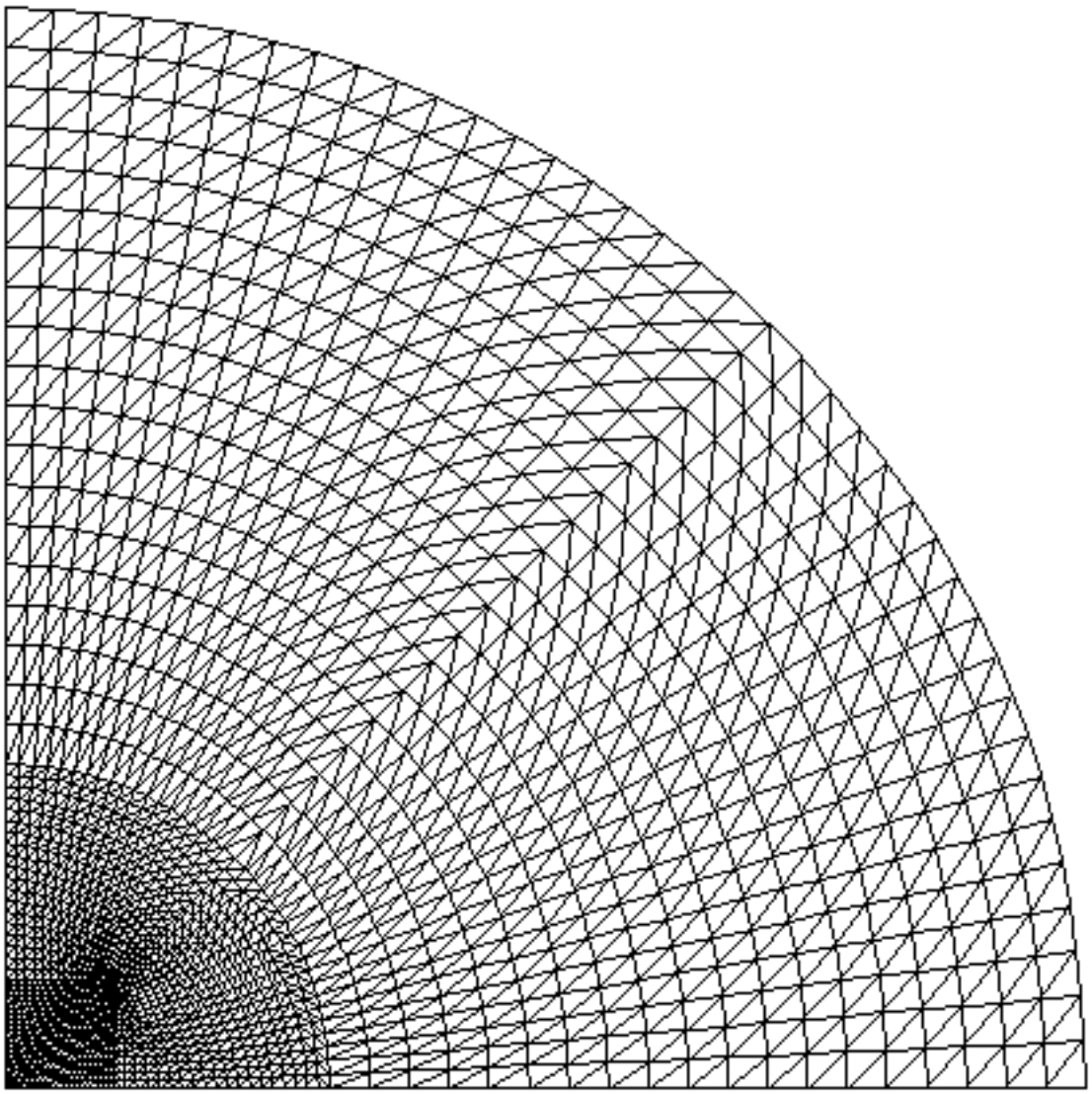

Fig 1.15.3a Generated mesh and boundary conditions

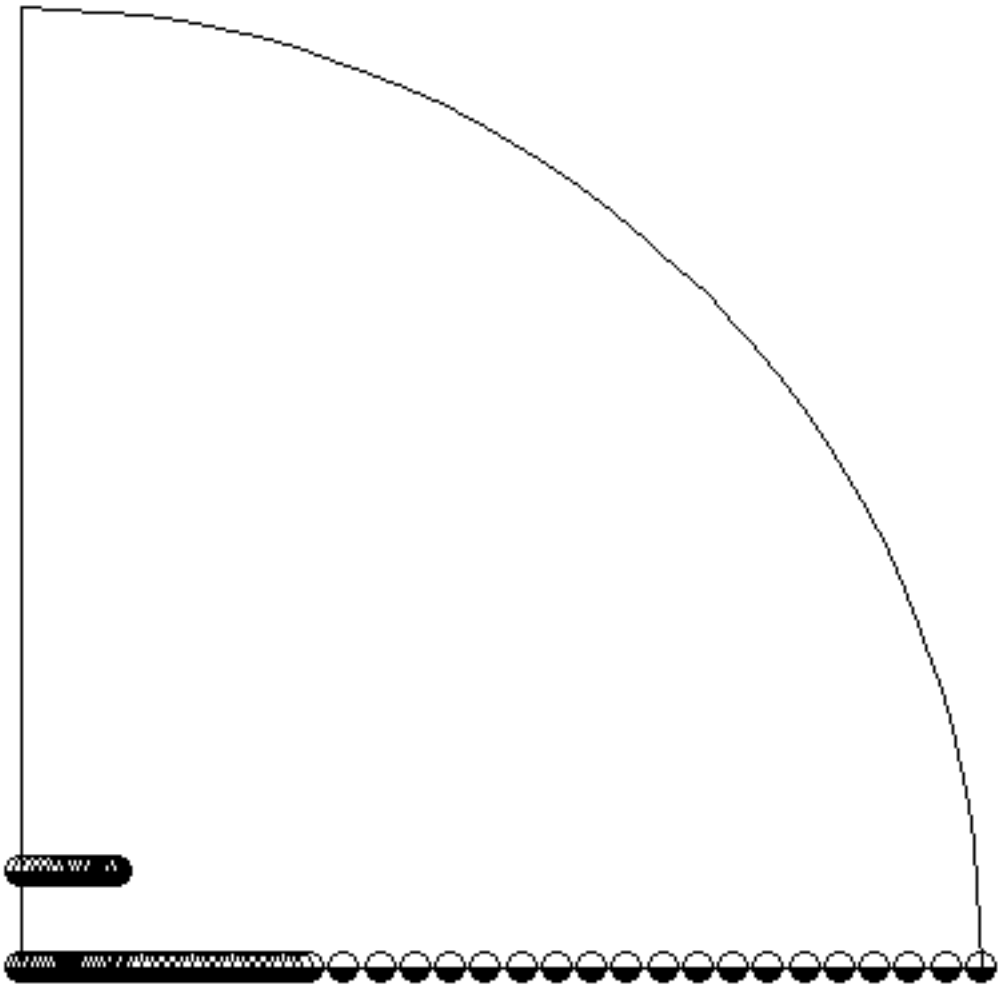

Fig 1.15.3b Generated mesh and boundary conditions

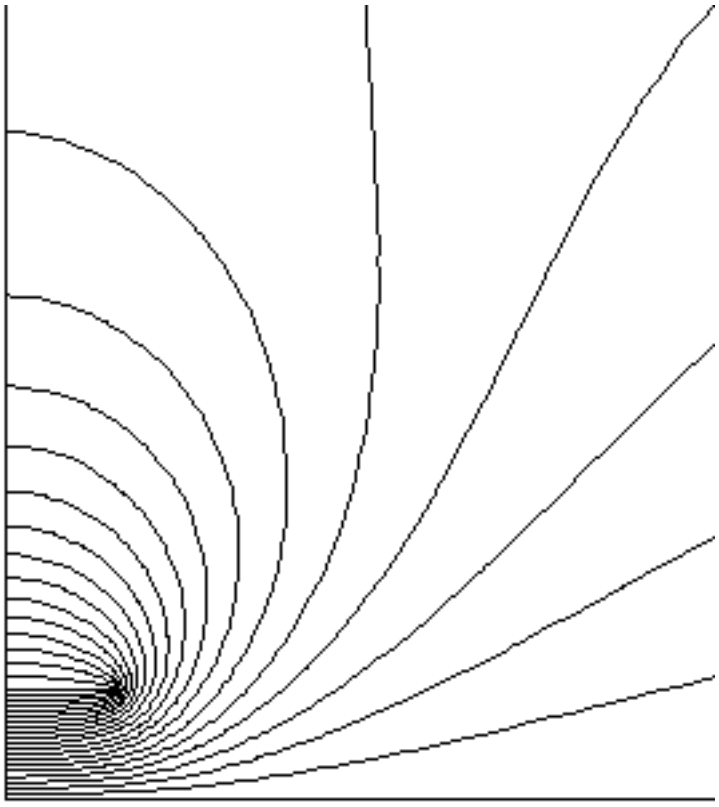

Fig 1.15.4a Constant potential lines

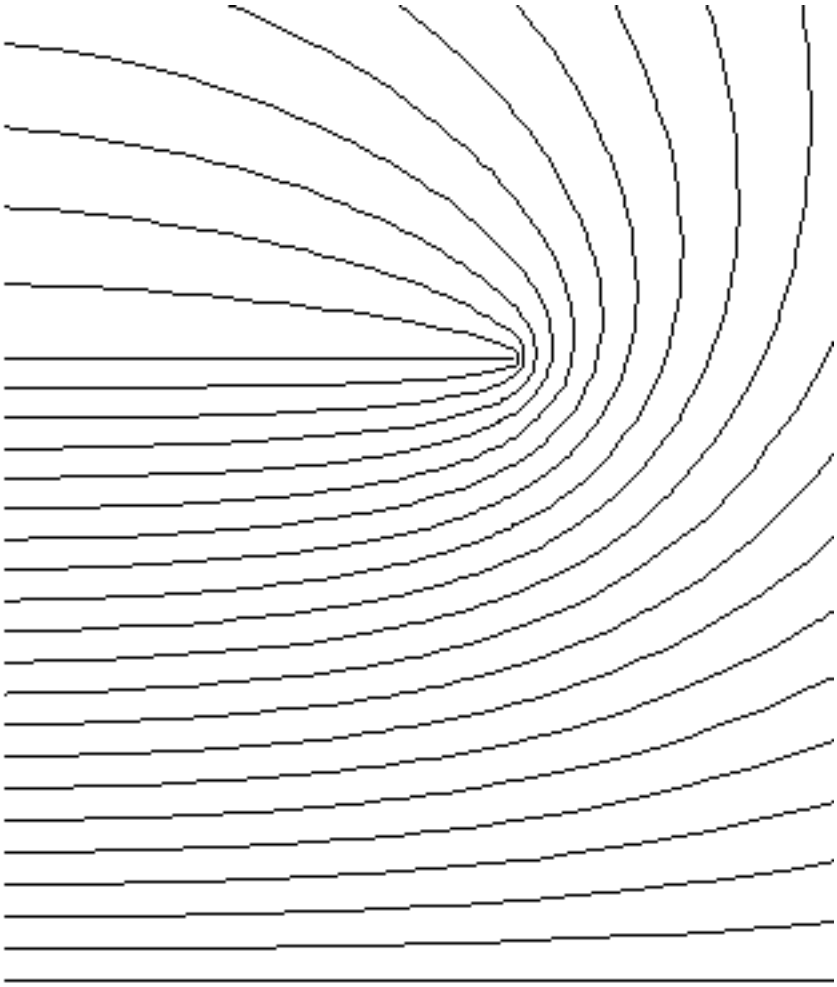

Fig 1.15.4 b Constant potential lines

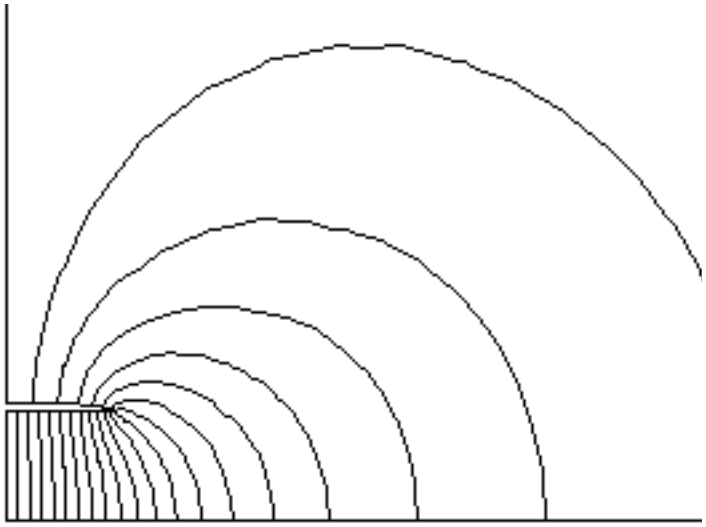

Fig 1.15.5a Flow lines and equipotential lines

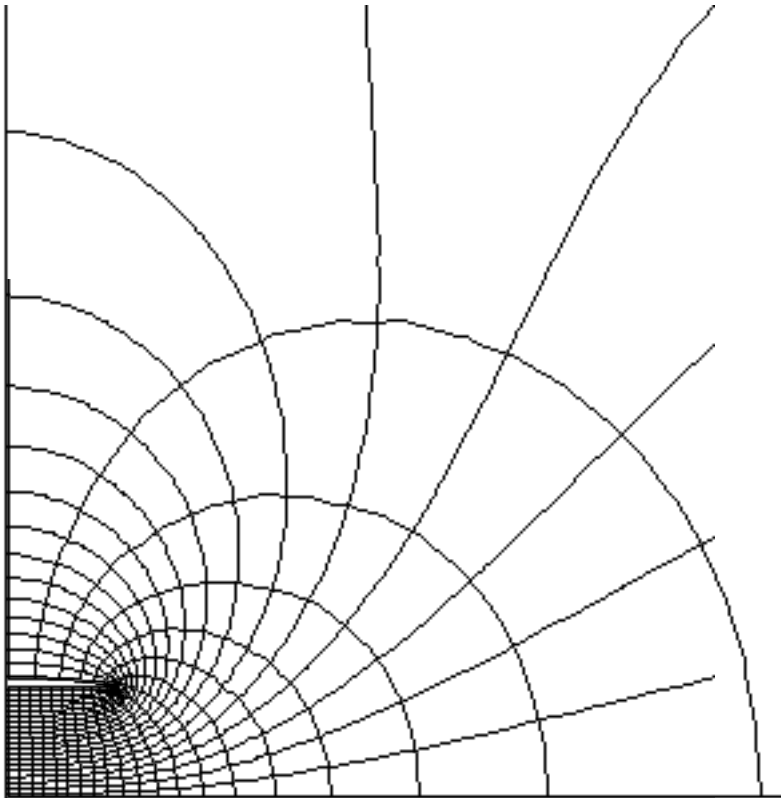

Fig 1.15.5b Flow lines and equipotential lines

The constant potential lines (Fig 1.15.4) turn abruptly at the edge of the capacitor. In fact, the exact solution is undefined at this sharp corner. Except in the immediate vicinity of this sharp corner the finite element solution reasonably approximates the conformal mapping result. Compute the conjugate problem (Fig 1.15.5) by swapping the boundaries of zero gradient and constant potential.

Reference: *Field Theory Handbook* (Moon and Spencer, 1971, p65 and Moon and Spencer, 1961, p341)

Project 16: Conducting cylinder in a uniform electrostatic field.

Folder: ElectroCylinder

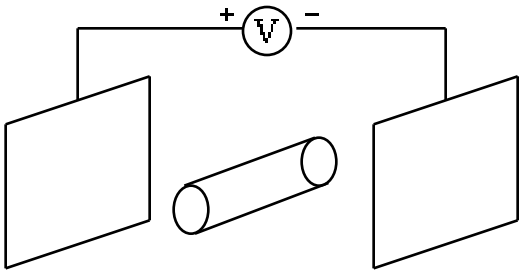

Fig 1.16.1 Conductor in uniform field

Let's look at an electrostatics problem which occurs in nearly every introductory textbook on electromagnetic theory. Suppose a conducting cylinder is placed perpendicular to a uniform electrostatic field.

This is a planar problem with results which agree well (10%) with the theoretical solution for the problem with a very coarse mesh. Some thought shows that the problem is symmetric about two axis; it is, therefore, possible to reduce computing time by modeling only one quadrant of the problem. There are at least two ways of dividing the problem space into regions. We have used the one which creates one triangular region and one curvilinear quadrilateral region with the entire quarter circle in it. The other division creates two mirror images along a line starting at the center of the circle and ending in the extreme corner of the problem space. At 91 D.O.F. the problem solves quickly.

For the case where the size of the conductor is small compared to the distance between the field-generating plates, the theoretical solution of the problem is found to be:

$$V = -E_0 \, r \cos\theta + \frac{E_0 \, a^2 \cos\theta}{r}$$

where E_0 = incident field

a = the radius of the cylinder

and r and q are cylindrical coordinates measured from the conductor's center.

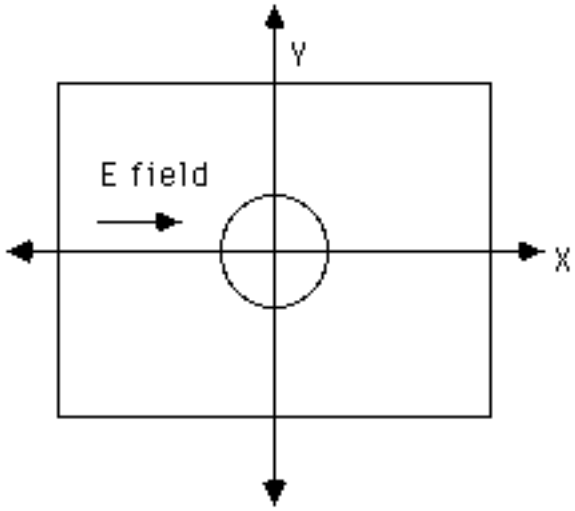

Fig 1.16.2 Conductor in uniform field

Fig 1.16.2 shows the symmetry about both axes.

You can achieve greater accuracy with less computation time if you use the symmetry of a problem to your advantage. In this case, you need model only one of the four quadrants of the problem, the other three being available through reflections across one or both axes. Use a radius of 2.5 meters for the conductor and an x-axis size of 10.0 meters. The quadrant we chose is shown in Fig 1.16.3.

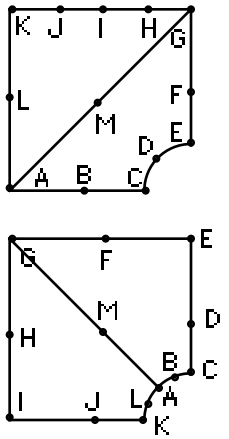

Fig 1.16.3 Generating region alternatives

Notice the line AG which divides the problem into two regions, both of which have the requisite eight points on their perimeters and neither of which has more than four sides. This division enables you to select curvilinear quadrangle ABCDEFGM as one region and (degenerate) quadrangle AMGHIJKL as the other region.

WARNING: USE THE SAME POINTS ON THE COMMON BOUNDARY FOR REGION GENERATION OR ERRORS RESULT!

MacPoisson prompts you for node per side values for all the borders of the problem. However, the nodes per side for sections CDE, AMG, and IJK are all set concurrently because they are

constrained by common side AMG. The geometry of the problem causes the greatest variations in field strength to occur near the conductor; it is, therefore, wise to concentrate nodes (and therefore computing resources) on the arc.

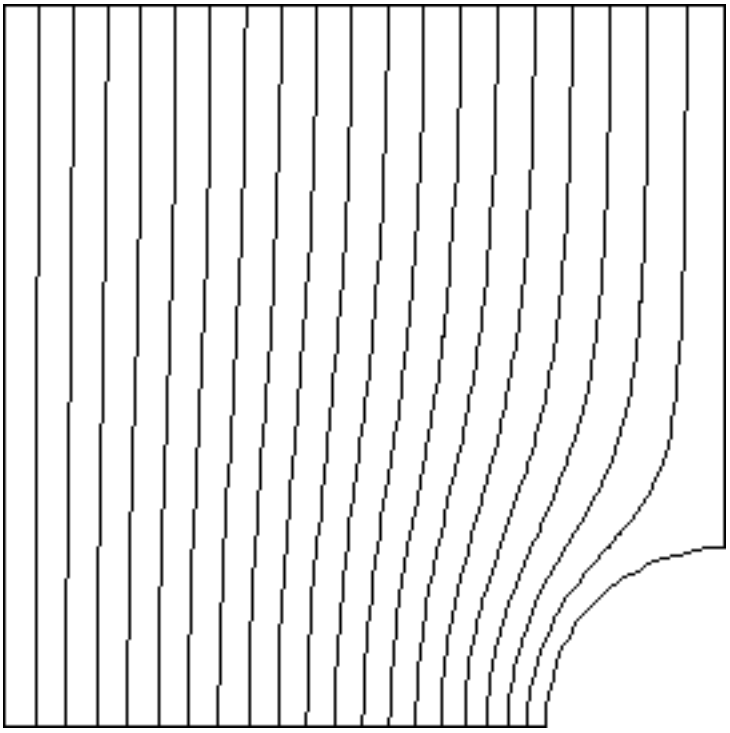

Fig 1.16.4 Constant potential lines

The electrostatic field produced by two conductors of opposite potential leads to the condition that the potential on the conducting cylinder and on the y-axis is zero. Therefore, we can model the situation in one quadrant by setting sides CDE and EFG to zero potential and setting side KLA to an appropriate potential to generate the desired field, i.e., for a 10V/m field, set V_{KLA} to 100 volts since there is a 10 meter separation between it and the zero potential line.

Using a fine mesh (dof=580), the program produces results (Fig 1.16.4) which agree with the theoretical solution within 10% everywhere except at the immediate boundary of the cylinder.

Pugh, E.M. and E.W. Pugh. 1970. *Principles of Electricity and Magnetism*. 2nd. Addison-Wesley Pub. Co. p100.

Project 17: Spheres in a uniform electrostatic field.

Folder: Sphere1, Sphere2, Sphere3

Consider now the axisymmetric case of a ***sphere*** in an initially uniform field.

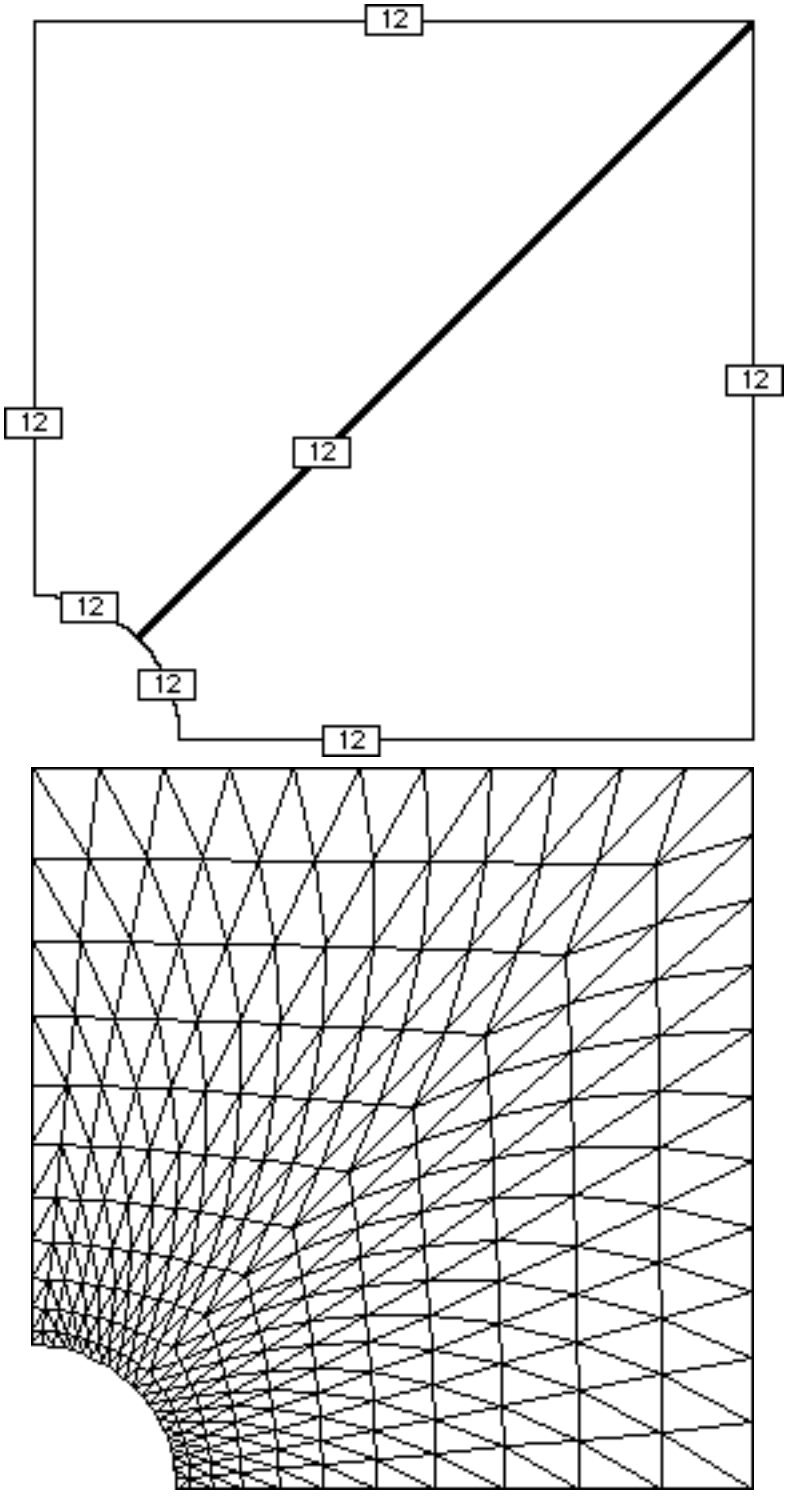

Fig 1.17.1 Mesh

Using the mesh shown in Fig 1.17.1 and the boundary conditions of Fig 1.17.2, we obtained the solution.

Moon and Spencer (1961, p226) present the Legendre polynomial solution (where the boundaries are a large distance from the sphere) as follows:

$$\varphi = V + E_0 \, r \cos\theta \, [\, 1 - (a / r)^3]$$

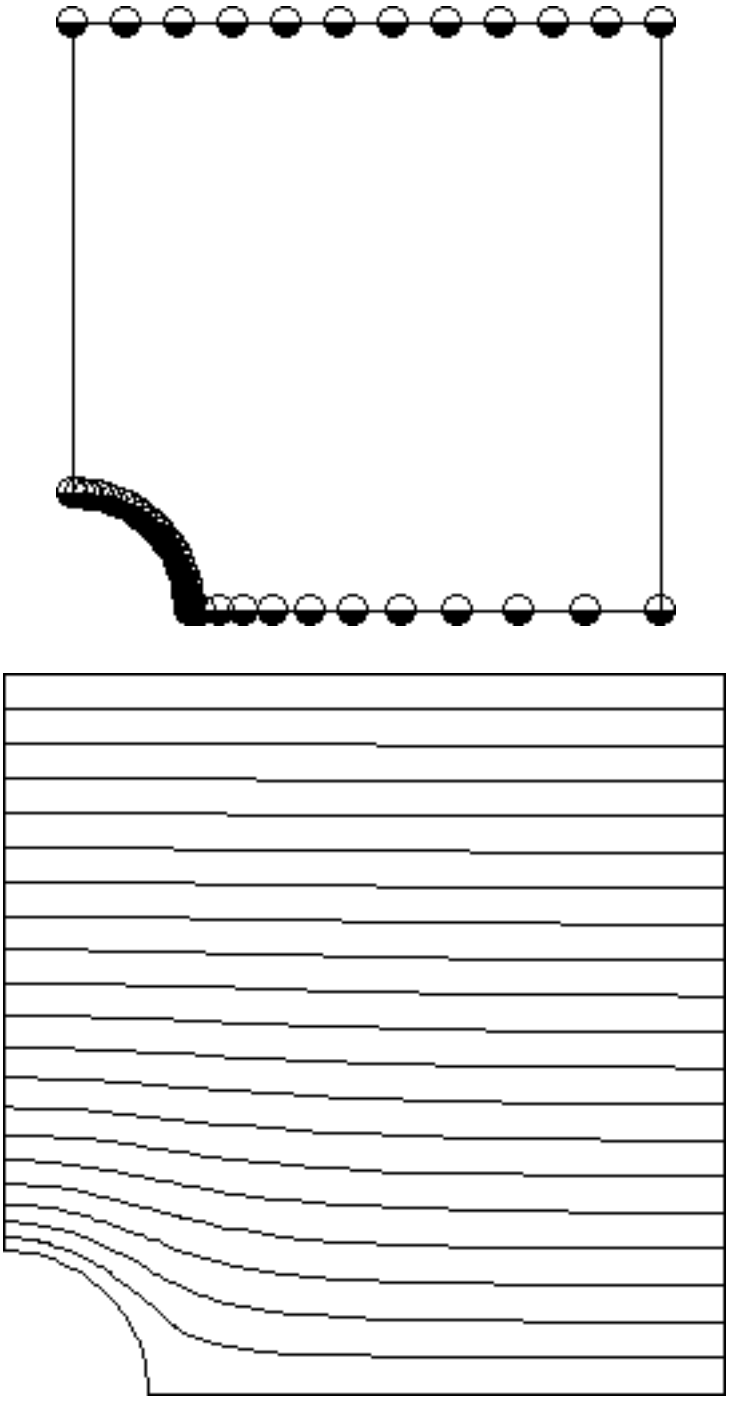

Fig 1.17.2 Spherical conductor

Compare this result with the prolate spheroid considered in Project 18.

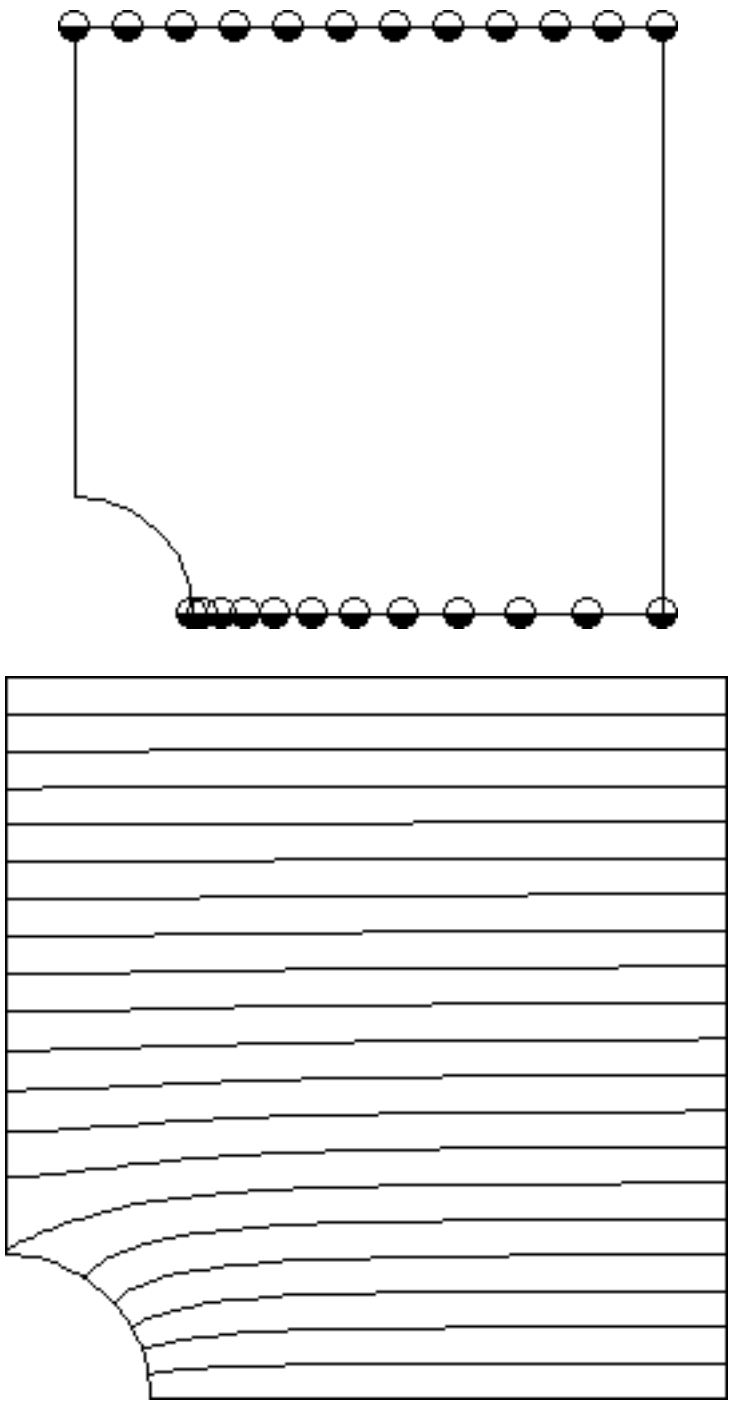

Fig 1.17.3 Spherical cavity

Suppose we consider the related problem of electric conduction (Moon and Spencer, 1961, p229) through a large casting having a spherical cavity. The solution is shown in Fig 1.17.3.

$$\phi = E_0 r \left[1 + (1/2) (a / r)^3 \right] \cos \theta$$

Finally, suppose that a metal sphere is introduced into a uniform field and maintained at 0 volts at a point where the undistorted field was 100 volts (Moon and Spencer, 1961, p228). In this case symmetry exists about the polar axis only. The resulting field is shown in Fig 1.17.4.

$$\varphi = V\,(a / r) + K\,(1 - a / r) + E_0\, r\,[\,1 - (a / r)^3]\cos\theta$$

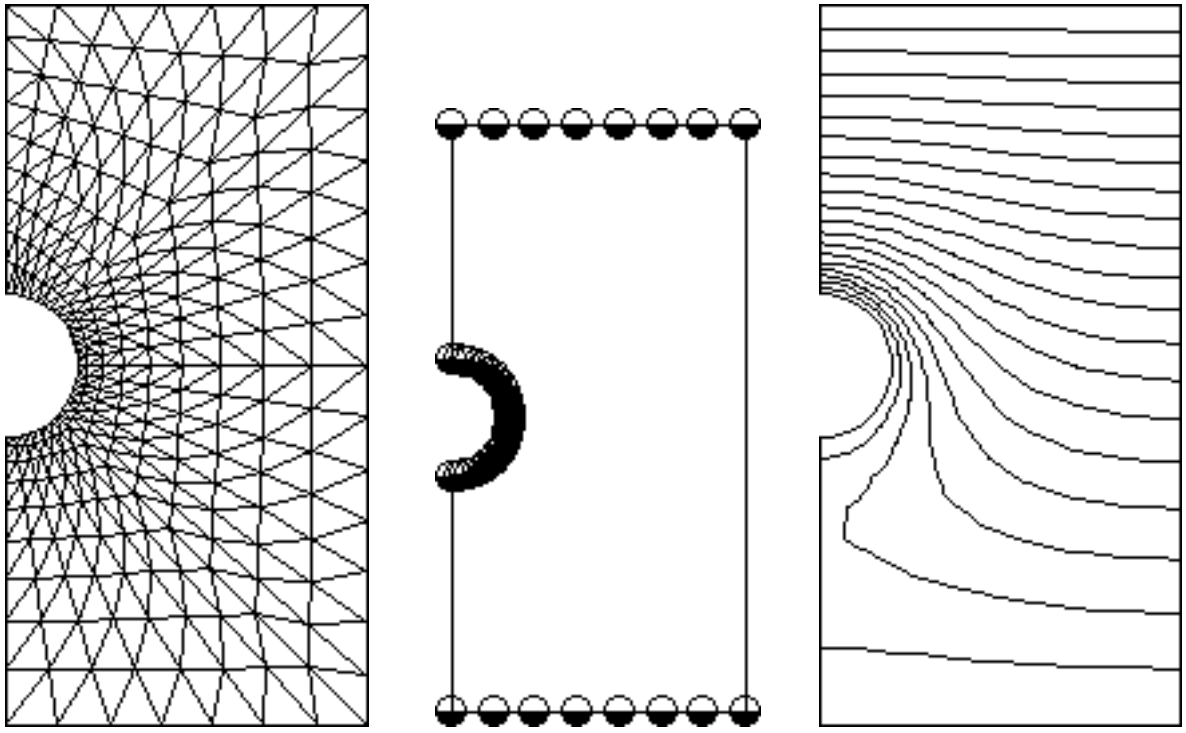

Fig 1.17.4 Electric field when sphere voltage is specified

Reference: Moon, Parry and Domina Eberle Spencer. 1961. Field Theory for Engineers. D. van Nostrand Co. Princeton. , pp. 226, 229

Project 18: Prolate spheroid dielectric in a uniform field.

Folder: Prolate Spheroid

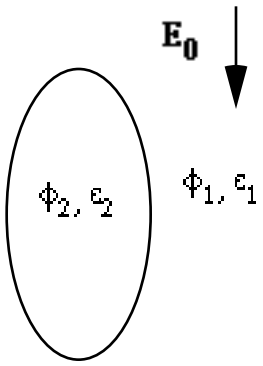

Fig 1.18.1 Dielectric spheroid in initially uniform field

Consider a prolate spheroid dielectric (Moon and Spencer, 1961, p252) of permittivity e_2 placed in an initially uniform electrostatic field $\mathbf{E}_0$ in a medium of permittivity e_1. The major axis is aligned with the field. What is the potential distribution inside and outside the spheroid?

Suppose the semi-minor and semi-major axes are 2.0 and 4.0, respectively, that $e_2 = 10$ and $e_1 = 1$, and that the potential is zero along the plane of the semi-minor axis and 100 volts at z = 10. This problem illustrates the use of the ellipse generation tool in geometry.

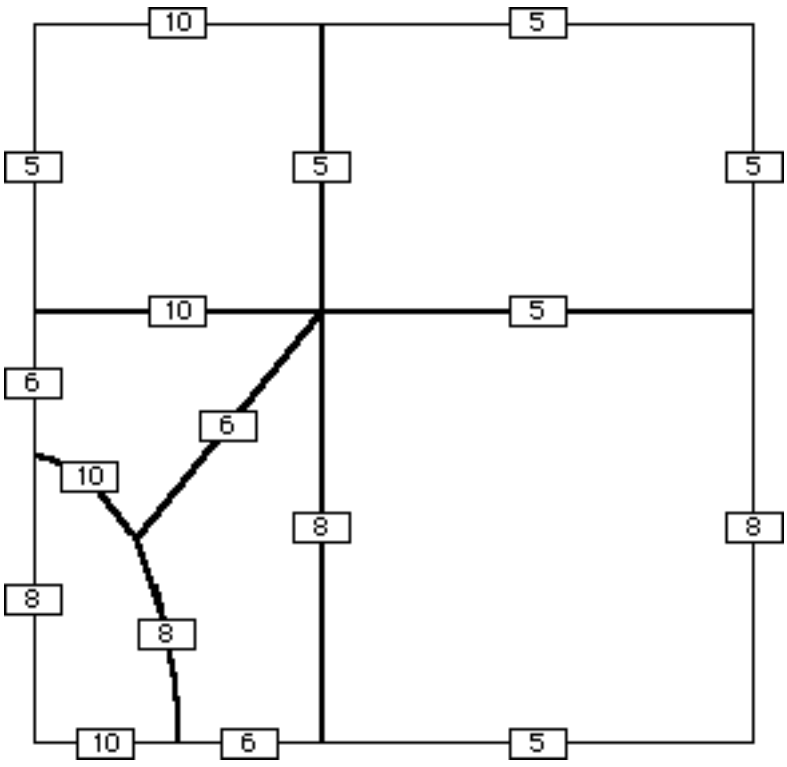

Fig 1.18.2a Mesh

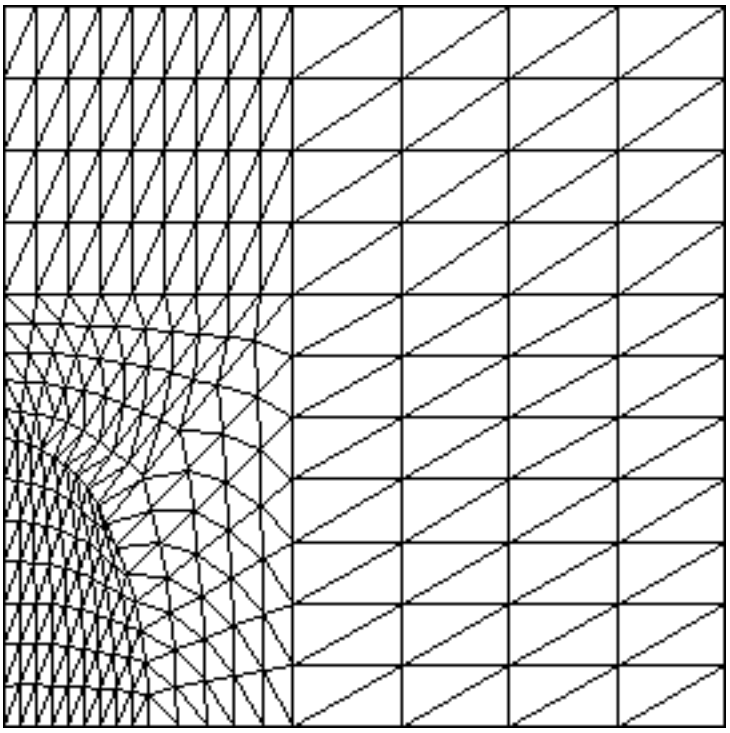

Fig 1.18.2b Mesh

Fig 1.18.2 Depicts the mesh used.

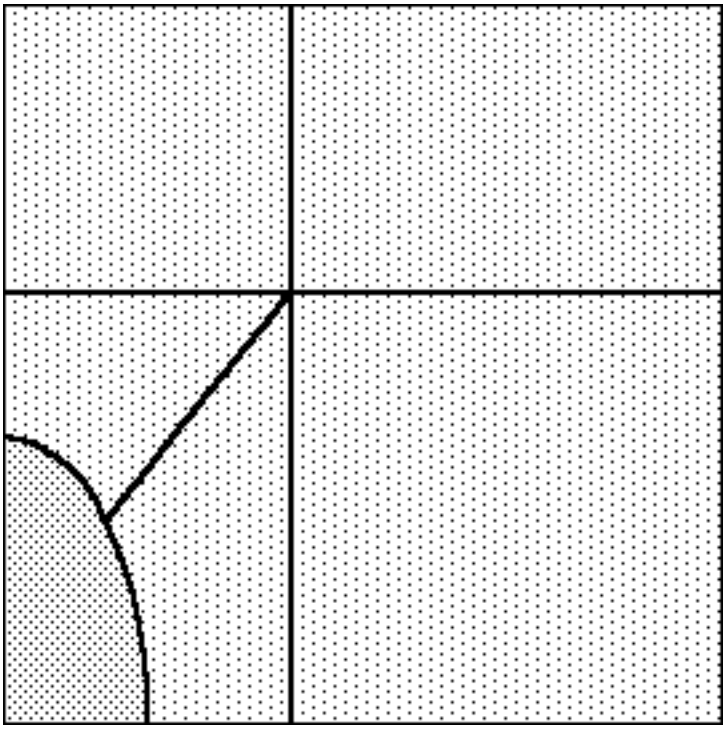

Fig 1.18.3a Properties

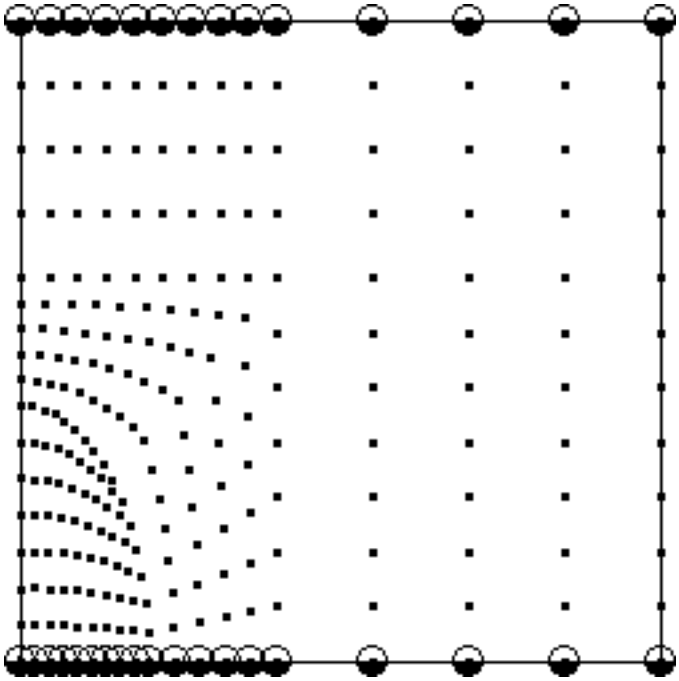

Fig 1.18.3b Constraints

Fig 1.18.3 shows the constraints.

Fig 1.18.4 shows the computed field. We have added the boundary of the spheroid. You can automatically overlay the mesh as an aid to understanding the performance of the mesh.

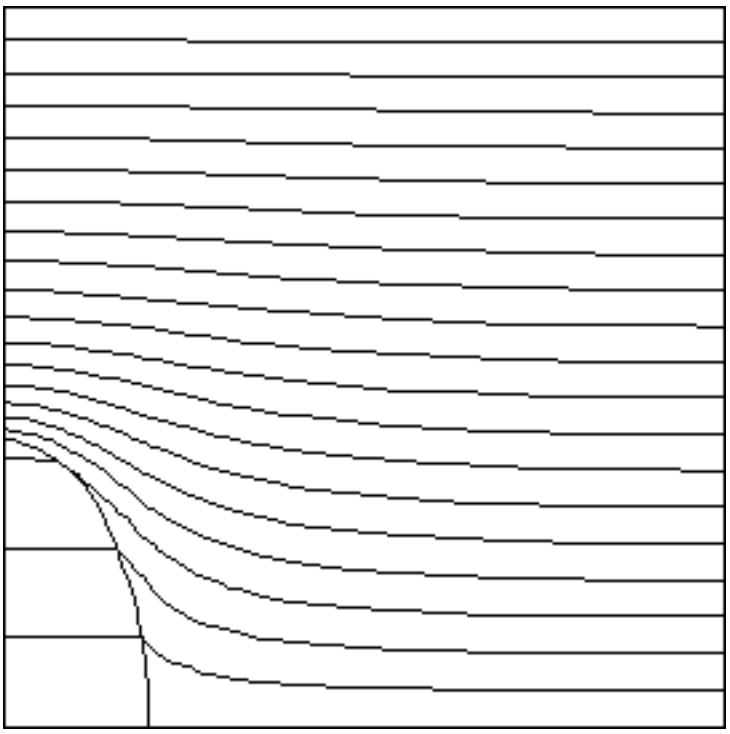

Fig 1.18.4a Computed fields

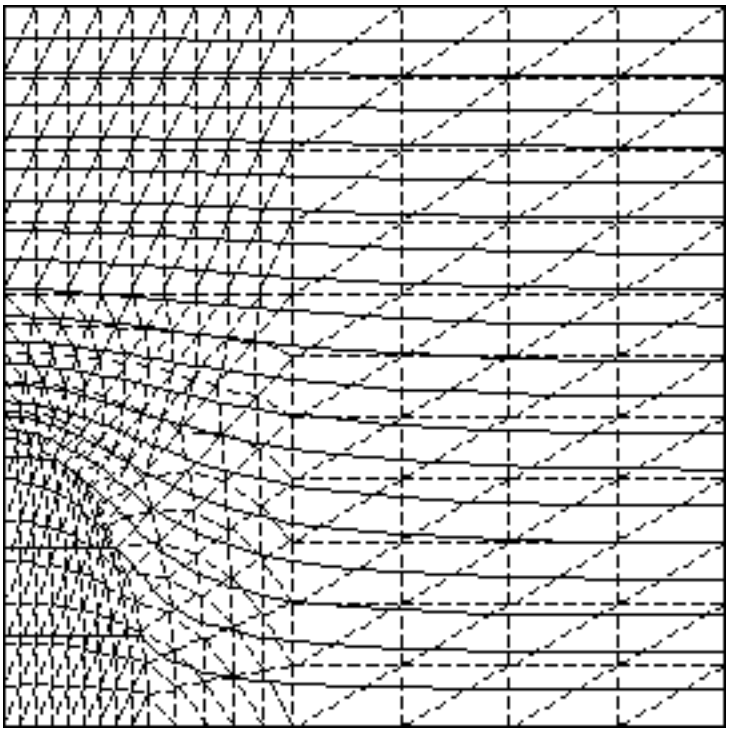

Fig 1.18.4b Computed fields

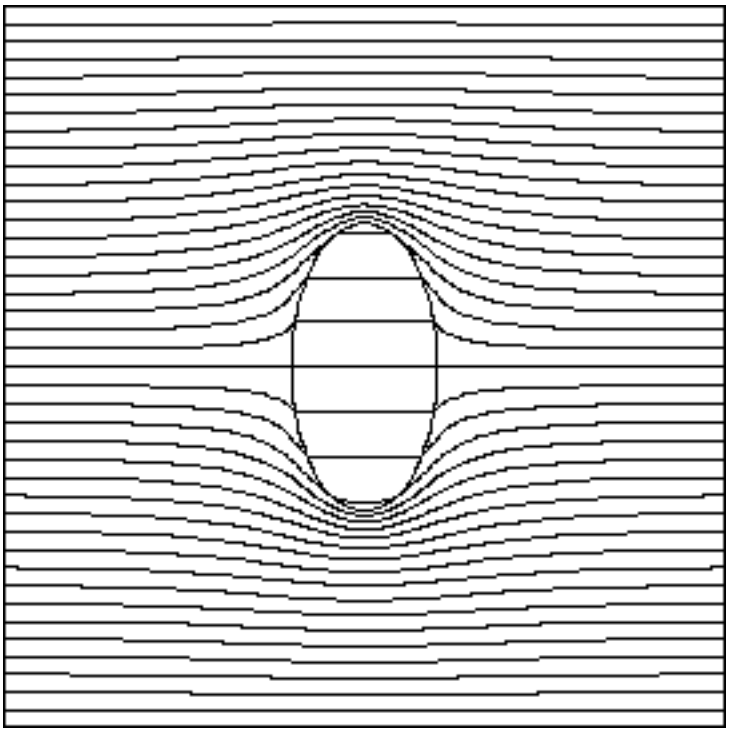

Fig 1.18.5 Composite plot

Notice the effect (Fig 1.18.5) of the dielectric on the field.

Project 19: Step change in boundary potential

Folder: Square

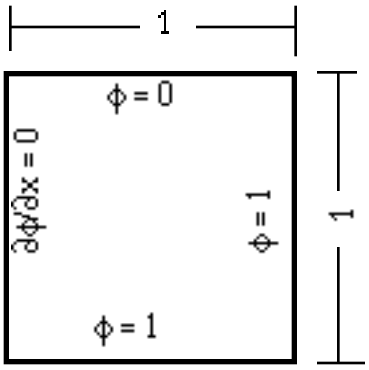

Fig 1.19.1 General

This problem illustrates the handling of an abrupt change in the boundary potential (Fig 1.19.1).

Fig 1.19.2 shows the mesh; Fig 1.19.3 depicts the boundary condition and solution. At the top right corner of the unit square, the potential makes an abrupt change between 0 and 1. We assigned the average value (0.5) as the boundary condition at the corner where the jump occurs because the series solution converges to the average.

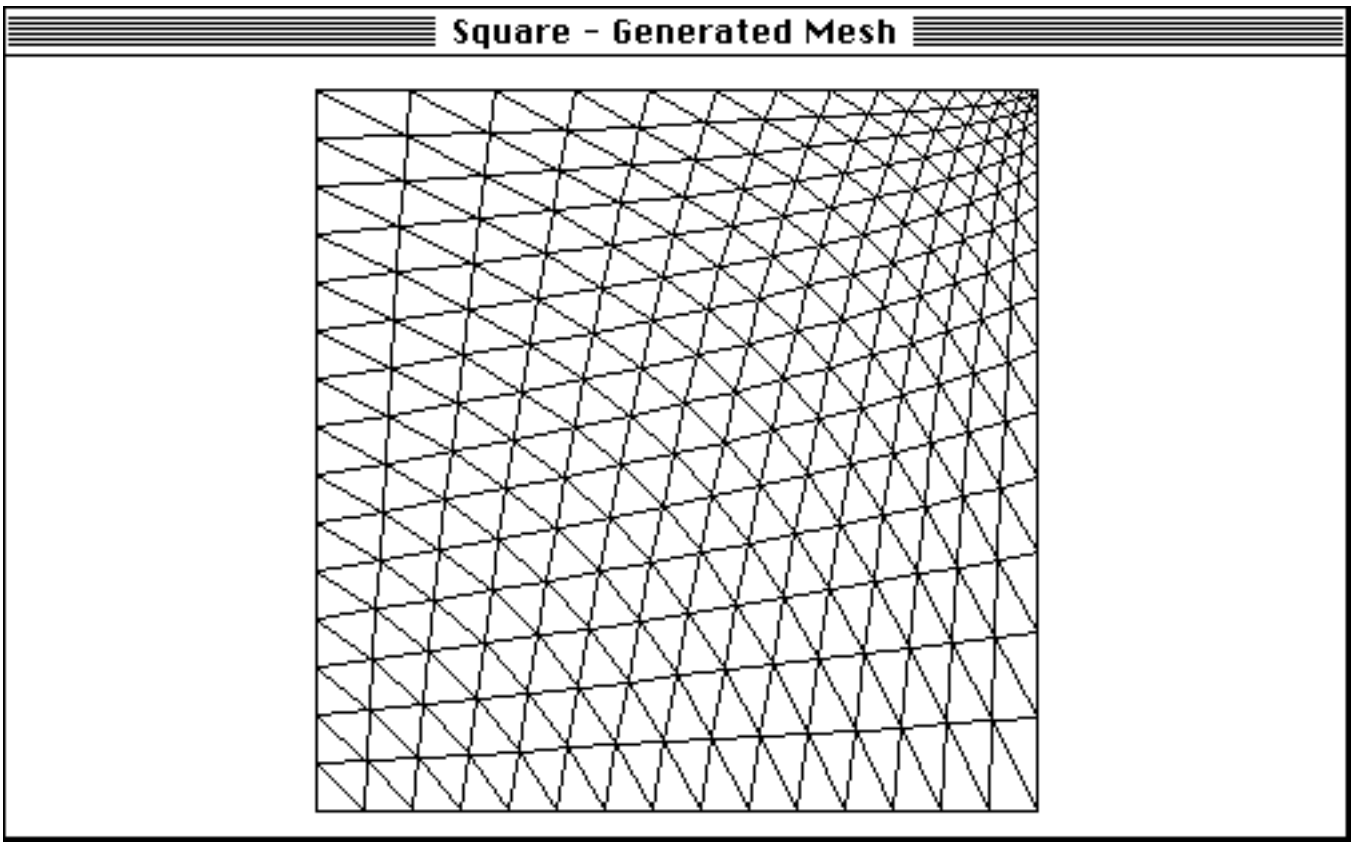

Fig 1.19.2 Mesh

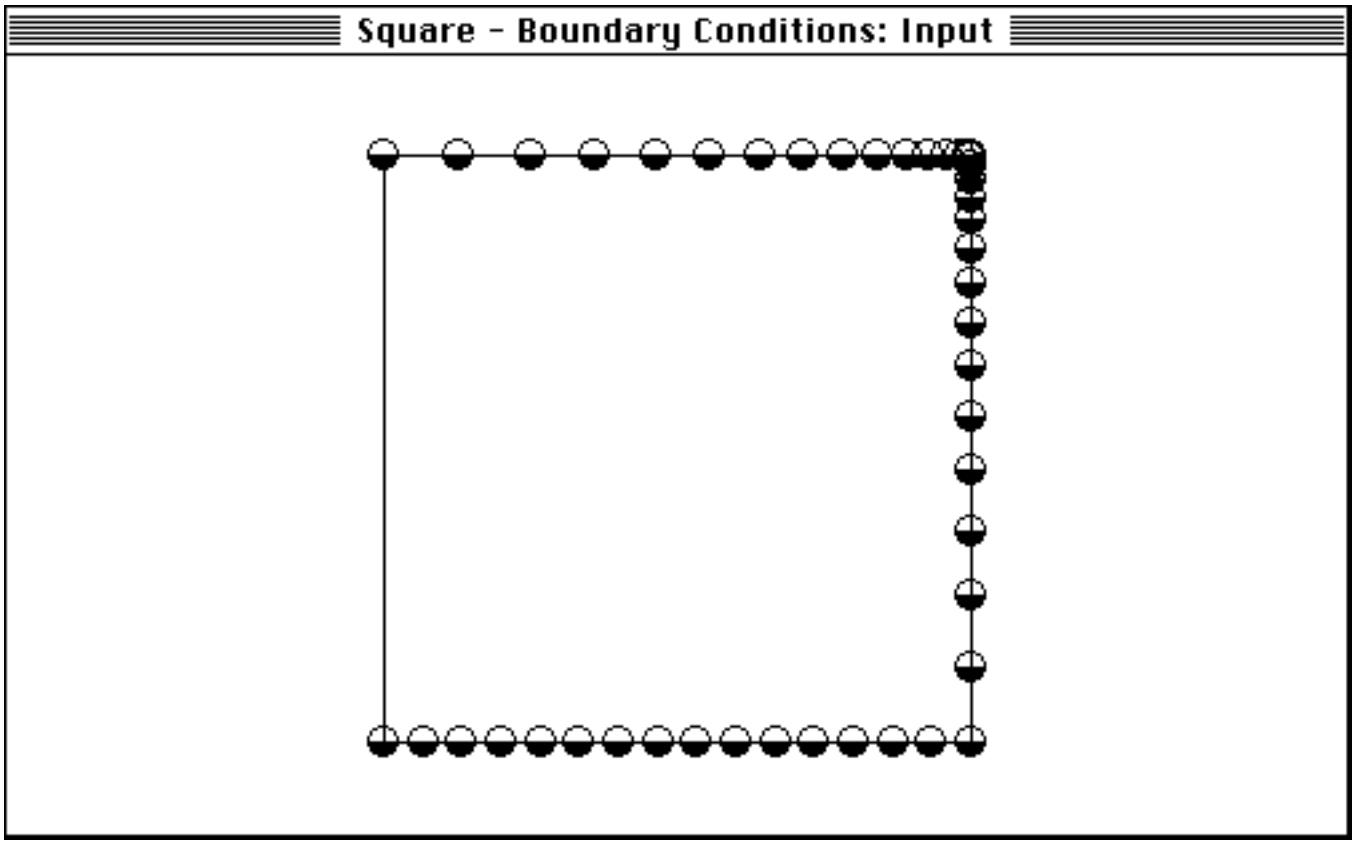

Fig 1.19.3a Constraint

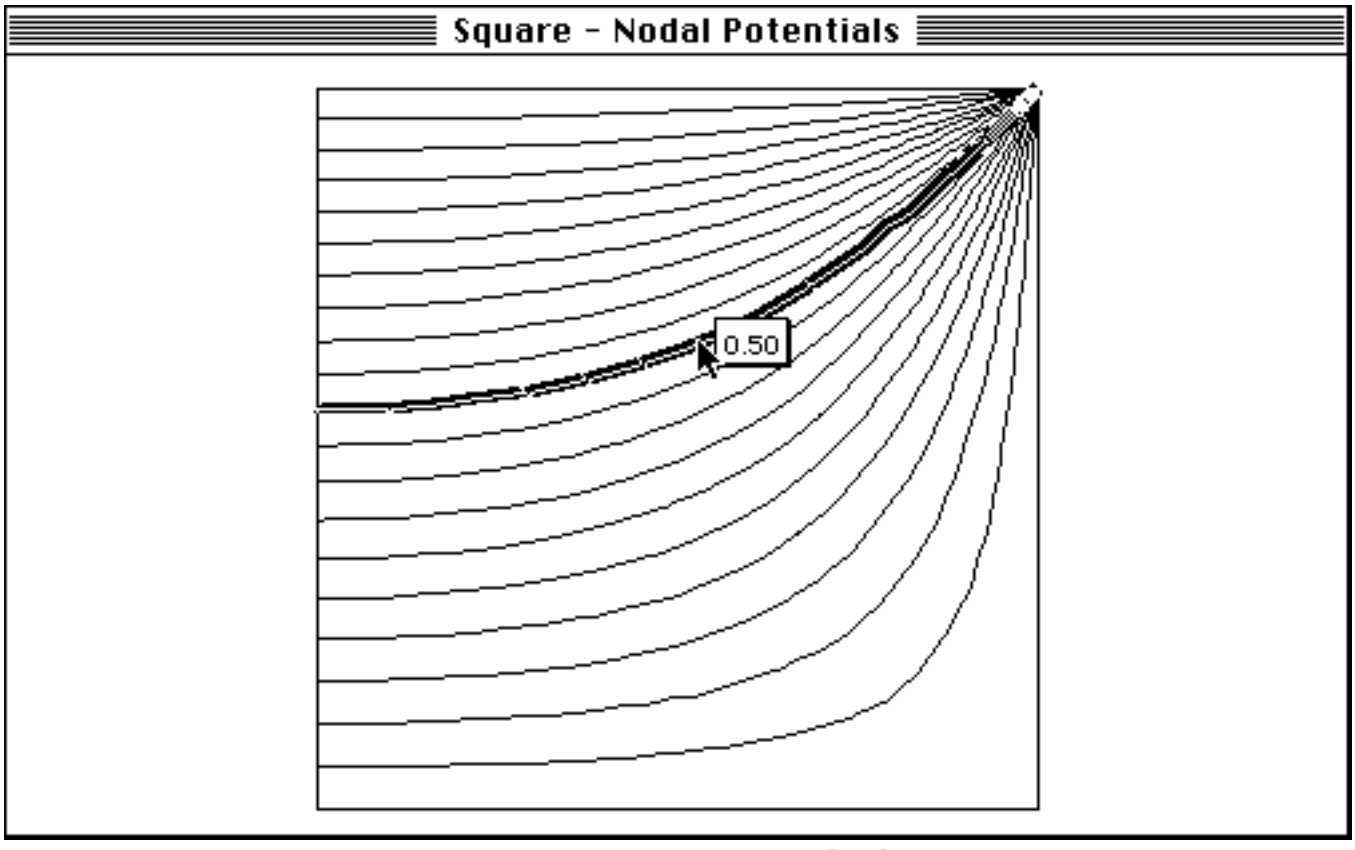

Fig 1.19.3 Constraint and solution

Project 20: Torsion of a square shaft.

Folder: Torque

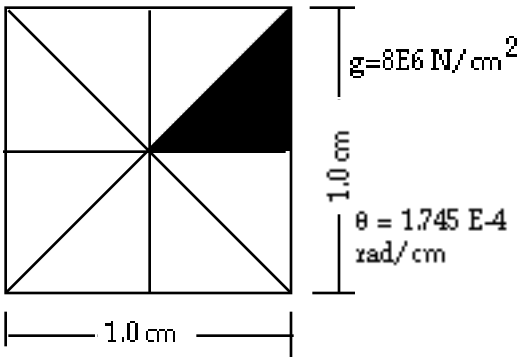

Fig 1.20.1 Square shaft

This example illustrates the application of Prandtl's theory to the twisting of a solid, noncircular shaft. A detailed discussion of this example has been presented by Segerlind (1984, 100-114). This problem is governed by Poisson's equation if the conductivity terms are unity, the stress function (or potential) is zero on the shaft boundary, and the "source term" is 2 times the shear modulus times the twist per unit length. The torque is calculated as twice the integral of the stress function over the cross-section.

Fig 1.20.1 depicts a 1 cm square shaft. By symmetry you only need consider one-eighth of the cross section. Three mesh generating regions (Fig 1.20.2) generated the mesh (Fig 1.20.3). The two triangular regions are degenerate quadrilaterals. The boundary conditions (Fig 1.20.4) are zero on the outside boundary, and the gradient is zero elsewhere (Fig 1.20.5). MP reports the torque for the eighth section (24.5 N cm) in the Solve window and at the end of the nodal potential file. The calculated torque (196 N cm) matches theory.

Reference: Timoshenko and Goodier, 1970, *Theory of Elasticity*. p313).

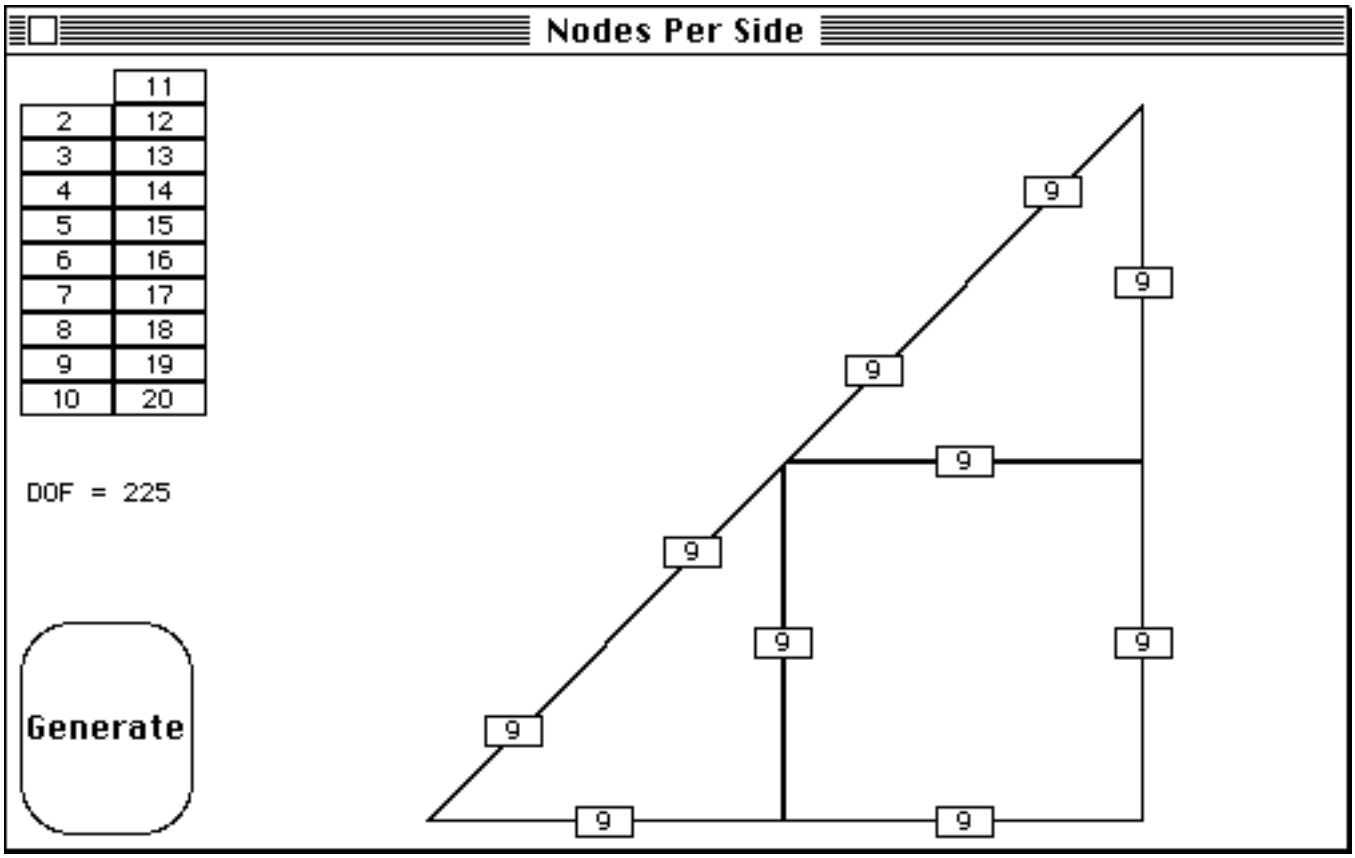

Fig 1.20.2 Generating regions

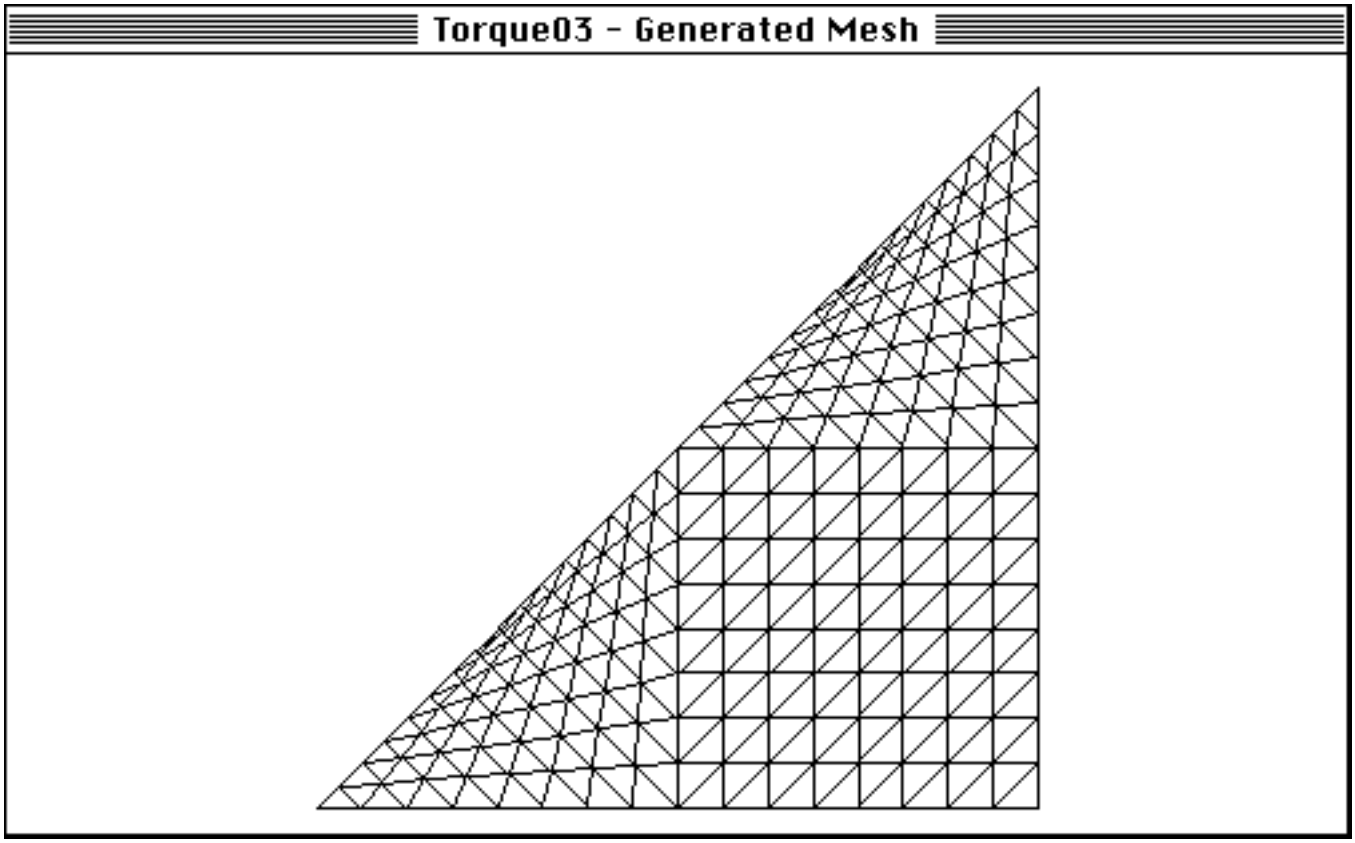

Fig 1.20.3 Mesh

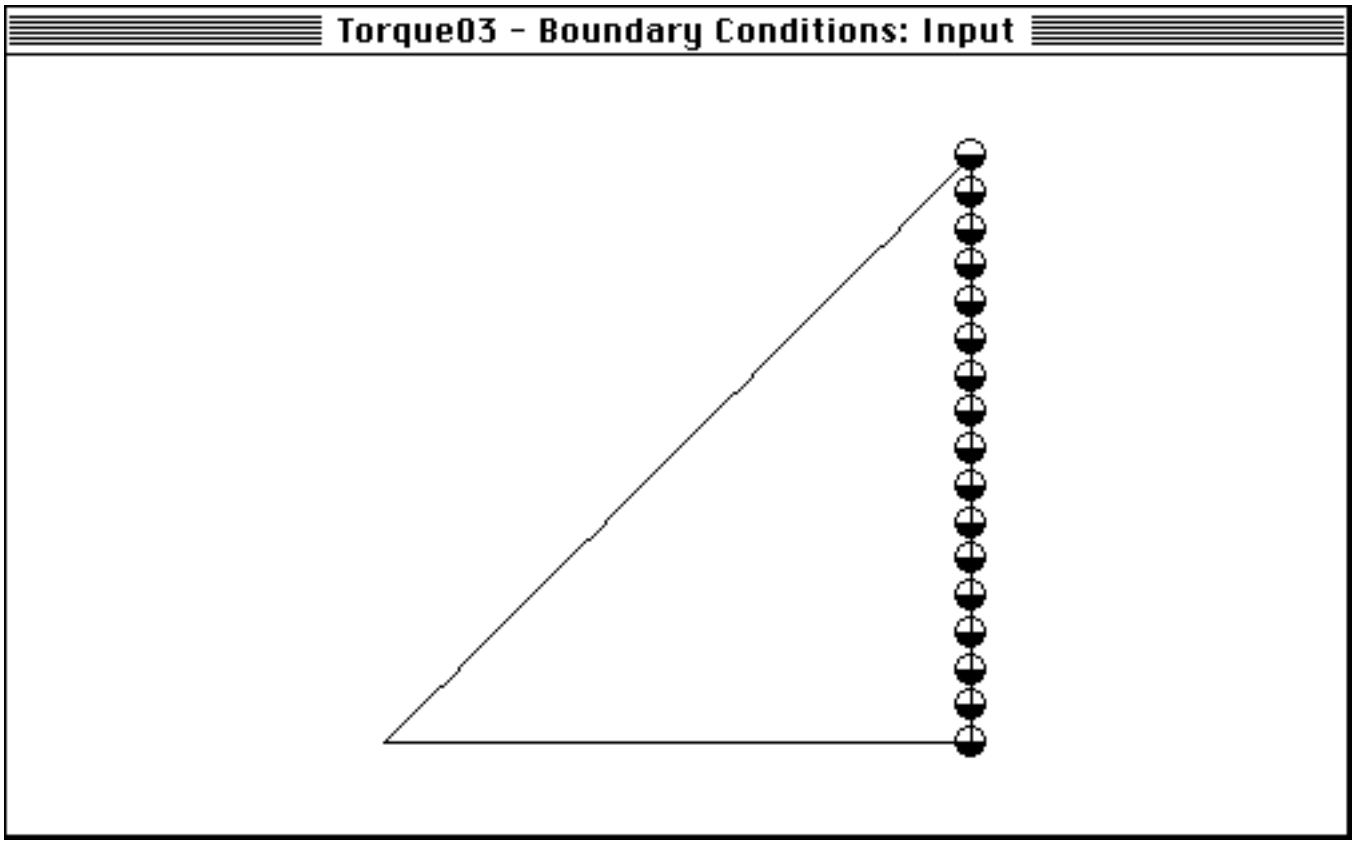

Fig 1.20.4 Boundary conditions

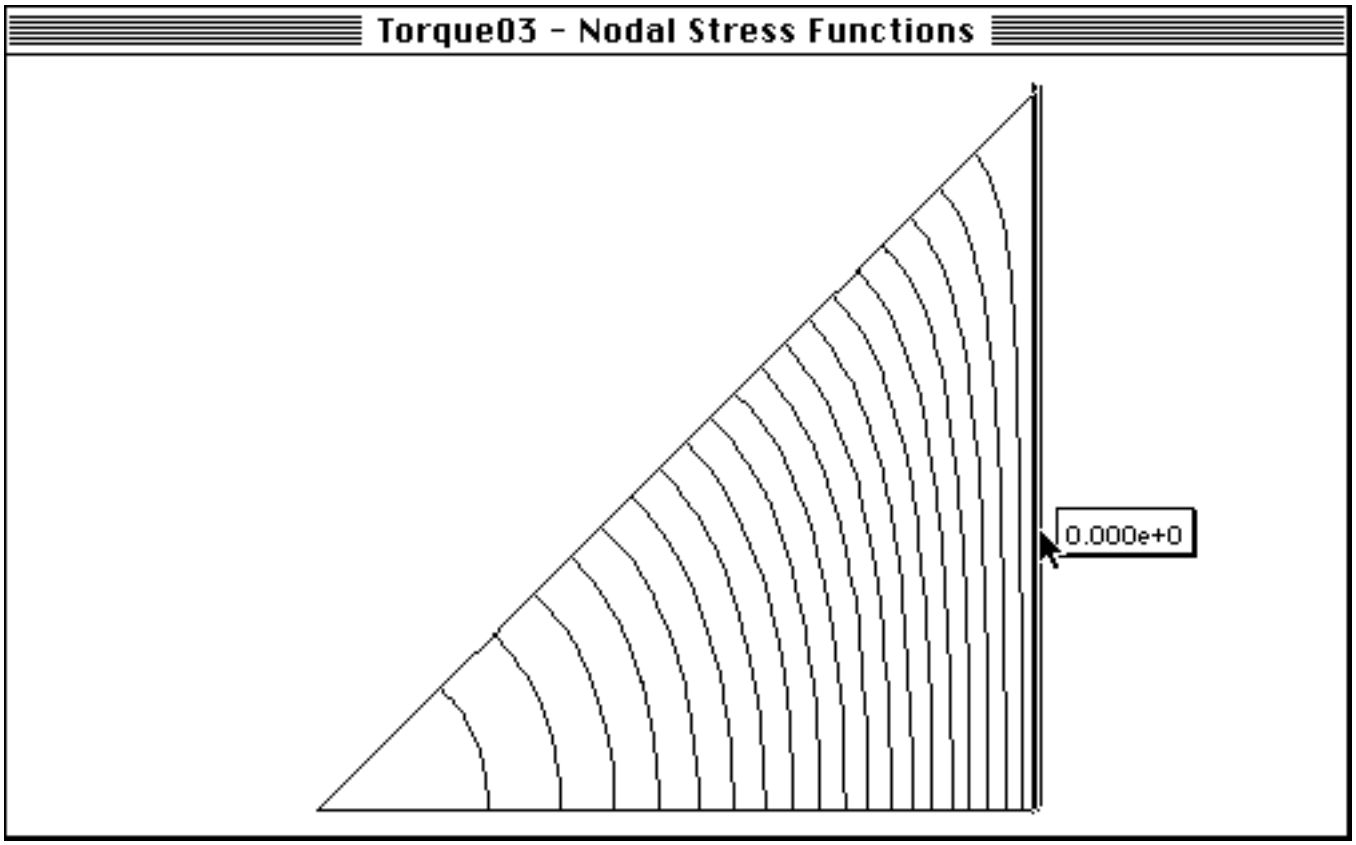

Fig 1.20.5 Constant stress function lines